Fall 12-3-2012

Dynamic Vulnerability Assessment of Highway and Railway Bridges

Mehdi Mohseni
University of Nebraska-Lincoln, mhsn.mehdi@gmail.com

Dynamic Vulnerability Assessment of Highway and Railway Bridges

by

Mehdi Mohseni

A DISSERTATION

Presented to the Faculty of

The College of Engineering at the University of Nebraska-Lincoln

In Partial Fulfillment of Requirements

For the Degree of Doctor of Philosophy

Major: Engineering

(Construction)

Under the Supervision of Professor Terri R. Norton

Lincoln, Nebraska

December, 2012

Dynamic Vulnerability Assessment of Highway and Railway Bridges

Mehdi Mohseni, Ph.D.

University of Nebraska-Lincoln, 2012

Adviser: Terri R. Norton

Dynamic loads can cause severe damage to bridges, and lead to malfunction of transportation networks. A comprehensive understanding of the nature of the dynamic loads and the structural response of bridges can prevent undesired failures while keeping the cost-safety balance. Dissimilar to the static behavior, the dynamic response of bridges depends on several structural parameters such as material properties, damping and mode shapes. Furthermore, dynamic load characteristics can significantly change the structural response. In most cases, complexity and involvement of numerous parameters require the designer to investigate the bridge response via a massive numerical study.

This dissertation targets three main dynamic loads applicable for railway and highway bridges, and explores particular issues related to each classification: seismic loads; vehicular dynamic loads; and high-speed passenger train loads. In the first part of the dissertation, highway bridge responses to the seismic loads are investigated using fragility analysis as a reliable probabilistic approach. The analysis results declare noticeably higher fragility of multispan curved bridges, compared to straight bridges with the same structural system.

Structural reliability of steel tension and compression members in highway bridges, and the effects of the vehicular dynamic load characteristics are studied in the second part

of the dissertation. Latest available experimental data have been used to re-evaluate current US design criteria for axially loaded steel members. The obtained results indicate conservative design of steel tension members for yielding of gross cross section, (β_{min}=3.7 compared to the target reliability β_T=3.0) and fracture of the net section (β_{min}=5.2 compared to the target reliability β_T=4.5). In addition, all monitored steel sections designed for axial compression show adequate safety in all cases.

Lastly, the resonance of railway bridge superstructures under passing high-speed passenger trains is examined and their dynamic response are presented using dynamic load factor diagrams, applicable in strength limit state design of railway bridges. Applying proposed response curves can guide designers to estimate the structural response of railway bridges in the initial design phase, and avoid any possible resonance by changing the superstructure system, or modifying design parameters and the consecutive vibration frequency.

Acknowledgements

I would like to express my deepest appreciation to my advisor, Professor Terri Norton, for her thoughtful guidance and through reviewing of this dissertation. I am very grateful for all her support, enthusiasm and concern which made this research possible. I also wish to thank other advisory committee members; Professor Andrzej Nowak, Professor George Morcous and Professor Ece Erdogmus for their valuable guidance and suggestions which enriched the contents of this dissertation. I would like to acknowledge Dr. Wu for sharing his valued research results and generated ground motions. Also, I want to thank my fellow officemate Mohammad Lashgari for his kind help and sharing his knowledge.

To:

Farzaneh Noghandokht
Ezzatollah Mohseni

Table of Contents

List of Tables

List of Figures

List of Symbols

A_g	*gross cross-sectional area*
A_n	*net section area*
DC	*component dead load*
DLF	*moment dynamic load factor*
DW	*wearing surface dead load*
C	*viscous damping per unit length*
d_{bl}	*nominal bar diameter (longitudinal)*
E	*modulus of elasticity*
F_y	*specified minimum yield stress*
F_u	*specified minimum tensile stress*
f_{ye}	*expected yield stress of reinforcement (MPa)*
HSLM	*high speed load models proposed by Eurocode*
I	*moment of inertia*
IM	*dynamic load factor*
K	*effective length factor*
L	*length*
LL	*live load*
LM71	*static load model proposed by Eurocode*
L_P	*plastic hinge length*
[M]	*lumped mass matrix*
M_t	*total unrestrained mass of the structure*
m	*mass per unit length*
n	*mode number*
P_i	*unique random natural number*
P_f	*probability of failure*
$P_{f\text{-}c}$	*probability of failure for each component*
$P_{f\text{-}sys}$	*probability of failure for system*
P_r	*factored compressive resistance*
p(x,t)	*load per unit length (at point x and time t)*

PGA	*peak ground acceleration*
$q_n(t)$	*time function*
R_i	*randomly selected number (0-1)*
r_i	*mass participation ratio of mode i*
r_s	*radius of gyration about the plane of buckling*
r'	*dead load to total load ratio*
S_c	*median capacity value*
S_d	*median seismic demand value*
T_i	*randomly generated target number*
t	*time (sec)*
U	*reduction factor to account for shear lag*
$u(x,t)$	*transverse displacement of beams (at point x and time t)*
V	*coefficient of variation*
x	*space coordinate*
y_{dyn}	*maximum dynamic response*
y_{stat}	*maximum static response*
β	*reliability index*
β_c	*capacity dispersion value*
β_d	*seismic demand dispersion value*
β_T	*target reliability index*
δ	*bias factor*
η	*Load modification factor*
λ	*slenderness related parameter*
λ_n	*n^{th} mode frequency related parameter*
ξ	*damping ratio*
Φ	*dynamic factor*
$\Phi_n(x)$	*n^{th} mode spatial function or mode shape*
$\{\phi_i\}$	*modal shape vector for mode i*
φ_c	*resistance factor for compression*
φ_y	*resistance factor for yielding on gross section of tension member*
φ_u	*resistance factor for fracture on net section of tension member*

ω	*natural circular frequency*
ω_n	*n^{th} mode natural frequency*

Chapter 1

Introduction

1.1. Motivation

Bridges are an important part of the surface transportation system. Failure in a bridge operation can cause severe economic, environmental and/or social consequence. A considerable number of bridge failures, caused by natural or human-made forces, can be prevented by theoretical studies, updating design criteria, re-evaluating safety and structural maintenance.

The structural response of bridges to dynamic loads contains common characteristics regardless of the load type and structural system. Dissimilar to the structural response to static loads, the dynamic response of a structure depends on several parameters such as material properties, damping, mass of the structure, accelerations, velocity of moving loads and modes of vibration. Recent findings in the nature of dynamic loads and their characteristics along with the continuous improvement in construction material properties should be involved in designing new bridges and also re-evaluation of the existing structures.

Using probabilistic approaches (in compare to deterministic approaches) is an efficient way to provide a better balance between cost and safety. By integrating the uncertainty of load characteristics, material properties, etc. code developers and designers have found a more reliable method to design structures and reduce possible environmental, economic and social damages.

1.2. Research Significance and Objectives

This dissertation aims to study the effects of three main dynamic loads applicable for bridges in the United States and abroad, and explores particular issues related to each classification. In the first part of the dissertation, bridge responses to seismic loads are investigated using fragility analysis as a reliable probabilistic approach. The main objective is to investigate the response of continuous curved bridges to seismic excitation and apply fragility curves to predict structural response both at the component and system level.

Effects of the vehicular dynamic load characteristics, as another major dynamic load for bridges, on the reliability of highway bridges have been studied in the second part of the dissertation. The obtained results can be used to re-calibrate current US design criteria for steel tension and compression members.

Lastly, resonance of railway bridge superstructures under passing high-speed passenger trains is examined and their dynamic responses are presented using dynamic load factor diagrams. Calculated diagrams are applicable in strength limit state design of railway bridges.

Using proposed response curves can guide designers to estimate the structural response of the superstructure in the initial design phase and avoid possible resonance by changing the superstructure system and the consecutive vibration frequency. The comprehensive results can be beneficial for the US transportation authorities in developing new design criteria regarding the ongoing high-speed rail projects in the United States.

1.3. Scope

This dissertation is organized in 6 chapters. This chapter briefly speaks about the motivations, research significance, objectives and the organization of the dissertation.

Chapter 2 discusses the vulnerability of existing bridges in the United States. Current status of existing bridges and an overview of bridge failures and causes are presented using some recorded data and statistics. Furthermore, future needs and challenges in the bridge industry are pointed to highlight the possible trends for reducing the risk of bridge structural failures.

In Chapter 3, general seismic load effects on bridge structures and components are discussed. Next, a continuous multispan curved bridge with steel I-shape girders is examined through a massive nonlinear analysis using fragility curves as a probabilistic approach. Generated ground motions and Monte Carlo simulation have been used to develop fragility curves for different damage levels for individual components and bridge system.

In Chapter 4, recorded dynamic loads in axially loaded steel members due to the passing traffic load are used to evaluate the reliability of current US design criteria. Latest probabilistic models have been used for both load and resistance parameters. Reliability indices are calculated using Monte Carlo simulation technique for both tension and compression members. Possible code adjustments are examined to observe the applicability of the recommendations.

In Chapter 5, dynamic response of bridges to passing high-speed trains is presented through a comprehensive analytical study. Based on a deterministic approach, the dynamic response of bridge superstructures are evaluated for any bridge structural system

and a variety of applicable velocities. Concluded results are presented as dynamic load factors and can be used to determine the possibility of resonance for any selected superstructure, based on its frequency of vibration. The results can be beneficial in the everyday design practices related to high-speed rail program in the United States and abroad.

Chapter 6 summarizes the findings and contributions of this dissertation and discusses possible research topics to be considered in future.

Chapter 2

Vulnerability of Existing Bridges in the United States

2.1. Current Status of Existing Bridges in the United States

Determining the existing condition of bridges is a key term in evaluating their response and vulnerability to different dynamic loads. With regard to the dynamic response of bridges (especially when resonance is a point of concern), in situ structural condition is important for new and aging bridges. About 600,000 bridges are currently in service in the US transportation network. Figure (2-1) shows the age of the US bridges in a modified graph based on an AASHTO document published in 2008 (AASHTO, 2008a).

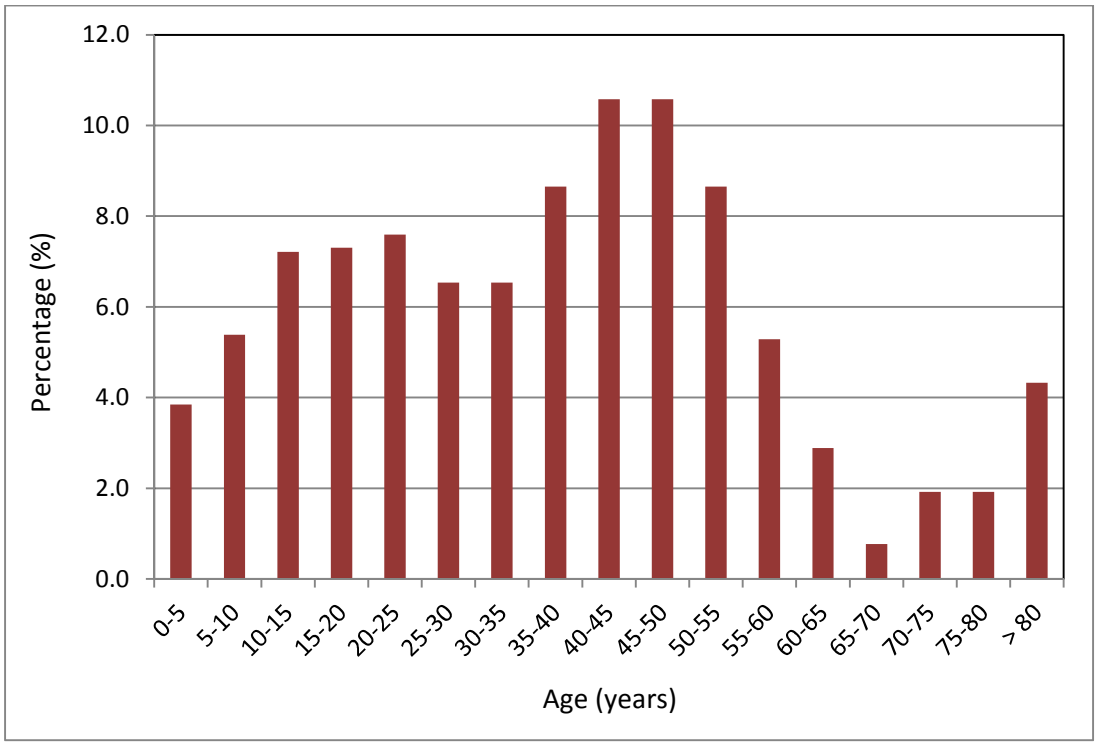

Figure 2-1. Age of bridges in the US transportation network

Today, about one half of the bridges in the United States have aged more than 40 years. On average, about 12% of existing bridges are already structurally deficient and need repairs, strengthening, maintenance and perhaps closure (AASHTO, 2008a). The critical situation can be where two or more failure causes happen at the same time. For example, a structurally deficient bridge under overloading conditions can be significantly in danger of collapse. One practical procedure is forcing "live load" limits for deteriorated bridges after a careful bridge inspection until enough funding is provided to repair the bridge, or other decisions for its functionality is made. However, this act does not protect bridge structures against environmental disasters and accidents. Regular inspection plans and bridge rating processes have considerably reduced the risk of failure for the huge number of aging bridges in the United States.

Figure 2-2. Plattsmouth Bridge over the Missouri River connecting Nebraska to Iowa built in 1929 (Image credit: http://www.wikipedia.org/)

By referring to the massive bridge construction in 1950s and 1960s (Fig. 2-1), the importance of bridge evaluations will be determined. Wang et al. (2011a; 2011b)

conducted a valuable study to involve reliability assessment to the conventional bridge rating process. Their study shows the results of different bridge rating methods as permitted by AASHTO's manual for bridge evaluation (AASHTO, 2008b) including allowable stress, load factor and load and resistance factor method can estimate different rated capacities for the same bridge structure. Using bridge rating data collected in 41 states, authors proposed a new guideline for the evaluation of existing bridges in the State of Georgia, based on a reliability approach. However, their study considers everyday loading condition (including permanent gravity loads and vehicular loads) for common highway bridges in Georgia such as reinforced concrete tee, prestressed concrete and steel girder bridges. Most dynamic loads such as earthquake loads were not reflected in the proposed guidelines.

2.2. Dynamic Loads and Bridge Failure

Bridge failures may happen at any stage of the bridge life time as reported in the United States and abroad. Reports declare collapse of older bridges, newly designed bridges, and even those which are under construction. Deterioration of the bridge elements and inadequate design criteria in older codes can be two main reasons for collapse of old bridge structures. After few bridge failures in the United States (Fig. 2-3), bridge inspection and rating policies were developed in late 1960s to mitigate future disasters (McLinn, 2009). The bridge inspections and ratings can highlight vulnerability of existing bridges and help authorities to make the best decision at the right time to avoid possible failures.

Figure 2-3. Silver Bridge failure over the Ohio River caused the death of 46 people in 1967 (Image credit: http://www.pbs.org/)

Beside deterioration and lack of regular inspection and maintenance, design errors and unpredicted loads can also cause collapse of bridges including new and/or old bridge structures. Hydraulic loads, collision, overloading, deterioration, earthquake and construction have been measured as the most destructive causes of bridge failures in the United States (Wardhana & Hadipriono, 2003). Table (2-1) shows the number and percentage of each cause for reported failures in the US between 1989 and 2000. The presence of two or more causes at the same time can significantly increase the failure threat. For example, deteriorated elements subjected to overloads or earthquake excitations might be a source of damage and possible structural collapse.

After each major earthquake event, numerous reports and research articles are frequently published base on field studies and observations. In some cases, field studies

reveal the need of justifying design codes to prevent future disasters (Sun et al., 2012; Yashinsky, 1998). Experimental and analytical studies on bridge failures during earthquake events can be used to investigate the adequacy of seismic codes and propose justified criteria (Cruz Noguez & Saiidi, 2012).

Table 2-1. The number and percentage of each cause for reported failures in the US for a 10-year period (Wardhana & Hadipriono, 2003)

Failure cause	No. of occurrence	Percentage
Hydraulic	266	52.9
Collision	59	11.7
Overloading	44	8.7
Deterioration	43	8.5
Earthquake	17	3.4
Construction	13	2.6
Other	61	12.1

The ongoing bridge engineering research projects show that the behavior of bridges under dynamic loads is still a point of concern. In addition, innovative bridge projects need to be verified based on enough experiments and theoretical studies. High-speed rail program in the US (to be accomplished by 2050) is a great example of new developments with broad uncertainties in bridge structural response. Learning from successful experience of utilizing high-speed trains in Europe and East Asia can significantly improve the structural engineering knowledge in the local US projects.

2.3. Future Needs and Challenges

Moving from deterministic approaches to probabilistic based designs and reliability assessments has led to the development of more trustworthy and economic criteria for

designing bridges in the United States. However, in most cases, researchers target the two main load categories: permanent dead loads and vehicular live loads for highway bridges. Implementing probabilistic techniques in evaluating structural response of bridges to dynamic loads can enhance the consistency of design criteria such as the AASHTO guide specifications for LRFD Seismic Bridge Design (AASHTO, 2011).

Furthermore, reliability evaluation of less applicable structural systems such as truss bridges, arch bridges, cable-stayed bridges, etc. can improve structural safety of these types of bridges. Same static or dynamic load can have a dissimilar effect on different bridges. Consequently, investigating the influence of a dynamic load on bridge structures should not only include girder bridges, but also other practical structural systems.

Chapter 3

Part I: Seismic Loads

3.1. Seismic Loads on Global Bridge Structures

Bridges, as a sensitive and relatively expensive part of the transportation networks, are critical to function after natural disasters such as earthquakes. Similar to other types of structures, bridges can be significantly damaged by large scale earthquakes. The unique structural configuration of bridges requires special attention to their dynamic response and characteristics. Numerous analytical and experimental studies are being accomplished every year to disclose particular issues regarding seismic response of bridges such as geotechnical considerations, analysis approaches, design philosophies, seismic damage assessment, retrofitting practices, energy dissipation techniques and soil-structure interaction.

Each particular research can be useful in determining general trends in the structural response of bridges to be applied for new designs and evaluating other similar bridge structures. However, irregularity and complexity of some particular bridges necessitates them to be evaluated case by case. Special attention should be made for each site seismicity, system response and individual component behaviors.

3.2. Seismic Load Effects on Bridge Components

Most sensitive bridge components may include pier columns, abutments, bearings and foundations. In some specific cases, such as large vertical excitations, bridge superstructure and girders might be damaged as well. Plastic deformation of pier columns

can occur in either longitudinal or transverse direction. It is desired to provide sufficient ductility by considering special seismic considerations in columns. The ductile behavior helps to transfer applied loads to other structural components before failure, while reduces the actual seismic loads by dissipating applied energy (Fig. 3-1).

Using energy dissipating devices and isolation bearings can significantly reduce the damage on bridge substructure components including columns, abutments and foundations. In areas with less seismic concerns, fixed bearing devices are still being used in highway bridge construction.

Figure 3-1. Plastic deformation of a bridge concrete column during the 1994 Northridge earthquake (Image Credit: NOAA/NGDC, M. Celebi, U.S. Geological Survey)

Insufficient longitudinal girder seat length is a common defect in older bridges in the United States which can cause in unseating of girders and eventually bridge failure (Wright et al., 2011). In addition, large vertical accelerations during an earthquake can cause outsized bending moments larger than girders capacity and lead to superstructure failure (Fig. 3-2). As the seismic loads were traditionally being considered for two horizontal directions, this fact shows the importance of vertical accelerations and the need of particular investigation of irregular bridges such as curved and skewed bridges.

Figure 3-2. A superstructure failure during the 1994 Northridge earthquake (Image Credit: www.usgs.org)

3.3. Fragility Analysis of Highway Bridges

3.3.1. Methodology

Bridge structures are one of the most expensive and vulnerable parts of transportation networks. Failure in a bridge operation may lead to the loss of lives and/or money during or after an earthquake event. Fragility analysis, a powerful tool of predicting seismic damage, provides a comprehensive seismic evaluation of bridge structures and transportation networks. The probabilistic approach in fragility analysis offers the cumulative probability of passing each damage state for a variety of earthquake demands.

Fragility curves can be developed empirically or analytically. Empirical fragility curves are mostly obtained by damage observation of existing bridges after an earthquake. This method is not applicable in most of the cases due to the lack of post-earthquake damage data (Hwang et al., 2001). The analytical method, which considers uncertainties in ground motion, site condition and bridge modeling parameters, is more common according to the accessibility of high speed computers for numerical calculations (Mohseni & Norton, 2010).

Fragility analysis is commonly used in earthquake damage assessment of a structural component or system. In seismic analysis, fragility curves illustrate the probability of exceeding demand (D) by capacity (C) of the structure or individual component for different levels of damage. This probability can be expanded for a variety of intensity measures (IM) which is a ground motion characteristic and can be defined with numerical parameters such as spectral acceleration (S_a) or peak ground acceleration (PGA). This simplified statement can be represented by following equation (Buckle et al., 2006):

$$\text{Fragility} = P\,[D \geq C \mid IM] \tag{3-1}$$

To calculate this probability, seismic demand and capacity of each component should be defined. Probabilistic seismic demand models (PSDM) can be developed by using analysis results of bridge samples. To generate PSDM for each component, the following equations were applied (Cornel et al., 2002):

$$S_d = a\,(IM)^b \tag{3-2a}$$

or:

$$\text{Ln}(S_d) = \text{Ln}(a) + b*\text{Ln}(IM) \tag{3-2b}$$

in which S_d is the median value of seismic demand for each component, and a and b are regression coefficients depending on sensitivity of each response to intensity of ground motions.

It has been shown that PGA and S_a are appropriate features of ground motions to be considered as the intensity measure for analysis of bridges (Padgett et al., 2008). In this study, using PGA rather than spectral acceleration resulted in lower logarithmic standard deviation values (β_d) for the probabilistic seismic demand models.

As the fragility function is expressed with a relation of demand to capacity, a lognormal distribution can be a suitable estimation for the fragility function. This statement is even more accurate when the capacity and demand models follow a lognormal distribution. As a result, Equation (3-1) can be rephrased as the following equation (Choi & Jeon, 2003):

$$Fragility = \phi\left(\frac{Ln(\frac{S_d}{S_c})}{\sqrt{\beta_d^2 + \beta_c^2}}\right) \tag{3-3}$$

in which $\phi(x)$ is the standard normal cumulative distribution function (CDF). The dispersion value (lognormal standard deviation) for seismic demand (β_d) can be calculated during probabilistic seismic demand analysis for each component applying following equation:

$$\beta_d = \sqrt{Ln[\left(\frac{\sigma_d}{\mu_d}\right)^2 + 1]} \tag{3-4}$$

where σ_d and μ_d are the standard deviation and mean value of the calculated demand data, respectively.

3.3.2. Fragility of Typical Straight Bridges

Several attempts have been made to develop fragility curves for different types of existing straight bridges (Choi & Jeon, 2003; Choi et al., 2004) and retrofitted bridges (Padgett & DesRoches, 2006; 2008; 2009). The most possible damages were observed in bearings, abutments and pier columns.

In seismic damage assessment of bridges, the difference between design assumptions and as-built parameters can significantly affect the estimation of demand and capacity. Multi-span curved bridges are even more sensitive to as-built details due to their more complicated dynamic response (Mwafy et al., 2007). However, as-built parameters are not deterministic and follow a probabilistic random distribution function. Random variables are not only materials and geometry of the structure, but also soil properties,

dead and live load values and earthquake intensity and direction (Nowak & Collins, 2000). In practice, to generate several probabilistic structural models for fragility analysis, Latin Hypercube method is widely used (Olsson & Sandberg, 2002; Ayyub & Lai, 1991). More details regarding the response of multi-span continuous steel bridges, calculated by others are presented in following sections to compare with the examined curved bridge response.

3.3.3. Curved Bridge Structures

Curved bridges need more attention than straight bridges, as a result of their irregularity and unknown modal behavior (Mohseni & Norton, 2011). The uneven stiffness distribution in different horizontal directions can cause severe damage to bridge components, depending on the direction of earthquake excitations. In addition, eccentricity in superstructure weight and accompanying live load could be an issue in vertical ground excitations.

Seo and Linzell (2012) have recently studied the seismic vulnerability of an existing inventory of horizontally curved, steel, I-girder bridges located in Pennsylvania, New York and Maryland. Selected bridges were all without skew. The focus of their study was an evaluation of the Response Surface Metamodels technique in conjunction with Monte Carlo simulation. This methodology effectively reduced the number of samples for fragility analysis. However, no comparison was made to other efficient techniques such as Latin Hypercube method. Results declared that for non-skew curved bridges, bearing radial deformation was the most fragile component in extensive to complete damage states.

An experimental research project at the NEEC facilities at the University of Nevada-Reno is underway to study seismic response of multispan curved bridges. The massive two-fifth scaled lab study focuses on a variety of issues including live load effects, base isolation, hybrid isolation, response of conventional columns and abutment pounding. Initial results declare the need of complete three dimensional modeling due to the torsional effects, columns-superstructure interaction and possible plastic deformation of columns (Levi, 2011).

3.4. Case Study: Fragility Assessment of a Multispan Curved Bridge

Horizontally curved bridges are a common practice in urban areas. The irregular geometry makes seismic response of curved bridges more dependent to bridge characteristics. To study the fragility of curved bridges and comparing the results with the same structural system in straight bridges, an existing multi-span curved bridge with continuous steel composite girders was examined against earthquake excitations. To follow a relatively reliable approach for seismic damage assessment of the bridge, fragility analysis was applied. This method assists to include the effect of uncertainties in loading/modeling assumptions. Three dimensional nonlinear finite element (FE) models were used to achieve more accurate analysis results in compare to simplified methods. Applying Latin Hypercube method, 60 different bridge models were generated considering uncertainty of each random parameter. Using the analysis results, probabilistic seismic demand models are developed for various bridge elements and fragility curves for each monitored element are plotted for considered qualitative damage levels. Furthermore, system fragility curves are presented for the bridge structure in terms

of upper and lower bounds. Analysis results declare the importance of various parameters including bridge geometry and ground motion direction, and also their impact on analysis results. Also, the bridge superstructure stayed elastic during vertical excitation with relatively high PGA's. Median PGA values which cause slight, moderate, extensive and complete damages were determined equal to 0.09g, 0.19g, 0.29g and 0.57g, respectively.

3.4.1. Analytical Modeling

3.4.1.1. Bridge characteristics

Curved bridges are very common in urban highway intersections. For normal to relatively long span lengths, steel I-shape girders in composite action with reinforced concrete slab make an economical choice to design a bridge superstructure. The selected bridge for this case study is located in Omaha (NE) connecting US-75 southbound to I-480 eastbound. The bridge consists of four continuous spans including two 47m spans on sides and two 59m spans in the middle.

A continuous composite superstructure with seven I-shape steel girders exists along all four spans of the bridge structure (State of Nebraska 2005). The horizontal radius of curvature is 162m constantly, providing almost 75 degrees of rotation (Fig. 3-3). Steel girders sit on radially fixed bearing devices at the central pier and guided bearings at two adjacent piers, while integral abutments connect the bridge superstructure to driven H-section steel piles at both abutments. Three double rectangular column piers with different heights stand on 1.20m thick pile caps on a group of driven H-section steel piles. For live load considerations, four design lanes were assumed the most bridge

capacity, based on deck's total width (AASHTO 2007). The bridge structure was designed according to AASHTO design specifications and guide specifications for horizontally curved steel girder highway bridges (State of Nebraska 2005).

All dissimilar nonlinear 3D models were subjected to direct integration time history analysis, using finite element based software SAP2000® (2009). P-delta effect and justified damping ratio were taken into account for each time history analysis.

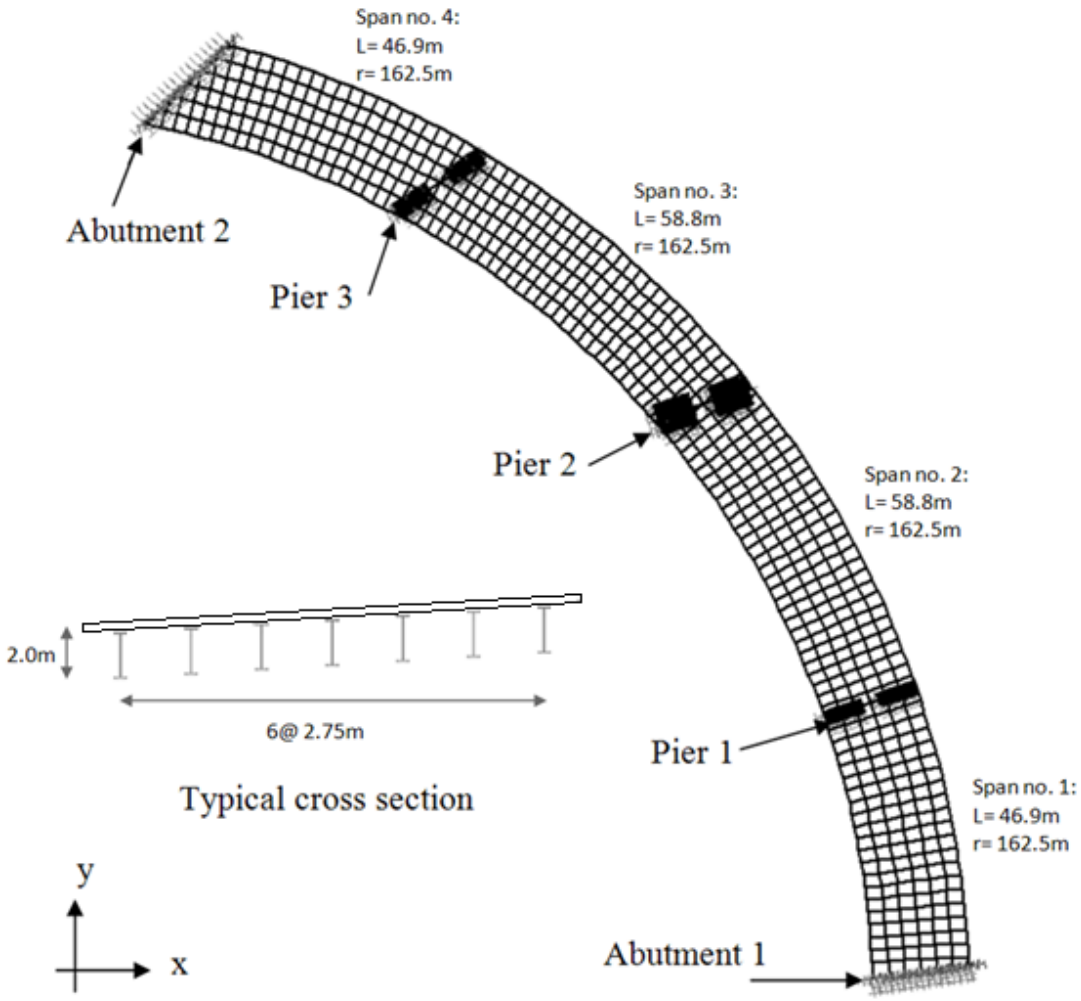

Figure 3-3. General plan and typical cross section of the existing curved bridge

3.4.1.2. Foundation modeling

A cohesive soil profile was observed in boring test results at pile locations. One row steel driven piles at abutments are rigidly connected to steel girders among a reinforced concrete pile bent. To include adjacent soil effects, equivalent stiffness of backfill soil was calculated for each abutment neglecting the effect of the approach slab and thin concrete slop protection in front of each abutment (Buckle et al., 2006). For this reason, 0.24 MPa passive pressure was considered in calculating equivalent soil stiffness at abutments. By using nonlinear gap elements in SAP2000© models, the backfill soil stiffness was imposed during passive displacements only (Fig. 3-4). Also, to include soil structure interaction in 3D models, equivalent stiffness for each H section steel pile was provided at location of each pile in all directions (Fig. 3-4). Stiffness values were subject to change in different models according to uncertainty in soil properties. Passive pressure from adjacent soil at each pier pile cap was also taken into account using line springs along pile cap edges (Buckle et al., 2006). Piles group action at abutments and piers were included due to the actual modeling of pile caps and abutments.

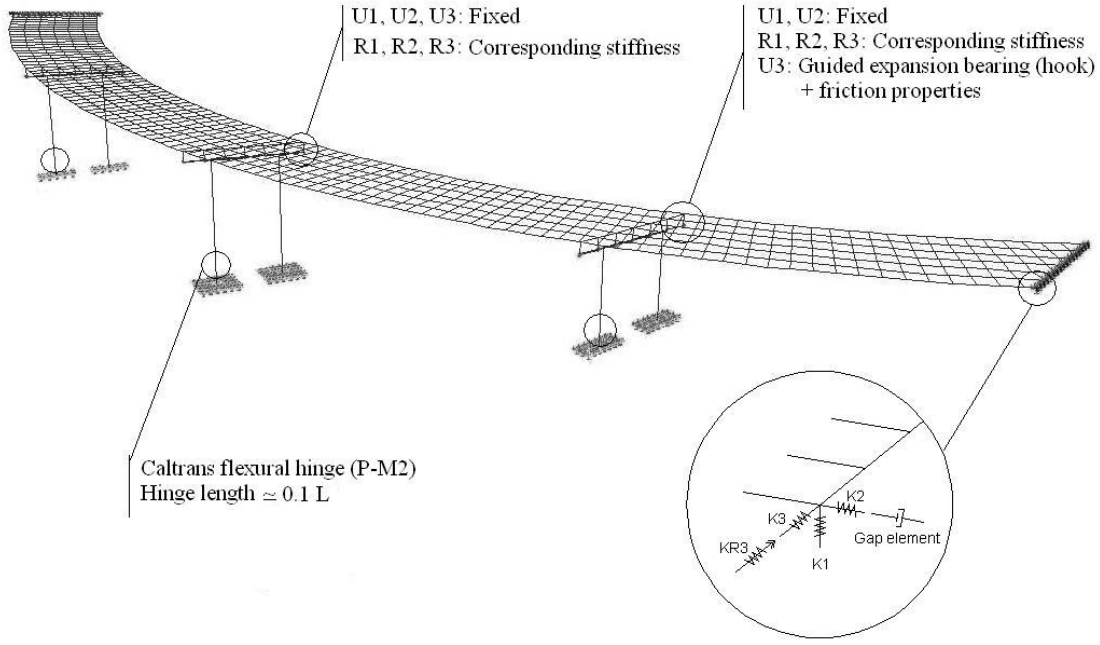

Figure 3-4. SAP2000© model for entire bridge using grid system for superstructure

3.4.1.3. Superstructure, piers and bearings

Based on previous studies on curved bridges (Agrawal & Jain, 2009), using a single linear-elastic frame element for the superstructure might considerably affect analysis results for this type of bridges. In this study, a grid model was used to provide superstructure properties in longitudinal and transverse direction (Fig. 3-4). Cross bracing was provided in almost every 6 meters to supply adequate lateral stiffness for the superstructure according to the bridge construction documents (State of Nebraska, 2005). Considering unlikely damages in bridge superstructure, more precise FE modeling was not determined necessary here. In positive moment areas a composite section with appropriate concrete deck was provided, while in negative moment areas, a reduction in moment of inertia due to the crack propagation in concrete deck was taken into account.

Section properties such as moment of inertia and corresponding stiffness were calculated using actual cross sections in finite element modeling. The superstructure mass was assumed linearly distributed along seven steel girders in grid modeling.

To monitor the bridge superstructure behavior, nonlinear sections (plastic hinges) were considered for each steel composite girder. Un-cracked and cracked sections were placed at mid-spans and at both ends of the girders, respectively. However, expectedly, all nonlinear plastic sections remained linear during horizontal ground motions. In addition, plastic hinges still showed elastic behavior during sample vertical ground motions with relatively high PGA values. Based on different studies summarized in FHWA Manual, the acceleration ratio of vertical to horizontal ground motion is assumed equal to 0.35 for this existing bridge period of vertical vibration (T=1.09 s) (Buckle et al., 2006).

The weight of the superstructure elements and additional dead loads including barriers and wearing surface were uniformly applied to girders. The presence of live load during earthquake was taken into account as one of the random variables in the fragility analysis. For this reason, a uniform static load equivalent to AASHTO LRFD live load models was considered along the steel girders.

Each pier consists of two square reinforced concrete columns. Nonlinear plastic sections (hinges) at lower part of each column were provided with the interaction of axial force and bending moments (Fig. 3-4). Hinge length along each reinforced concrete column was calculated using the following equation (CALTRANS, 2006):

$$L_P = 0.08L + 0.022 f_{ye} d_{bl} \geq 0.044 f_{ye} d_{bl} \quad (3\text{-}5)$$

where L is the column height (mm), f_{ye} is the expected yield stress for reinforcement (MPa), and d_{bl} is the nominal bar diameter of longitudinal reinforcement (mm). It should be noted that all plastic hinge lengths were tightly close to 0.1L as it is suggested for simplified calculations.

Radially fixed bearing devices connect steel girders to the pier cap at Pier 2. These bearings allow limited rotation (R1, R2 and R3) and no transverse movement (U1, U2 and U3). Girders sit on guided expansion bearings, on pier caps 1 and 3. The total nominal movement of guided expansion bearings is equal to 4.5 cm (along the longitudinal bridge direction) according to bridge construction documents. This tolerance was also assumed as a random variable with uniform distribution in fragility analysis. To model the guided bearings, including the provided gap and existing friction, one "hook" and one "friction isolator" element were used at each guided bearing location. Coefficient of friction for guided expansion bearing was considered according to previous studies (Nielson & DesRoches, 2007). The "hook" element in SAP2000© allows a certain amount of free displacement followed by predefined stiffness.

3.4.2. Ground Motions

To evaluate nonlinear behavior of bridge models, 60 ground motions for Mid-American cities were applied in this study (Wen & Wu, 2001). Mentioned ground motions had been generated for three different sites in the area (Memphis TN, St. Louis MO and Carbondale IL).

In each time history analysis, the direction of earthquake excitations was randomly selected using the Latin Hypercube method. Selected ground motions comply with the

target uniform hazard response spectra for each site with 2% and 10% probability of occurrence in 50 years. The coefficient of variation for median response spectra of each group including 10 ground motions is less than 10% compare to the target response spectra at each period.

The uncertainty in magnitude, focal depth, epicentral distance, path attenuation, fault parameters and soil profiles were considered in generated ground motions. Table (3-1) shows the mean Peak Ground Acceleration (PGA) values for each city with different probability of exceeding in 50 years.

Table 3-1: Mean PGA values (g) for 2% and 10% probability of exceeding in 50 years

Exceeding probability	10% in 50 yrs	2% in 50 yrs
Memphis, TN	0.075	0.375
St. Louis, MO	0.106	0.326
Carbondale, IL	0.167	0.505

3.4.3. Probabilistic Modeling

Statistically generated bridge samples were used in probabilistic damage assessment of the bridge structure. For this reason, 60 different bridge models were generated applying various geometry, material properties and load conditions. This sample size, provide 95% confidence level with the confidence interval percentage about 12%. Latin Hypercube method (Eq. 3-7) was used to generate uncorrelated random bridge models. Applying this method facilitates using smaller number of samples with respect to Monte Carlo

simulation technique (Eq. 3-6), while covering the entire sample space (Nowak & Collins, 2000):

$$T_i = \phi^{-1}(R_i) \tag{3-6}$$

$$T_i = \phi^{-1}(\frac{P_i - R_i}{n}) \tag{3-7}$$

In the equations above, R_i is a random number between 0 and 1, ϕ^{-1} is the inverse of the specific cumulative distribution function, P_i is a random unique natural number from 1 to n, and T_i is randomly generated target number. By applying Eq. (3-7), 60 uncorrelated random values were generated for each variable parameter in the bridge structure (Table 3-2).

Table 3-2: Random parameters considered in bridge modeling

Random variable	Distribution	Corresponding parameters		units
direction of ground motions	uniform	min= 0	max= π	rad.
coefficient of variation of the inelastic subgrade modulus (f)	uniform	min= 0.55	max= 1.10	kg/cm3
concrete compressive strength (slab)	normal	μ = 35.85	σ = 4.56	MPa
concrete compressive strength (other)	normal	μ = 33.78	σ = 4.30	MPa
reinforcing steel (Fy)	lognormal	μ = 463.0	V = 0.08	MPa
girders structural steel (Fy)	lognormal	μ = 413.7	V = 0.08	MPa
damping	normal	μ = 0.045	σ = 0.0125	-
expansion bearings coefficient of friction	lognormal	μ = 0.1	V = 0.5	-
expansion bearings gap	uniform	min= 3.17	max= 5.72	cm
dead load/mass factor	normal	μ = 1.05	σ = 0.095	-
live load factor	uniform	min= 0	max= 0.8	-

Variable parameters included ground motion direction, soil properties, damping, dead load/mass factor, live load factor, bearings properties and material properties. These selected parameters act as the most effective terms in the analysis of a bridge structure. Probability distribution type and related statistical parameters for each random variable were selected according to previous studies and bridge construction documents (Padgett & DesRoches, 2009; Nowak & Collins, 2000; State of Nebraska, 2005; Nielson and DesRoches, 2007).

Table (3-2) summarizes considered random variables and corresponding probabilistic parameters. For soil properties and the live load presence factor during earthquake events, uniform distributions were assumed, due to the lack of information in literature.

3.4.4. Modal Analysis

To identify the predominant modes of vibration, a comprehensive modal analysis was completed using SAP2000© software. The finite element model incorporated all components using a grid system for superstructure modeling (Fig. 3-4). The contribution of each mode in dynamic response of structures is indicated with its mass participation ratio r_i:

$$r_i = [\frac{(\{\varphi_i\}^T[M]\{I\})^2}{\{\varphi_i\}^T[M]\{\varphi_i\}}]/M_t \tag{3-8}$$

where $[M]$ is the lumped mass matrix, $\{\phi_i\}$ is the modal shape vector for mode i, and M_t is the total unrestrained mass of the structure (CSI, 1998).

Table 3-3: Predominant modal shape characteristics

No.	Period	UX[a]	UY[a]	UZ[a]	RX[a]	RY[a]	RZ[a]	Eigen value (rad/s)2	Mode shape
1	1.09	0.000	0.000	0.001	0.000	0.000	0.000	33.255	Vertical vibration
2	0.85	0.009	0.004	0.031	0.015	0.023	0.000	54.983	Ver. vibration (sym.)
3	0.77	0.451	0.075	0.032	0.083	0.438	0.023	66.158	Ver. vib. & hor. disp.
4	0.76	0.611	0.153	0.036	0.145	0.561	0.024	68.059	Ver. vib. & hor. disp.
5	0.73	0.678	0.588	0.036	0.556	0.626	0.248	73.320	Horizontal displacement
6	0.65	0.679	0.589	0.068	0.559	0.629	0.250	92.948	Vertical vibration
.									
.									
.									
48	0.12	0.984	0.960	0.715	0.939	0.954	0.955	2910.8	-
112	0.05	0.999	0.999	0.950	0.995	0.994	0.999	14953	-

[a]Mass participation values are cumulative numbers in each global direction (UX, UY, UZ: displacements, RX, RY, RZ: rotations)

To achieve reasonable cumulative mass participation ratios for all degrees of freedom, the first 48 modes were estimated to be sufficient. For the first 48 modes of vibration, the cumulative mass participation ratio for each translational or rotational degree of freedom varies from 94% to 98%, except for the displacement in the vertical direction which reaches to 72% (Table 3-3). By increasing the number of vibration modes to 112, all the mass participation ratios will be greater than 95%. Applying the Eigenvalue method, this single analysis was completed on a bridge sample with the mean values for random parameters.

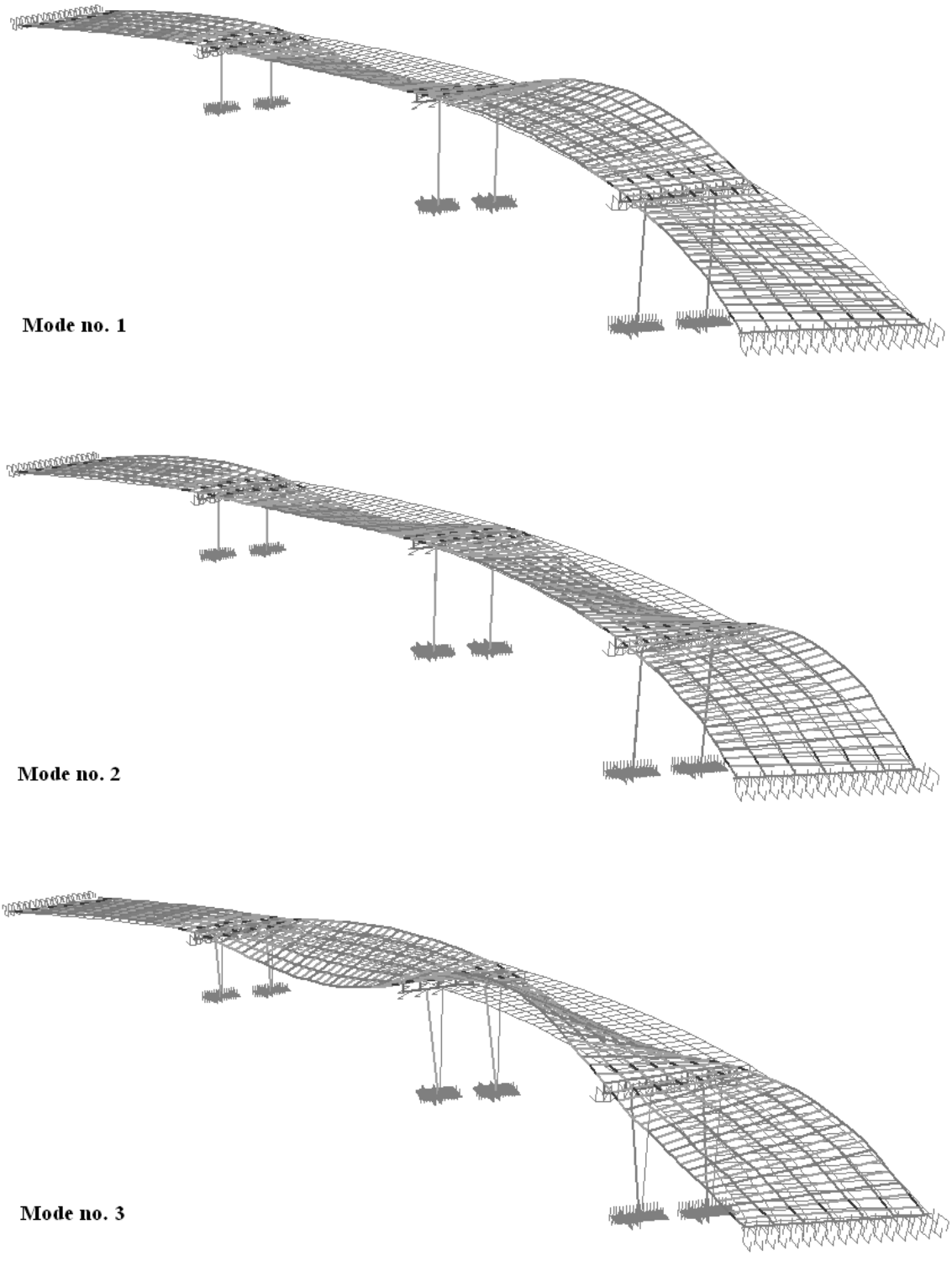

Figure 3-5. Predominant modal shapes

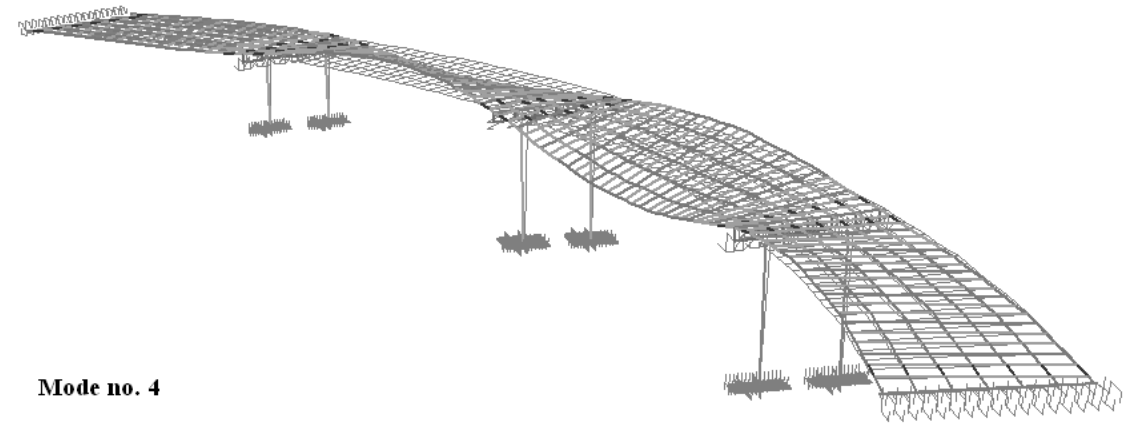

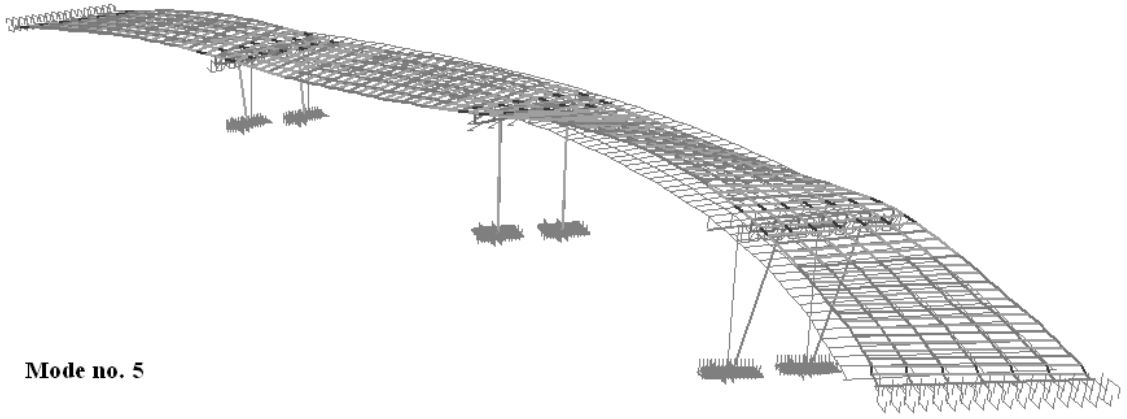

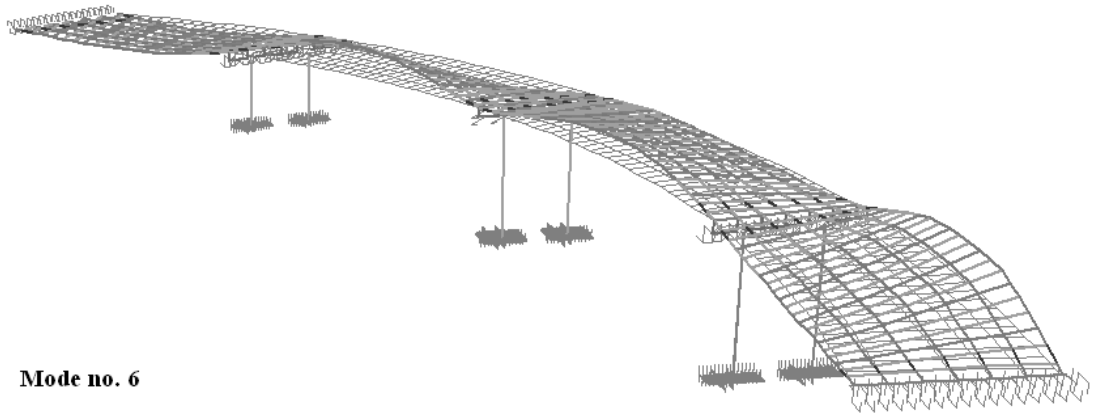

Figure 3-5 (Cont.). Predominant modal shapes

Based on modal analysis results (Fig. 3-5), the first two mode shapes were vertical vibration and swinging of the bridge superstructure due to the existence of long spans and eccentricity. Nevertheless, the bridge superstructure did not show any plastic response against vertical ground motions. The next three predominant modes (3, 4 & 5) declared horizontal movement of the bridge superstructure which causes the most damages in pier columns and abutments. Table (3-3) provides modal characteristics for first 6 modes and cumulative data for 48 modes of vibration.

3.4.1. Fragility Analysis

In order to develop component and system fragility curves, demand and capacity of structural components should be determined. The capacity of monitored bridge components should be expressed for each considered damage state. Based on the accepted methodology in HAZUS (FEMA, 2003), four qualitative damage states – slight, moderate, extensive and complete damages – were assumed to evaluate functionality of bridge components and structure.

The capacity of bridge components can be obtained by using analytical methods or empirical data. Table (3-4) displays selected medians and dispersion capacity values (S_c, β_c) for bridge components at each damage level according to previous studies (Nielson & DesRoches, 2007; Nielson, 2005). The assumed values for steel girders curvature ductility are based on building code recommendations, due to the lack of literature in this area (FEMA, 2003).

Table 3-4: Medians and dispersion capacity values for bridge components at each damage state

Component	Slight		Moderate		Extensive		Complete	
	med	disp	med	disp	med	disp	med	disp
Column curvature ductility (μ_φ)	1.29	0.59	2.10	0.51	3.52	0.64	5.24	0.65
Girders curvature ductility (μ_φ)	1.00	0.60	3.00	0.60	6.00	0.60	8.00	0.60
Abutment-trans (cm)	1.0	1.8	3.78	2.28	7.72	2.16	NA	NA
Abutment-active (cm)	1.0	1.8	3.78	2.28	7.72	2.16	NA	NA
Abutment-passive (cm)	3.7	1.17	14.6	1.17	NA	NA	NA	NA

Figure (3-6) shows Probabilistic Seismic Demand Models (PSDM) for column curvature ductility and active, passive and transverse deformation of abutments. According to analysis results, there was no other significant damage to other bridge components. For example, the bridge superstructure did not experience any plastic deformation during vertical ground motions (even for those with higher PGA values and considering the eccentricity of gravitational loads for the curved bridge plan in vertical excitations). Also, the induced forces in the bearings were less than their elastic capacity.

In Figure (3-6a), maximum curvature ductility of columns is plotted against PGA in a logarithmic scale. The best linear regression equation is chosen as the seismic demand model. Similarly, maximum displacement of abutments in transverse, active and passive directions are plotted to determine PSDM's for each case (Fig. 3-6b to d). Table (3-5) summarizes PSDM parameters for each monitored bridge component. To calculate column curvature ductility, maximum response among six rectangular columns was taken. Also, the maximum displacement in abutments was measured as the bridge response to corresponding ground motion.

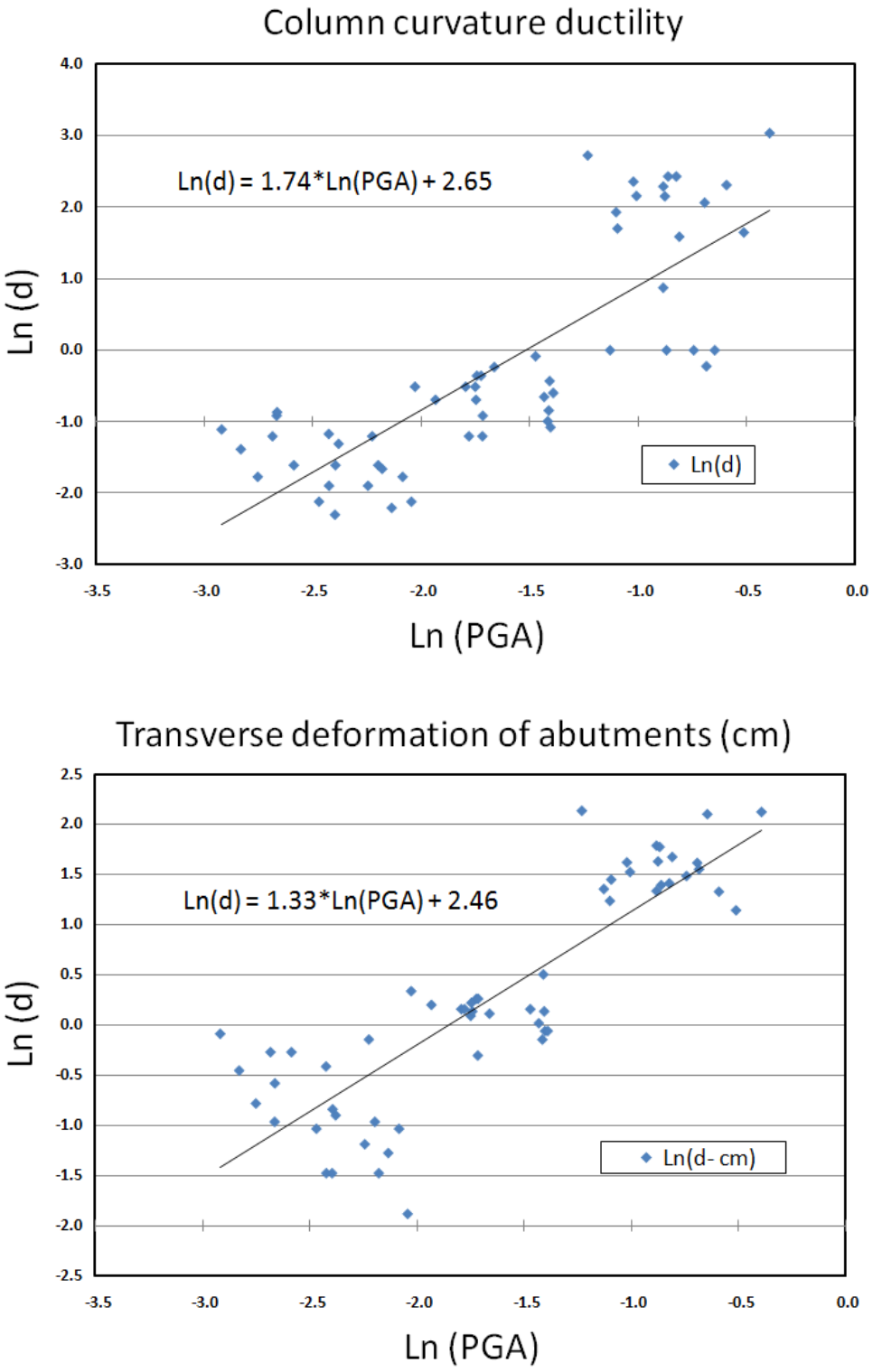

Figure 3-6. Probabilistic seismic demand models: (a) column curvature ductility, (b) transverse deformation of abutments

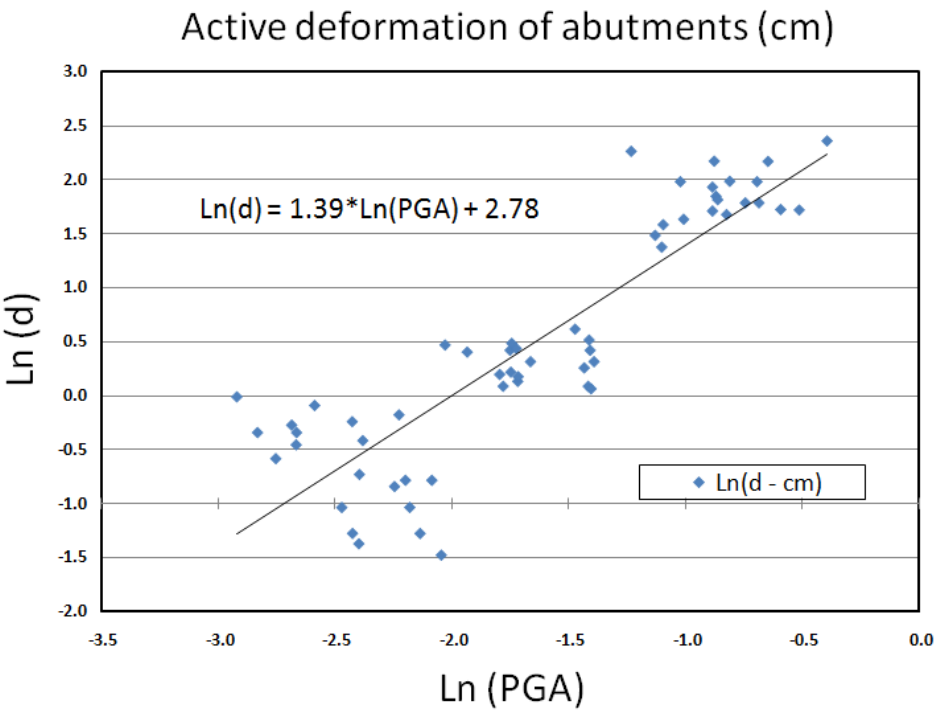

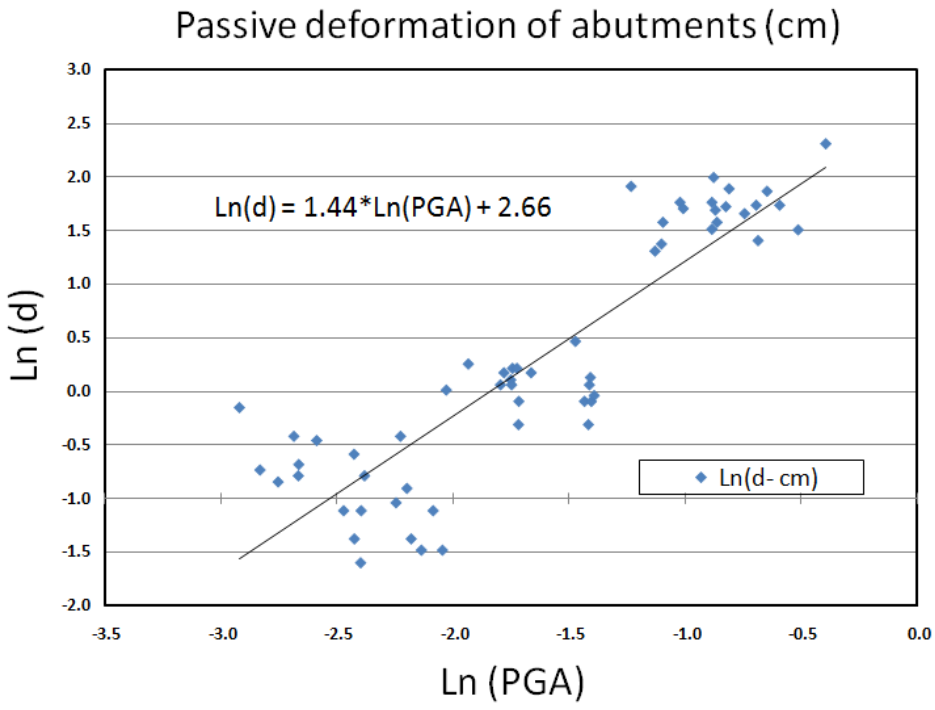

Figure 3-6 (Cont.). Probabilistic seismic demand models: (c) active deformation of abutments, (d) passive deformation of abutments

Table 3-5: Probabilistic seismic demand models (PSDM) for bridge components

Component	Ln(a)	b	β_d *(averaged)*
Column curvature ductility (μ_φ)	2.65	1.74	1.15
Abutment-trans (cm)	2.46	1.33	0.83
Abutment-active (cm)	2.78	1.39	0.84
Abutment-passive (cm)	2.66	1.44	0.85

In some cases, a polynomial function of higher degree (2 or 3) could be a better match for the demand data. However, the regression function needs to have positive slope in a specific domain to be applicable in fragility analysis which was not the case here. In other words, Equation (3-3) as a cumulative distribution function, need to be supplied with increasing values for observing domain. Due to the fact that other regression functions experienced a minimum for observing PGA values, the linear function in Equation (3-2b) ended up being the best choice for developing fragility curves.

By applying PSDM results into Equation (3-3), fragility curves for monitored bridge components was calculated for each considered damage state. Figure (3-7) shows fragility curves for slight, moderate, extensive and complete damage states for different components. It can be concluded that for slight damage (Fig. 3-7a) transverse and active deformation of abutments are the most fragile parts. For higher damage levels, columns turned out to be the most fragile components. Complete damage level is not applicable for abutments due to the fact that any large displacement in abutments cannot be taken as a complete damage.

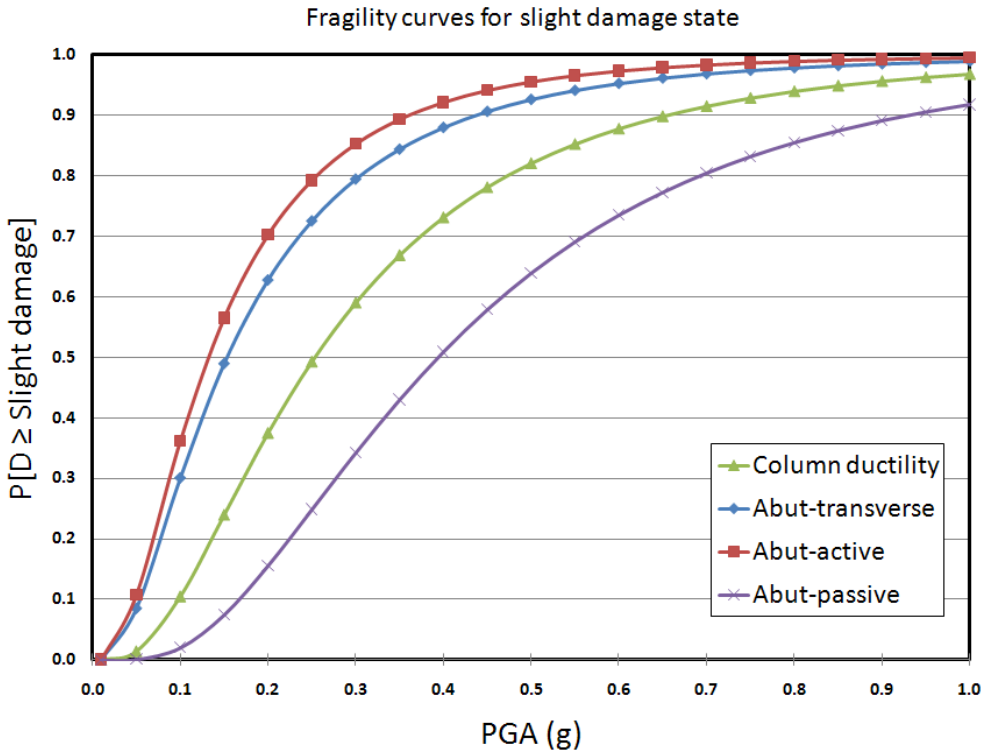

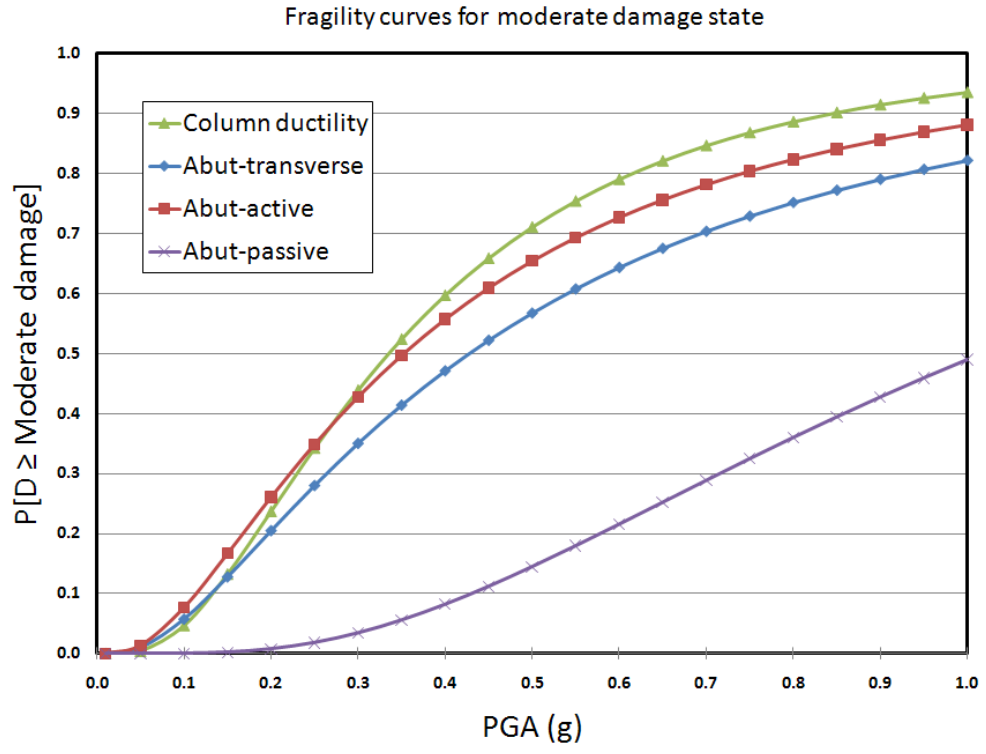

Figure 3-7. Fragility curves for (a) slight, (b) moderate

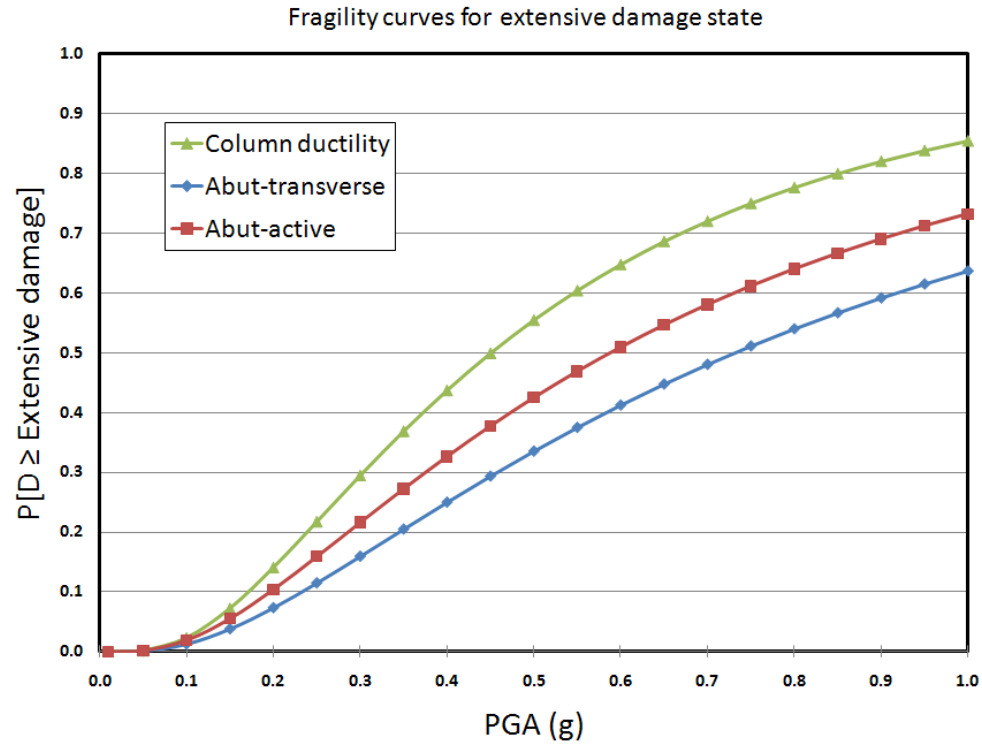

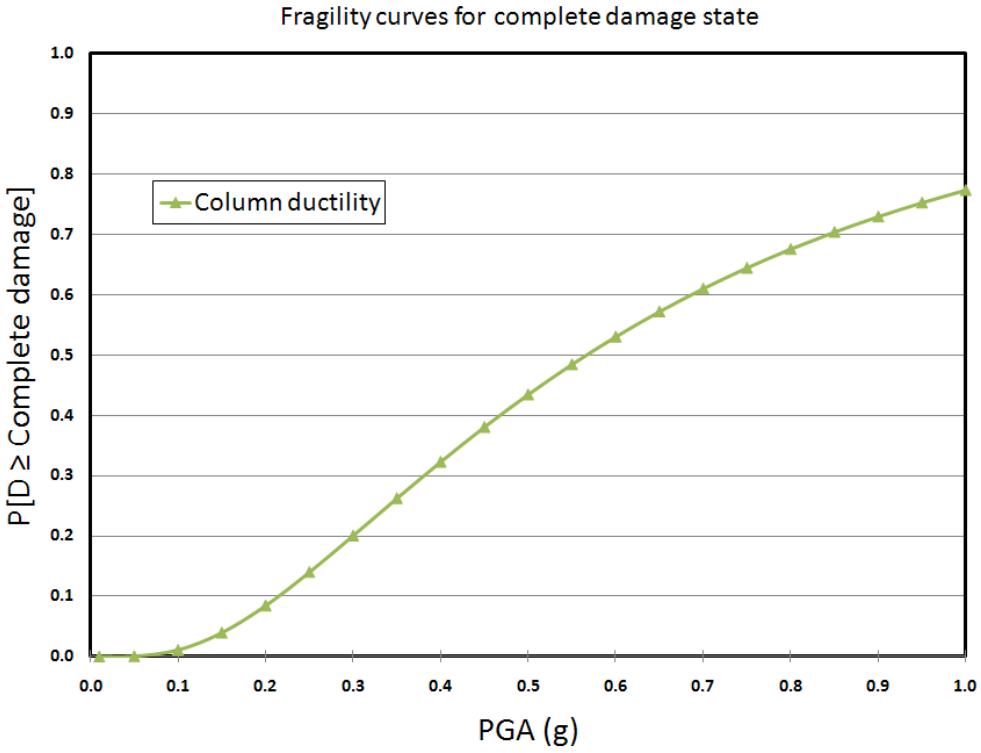

Figure 3-7 (Cont.). Fragility curves for (c) extensive, (d) complete damage state

Median PGA value for each damage level can be considered as the equivalent PGA for 50% probability of failure. For slight damage, the median PGA values for abutment displacement in active and transverse directions are 0.13g and 0.15g, respectively. Also, calculated values for columns and passive displacement of abutments are 0.25g and 0.39g, indicating less vulnerability with respect to other components. For moderate damage level, columns and active displacements in abutments are the most fragile components with 0.33g and 0.35g median PGA's. For higher damages, such as extensive and complete damage, columns are also the most fragile members with 0.45g and 0.57g median PGS values, respectively. Median PGA's for all components facing qualitative damage states are presented in Table (3-6) and Figure (3-8).

Table 3-6: Median PGA values for each damage state (g)

Component	slight	moderate	extensive	complete
Col. curvature ductility (μφ)	0.25	0.33	0.45	0.57
Abut-trans	0.15	0.43	0.73	NA
Abut-active	0.13	0.35	0.59	NA
Abut-passive	0.39	1.00	NA	NA

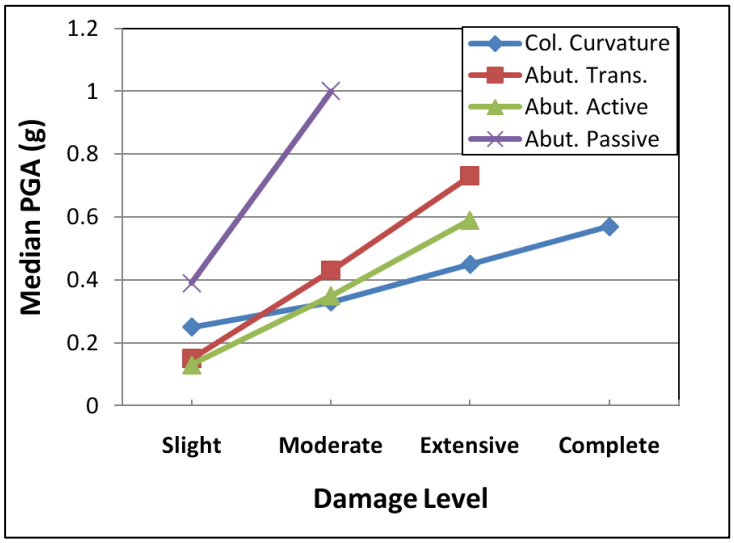

Figure 3-8. Median PGA values for each damage state (g)

3.4.2. System Fragility

Fragility curves for bridge structure, as a series system, can be derived from fragility analysis results for each observed component. In a series system, such as a chain, failure of one component will cause failure of the system. Hence, the probability of failure for a series system ($P_{f\text{-}sys}$) cannot be less than probability of failure for each component ($P_{f\text{-}c}$). This declaration means the bridge function will fail if any of components fails. Thus, the critical component fragility can be taken as the lower bound for bridge system fragility (Eq. 3-9a).

$$P_{f\text{-}sys} \geq \max_{1 \leq i \leq n} [(P_{f\text{-}c})_i] \tag{3-9a}$$

where $(P_{f\text{-}c})_i$ is the probability of failure for the i^{th} component (Nowak & Collins, 2000).

In a system with perfectly correlated components, the lower bound will be the exact system fragility curve. However, by decreasing the correlation coefficient between each

pair of elements, the probability of failure for the system will be increased up to the upper bound in Equation (3-9b).

$$P_{f\text{-}sys} \leq 1\text{-}\Pi_{i=1}^{n}\,[1\text{-}(P_{f\text{-}c})_i] \qquad (3\text{-}9b)$$

This conservative upper bound is usually taken as the fragility curve for the total system. Although, it has been shown that based on more realistic correlation coefficients, the actual system fragility is about 10% less than the upper bound (Nielson & DesRoches, 2007). Figure (3-9) shows the upper and lower bounds of bridge fragility curves for different damage states. In this bridge, for complete damage state, system fragility can be taken equal to column curvature fragility, due to the fact that this element was the only applicable component for this limit state, and any large displacement in abutments was not considered as a complete damage.

Table (3-7) provides median PGA values for system fragility curves. Similar to component fragility curves, PGA values corresponding to 50% probability of failure were taken as the medians. As mentioned earlier, the upper bound can be taken as the actual fragility curve for bridge system with about 10% overestimation.

Table 3-7: Medians PGA values for bridge system fragility curves (g)

Damage level	slight	moderate	extensive	complete
Lower bound	0.13	0.34	0.45	0.57
Upper bound	0.09	0.19	0.29	0.57

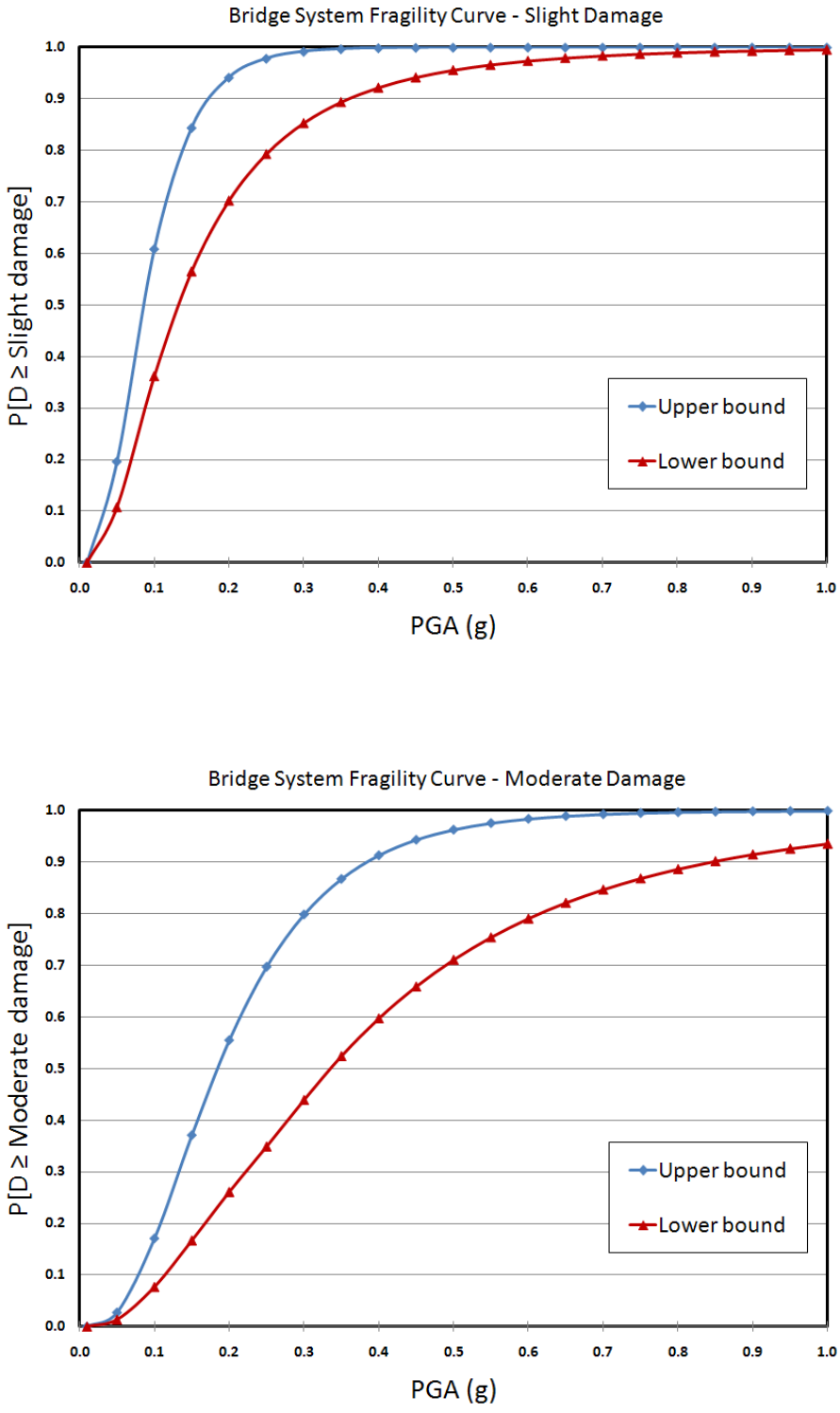

Figure 3-9. Upper and lower bounds for bridge system fragility curves, (a) slight damage level and (b) moderate damage level

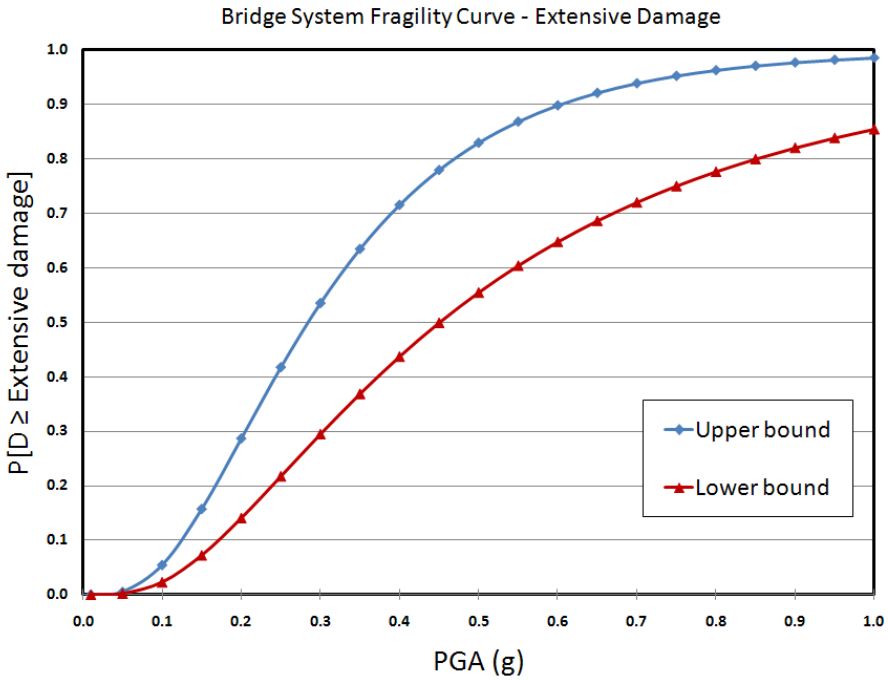

Figure 3-9 (Cont.). Upper and lower bounds for bridge system fragility curves (c) extensive damage level

To compare the fragility of the examined curved bridge, with 162m horizontal curvature, with the fragility of straight bridges with the same structural system, the results of the analysis of typical multi-span straight bridges in the Central and Southern United States (Choi & Jeon, 2003), with continuous steel girders are shown in Table (3-8). Higher median PGAs for straight bridges mean they might experience the same amount of damage during stronger earthquakes. Determined median PGA values for slight, moderate, extensive and complete damage states for the examined bridge are 2.33, 1.84, 1.69 and 1.19 times smaller than the corresponding values calculated for the straight bridges. This fact highlights the priority and need of more attention to curved bridges for retrofitting purposes.

Table 3-8: Medians PGA values for the examined curved bridge and straight bridges (g)

Damage Level	Slight	Moderate	Extensive	Complete
Examined Curved Bridge	0.09	0.19	0.29	0.57
Straight Bridges	0.21	0.35	0.49	0.68

3.5. Conclusions

In this chapter, seismic vulnerability of an existing curved bridge structure was evaluated using fragility analysis. This case study provides a step-by-step procedure for fragility analysis of multispan horizontally curved bridges focusing on major issues for curved bridge structures. Due to the fact that seismic response of curved bridges relies on multiple parameters assembling the stiffness matrix -including radius of horizontal curve, skew angles at abutments and piers, superstructure stiffness, pier heights, bearings, materials, etc.- and also the direction of possible strong earthquake excitations, it is suggested to evaluate each specific bridge rather than using general recommendations for curved bridges. A seismic hazard analysis for curved bridge site location can effectively improve the accuracy of fragility analysis results. By identifying possible earthquake sources, magnitudes and direction, more accurate probabilistic distribution can be selected for ground motions. For instance, current uniform distribution for earthquake directions (0 to π radians) could be replaced by a normal distribution function using the specified direction as the mean value.

Based on the nonlinear analysis results for vertical ground motions, the superstructure remained elastic with no major damage. However, possible live load presence on bridge deck during an earthquake, will affect the response of the superstructure. Future studies

on suggesting a percentage of maximum live load, to be considered during an earthquake event, can increase the consistency of analysis results.

The obtained fragility curves declared that the transverse and active deformation of abutments are the most vulnerable issues for slight damage state, while for higher damage levels plastic rotation at the lower part of columns is the critical possible damage. More likely, the repair or replacement of columns is considerably more expensive than repairing abutments. Hence, using isolation bearings or other energy dissipating devices could effectively reduce the possibility of plastic damage in columns and associated repair cost for the bridge structure.

Lastly, median PGA values which cause slight, moderate, extensive and complete damages (upper bounds) were determined equal to 0.09g, 0.19g, 0.29g and 0.57g, respectively. Compared to the measured fragility of typical straight multispan continuous bridges in the Central and Southern United States by Choi and Jeon (2003), with the median PGA values for 4 damage levels equal to 0.21g, 0.35g, 0.49g and 0.68g, this examined curved bridge is considerable more fragile. By applying calculated system fragility curves for each damage level and possibility of the earthquake intensity in the area, expected damage level and accompanying maintenance costs for each time period can be estimated for this examined bridge structure.

Chapter 4

Part II: Reliability of Steel Axial Members in Bridges

4.1. Vehicular Impact on Different Types of Bridges

Dynamic effects of passing vehicles on highway bridges should be considered in addition to their static load. This effect can be categorized in two parts: local hammer effect which is caused by vehicle wheels beating discontinuous surface areas such as expansion joints; and the global vibration effects caused by the motion of vehicles over bridge superstructure (Duan et al., 2000). The global vibration has a broader impact and affects superstructure components. In most cases, this dynamic effect magnifies stresses in superstructure element which need to be accounted.

Each bridge system responds differently to dynamic excitations due to the passing traffic loads. Several numerical and experimental studies have been done to investigate the most precise dynamic load factor for bridge systems such as concrete I-girders (Li et al., 2008), steel box girders (Samaan et al., 2007), arch bridges (Huang, 2012; Huang, 2005), suspension bridges (Ren et al., 2004), culverts (Chen & Harik, 2012) and truss bridges (Hag-Elsafi et al., 2012; Laman et al., 1999). However, mentioned studies mostly rely on studying one single bridge, which cannot be simply expanded for all cases.

To develop design criteria and provide adequate dynamic load factors for each system, more comprehensive data should be collected and used. Nowak (1999) concluded a probabilistic based research to develop new load and resistance factors for AASHTO LRFD bridge design code. Collected experimental data is presented and explained in detail for each essential load or resistance parameter. Impact factor distribution functions

for steel and concrete I-girder bridges were applied in calculating new load factors for the AASHTO code. However, the response of truss bridges was not considered in the code recalibration due to the less number of truss bridges with respect to other types of bridges.

4.2. Axial Members in Steel Truss Bridges

Compare to other superstructure load carrying systems, steel truss bridge is not a dominant design and relatively less experimental data is available for this bridge system (Kwon et al., 2011). Billing (1984) has studied dynamic response of different types of bridges, including steel truss bridges and proposed the cumulative distribution function of the dynamic load factor (DLF) for each bridge system. His study shows relatively high coefficient of variation for DLFs in truss bridges. This fact declares less uncertainty in predicting design forces for axial members in truss bridges.

In order to evaluate the adequacy of current design criteria in the United States for axial members, a reliability analysis has been done using latest available load and resistance data. Latest AASHTO LRFD bridge design specifications (AASHTO, 2007) is examined through a massive numerical study for both tension and compression design equation.

4.3. Recalibration of the Current US Design Criteria for Axial Members

Reliability based structural design insures a uniformly designed structure, in terms of safety. By considering an adequate reliability index (or probability of failure) for

different parts of a structure, a reasonable balance between cost and safety of the structure can be achieved.

In this chapter, the reliability of steel tension and compression members designed with AASHTO LRFD bridge design specifications (AASHTO, 2007) is evaluated. These members are prevalent in different types of truss or arch bridges. Various conditions such as redundancy, ductility and importance of the bridge are taken into account by changing load modification factor, η. To include the effect of the span length, a variable ratio of dead load to total load is considered. Current load factors in AASHTO LRFD code are accepted due to their verification in a comprehensive study for reliability of girder-type bridges. Furthermore, load and resistance distribution models are chosen based on the latest existing experimental data.

4.3.1. Background

Providing a reasonable balance between cost and safety of a structure has always been the major concern in developing design codes and specifications. A conservative design will enhance structural safety along with increasing cost of the construction. By converting all significant terms to an equivalent cost value including failure of the structure -product of the probability of failure and damage cost due to the failure-, the final cost should be minimized to obtain the most optimum design.

The re-calibration of existing design criteria including reliability-based ones is unavoidable due to numerous technical improvements and changes in the cost factors. As an example, the application of fast computers in numerical calculations may increase the precision of analysis results and reduce human errors in design procedure. Also, material

quality enhancement can reduce structural component imperfection and subsequently probability of failure. Moreover, load characteristics may change with time for each specific structure. For instance, more restrictive traffic rules may reduce the probability of overweight trucks passing on bridges. In fact, the latest dependable experimental data for both load and resistant parameters should be considered for any re-evaluation of the design criteria. However, simplification of design equations offers more conservative criteria in most cases.

A summary of various reliability studies, utilized as the backbone of the LRFD Bridge Design Code (AASHTO 2007), is provided in NCHRP-368 (Nowak 1999). Examining four different types of bridges with reinforced concrete girders, prestressed concrete girders, and composite and non-composite steel girders, as the most typical solutions in designing bridge structures, load and resistant factors were recalibrated to current factors. However, other types of bridge components such as axial members in trusses were not covered in the recalibration procedure (Mohseni & Norton, 2011).

Bennett and Najem-Clarke (1987) evaluated reliability of bolted steel tension members, designed according to AISC LRFD steel design code. Considering two failure modes; yielding of the gross section and fracture of the net section, the reliability index for each mode and combined system was derived, based on the correlation coefficient between yielding strength, F_y, and fracture strength, F_u. It was shown that for different levels of safety for yielding and fracture modes, the effect of correlation between F_y and F_u is negligible. This fact is particularly true when the practical target reliability index for yielding and fracture is taken equal to 3.0 and 4.5, respectively. Load models applied in their study were based on the latest data at that time gathered by Ellinwood et al. (1980).

Resistance models and correlation concern were characterized in a different study by Najem-Clarke (1985).

Schmidt and Bartlett (2002-a) have collected statistical data for tension and compression members for four most popular sections. Collected date regarding geometry and material strength for wide flange (W), welded wide flange (WWF) and hollow structural sections (HSS-class C and H) declared slight changes in resistance parameters compare to previous data from 1980's. In some cases new test results disclosed higher coefficient of variation for resistance of steel tension members. Considerable quantity of new collected data was based on experimental evaluation of steel sections produced in 1999 and 2000 by major suppliers to the USA and Canadian market. In a companion paper, Schmidt and Bartlett (2002-b) utilized mentioned data to re-calibrate the resistance factors in the 1995 National Building Code of Canada. Based on available experimental data, most resistance parameters including geometry, material and discretization factors are proposed in their study. However, professional factors for resistance of axially loaded steel members were chosen from values reported by Chernenko and Kennedy (1991) and Kennedy and Gad Aly (1980).

The objective of this chapter is re-calibrating steel tension and compression members design criteria in current AASHTO LRFD bridge design code based on the latest applicable load and resistance models. As the fundamentals of reliability evaluation, approaching a uniform reliability close to target level was pursued in this study. Applied load and resistance models and reliability analysis results are presented in following sections. Finally, suggested modifications based on analysis results are discussed thoroughly.

4.3.2. Load Models

Most important applying loads on highway bridges are dead load, live load (including dynamic effect), wind, earthquake, temperature, etc. In most cases, a combination of dead and live load governs design of a bridge superstructure. Clearly, each load component should be considered as a random variable due to the uncertainty in the actual amount of each load.

In this study, latest load models based on existing statistical data are used. A summary of collected data and observations is provided in Calibration of LRFD Bridge Design Code – NCHRP 368 (Nowak 1999). It should be noted that current load factors in AASHTO Bridge Design Code, are based on a comprehensive reliability study for design of girder-type bridges as the most common bridge system. Hence, it is preferred to use these load factors for all types of bridges to keep an acceptable simplicity in design code. Table (4-1) shows two load combinations, offered for maximum dead and live loads.

Table 4-1. Load combinations and load factors (AASHTO 2007)

Limit state	DC	DW	LL	IM
Strength I	1.25	1.50	1.75	1.75
Strength IV	1.50	1.50	-	-

DC: components dead load, DW: wearing surface dead load, LL: vehicular live load, and IM: vehicular dynamic load allowance

Strength I limit state presents basic load combination related to the normal vehicular use of the bridge, while Strength IV limit state is applicable for very high dead load to live load ratios (r >7). Values of r may represent the span length in bridge structures in

such a way that higher and lower r values stand for longer and shorter spans, respectively. By defining *r*' as the dead load to total load ratio (Eq. 4-1), Strength I limit state is applicable for $r' \leq 0.875$ and Strength IV limit state should be taken for $r' > 0.875$. In fact, a practical range of *r'* values (0.2-0.8) covers most bridges. Consequently, in calculation of reliability indices, the main focus should be on this range.

$$r' = \frac{DL + DW}{DL + DW + IM} \tag{4-1}$$

According to existing statistical data (Nowak 1999), most suitable distribution functions and their related random parameters has been taken for each load component (Table 4-2).

Table 4-2. Load models random parameters

	DC-Concrete	DC-Steel	DW	LL+IM (trucks)	LL
Distribution function	normal	normal	normal	lognormal	lognormal
Bias factor (δ)	1.05	1.03	1.40	1.40	1.27
Coefficient. of variation (V)	0.10	0.08	0.25	0.18	0.12

Based on the cumulative distribution functions for recorded dynamic load factors, IM, for through trusses, deck trusses and rigid steel frames, the average Coefficient of Variation (COV) is larger than calculated COV for steel or concrete girders (V=1.125 vs. V= 0.71 for steel girders and V= 0.56 for P/C AASHTO concrete girders). However, mentioned values reflect the impact of single trucks passing over examined bridges. For at least two lanes loaded at the same time, the bias factor and COV will be reduced. Also, according to the Turkstra's law (Nowak & Collins, 2000), maximum live loads should

not be taken with the maximum recorded impact values simultaneously. Hence, for the heavy trucks and their corresponding impact, combined values are taken.

4.3.3. Resistance Models

The actual resistance, R, is defined as the product of nominal resistance, R_n, and the factors considering the uncertainty in geometry, G, material, M, model error, P, and discretization factor, d. Thus, the mathematical model of resistance is of the form:

$$R = R_n GMPd \tag{4-2}$$

Adding discretization factor to conventional resistance model is due to limited number of available sections with discrete properties. Hence, by choosing the next available section for required section properties, this unavoidable overdesign factor conservatively affects the reliability of designed element. Assuming negligible correlation between mentioned terms in Equation (4-2), the resistance, R, follows a lognormal distribution with bias factor, δ_R, and coefficient of variation, V_R, as shown by Equations (4-3) and (4-4):

$$\delta_R = \delta_G \delta_M \delta_P \delta_d \tag{4-3}$$

$$V_R = \sqrt{(V_G{}^2 + V_M{}^2 + V_P{}^2 + V_d{}^2} \tag{4-4}$$

4.3.3.1. Tension

Applying new collected data, Schmidt and Bartlett (2002-b) utilized the aforementioned model to develop resistance statistical parameters for rolled wide flange (W), welded

wide flange (WWF) and hollow structural sections (HSS-class H and C). Table (4-3) shows their suggested resistance parameters for steel tension members for both yielding and fracture failure modes. As it is mentioned earlier, these parameters are based on collected data from thousands of tested steel products made by major suppliers in North-America.

Table 4-3. Tensile resistance statistical parameters

Steel section	Yielding [a]		Fracture [a]	
	δ_R	V_R	δ_R	V_R
WWF	1.18	0.070	1.28	0.077
Rolled W	1.09	0.081	1.19	0.080
HSS-C	1.36	0.103	1.20	0.088
HSS-H	1.32	0.094	1.24	0.084

[a] For tested steel equivalent to M270/A702 Grade 50 (F_y=345 MPa, F_u=450 MPa)

According to AASHTO LRFD Bridge Design Code (AASHTO 2007), the factored tensile resistance, P_r, shall be taken as the smallest value of the yield and fracture resistance of the section:

$$P_r = \varphi_y F_y A_g \tag{4-5a}$$

$$P_r = \varphi_u F_u A_n U \tag{4-5b}$$

where F_y and F_u are the yield and fracture strength of steel, A_g and A_n are the gross and net cross sectional area of the member, and U is the reduction factor due to the shear lag effect in connections. Resistance factors, φ_y and φ_u, assure a safer design by considering uncertainty of the predicted yield and fracture resistance of the steel member. Clearly, shear lag reduction factor, U, is the key parameter in determining governing design

equation. In current analysis, by choosing $(A_nU)/A_g$ ratio equal to 0.913, both design equations are involved in design of the steel tension members.

4.3.3.2. Compression

Using AASHTO LRFD Bridge Design Code (AASHTO 2007), the factored compressive resistance, P_r, should be taken as:

$$P_r = \varphi_c 0.66^{\lambda} F_Y A_S \rightarrow \lambda \leq 2.25 \quad (4\text{-}6a)$$

$$P_r = \varphi_c \frac{0.88 F_Y A_S}{\lambda} \rightarrow \lambda \succ 2.25 \quad (4\text{-}6b)$$

in which φ_c is the resistance factor for compression. The value of λ is expressed as follow:

$$\lambda = \left[\frac{Kl}{r_s \pi}\right]^2 \frac{F_Y}{E} \quad (4\text{-}7)$$

where K represents the effective length factor, l is the unbraced length of the member, r_s is radius of gyration about the plane of buckling, and E is the modulus of elasticity.

Table 4-4. Compression resistance statistical parameters

Section	A_s		r_s		D		F_y [a]		E [a]	
	δ	V	δ	V	δ	V	δ	V	δ	V
WWF	1.02	0.012	1.00	0.005	1.03	0.023	1.105	0.056	1.038	0.026
Rolled W	1.01	0.031	1.00	0.016	1.04	0.033	1.030	0.063	1.036	0.045
HSS-C	0.97	0.014	1.00	0.005	1.04	0.033	1.350	0.084	1.036	0.045
HSS-H	0.97	0.014	1.00	0.005	1.04	0.033	1.310	0.083	1.036	0.045

[a] For tested steel equivalent to M270/A702 Grade 50 (F_y=345 MPa, F_u=450 MPa)

Table (4-4) shows the latest resistance parameters for steel sections suggested by Schmidt and Bartlett (2002-b). The statistical parameters were obtained for different sections including Rolled W, WWF, HSS-C and HSS-H sections.

As mentioned before, an important factor contributing to the reliability analysis is the model error (also known as professional factor). This factor includes the uncertainty of analysis methods and proposed design equations. Table (4-5) presents the professional factors for various λ values calculated and normalized for AASHTO criteria, based on the study by Kennedy and Gad Aly (1980). The λ values in this table were chosen as to cover the entire acceptable range of slenderness for compression members.

Table 4-5. Professional factors

λ	WWF		W		HSS-C		HSS-H	
	δ	V	δ	V	Δ	V	δ	V
0.00	0.995	0.050	0.995	0.050	0.932	0.040	0.932	0.040
0.04	1.004	0.051	1.013	0.052	0.963	0.040	0.963	0.040
0.16	1.023	0.055	1.049	0.060	0.983	0.040	0.983	0.040
0.36	1.002	0.056	1.074	0.083	0.996	0.040	0.996	0.040
0.64	0.999	0.060	1.107	0.112	1.011	0.040	1.011	0.040
1.00	1.047	0.070	1.182	0.122	1.042	0.040	1.042	0.040
1.44	1.162	0.077	1.279	0.114	1.107	0.040	1.107	0.040
1.96	1.171	0.073	1.213	0.098	1.102	0.040	1.102	0.040
2.56	1.101	0.069	1.126	0.081	1.035	0.040	1.035	0.040
3.24	0.992	0.068	1.039	0.075	0.974	0.040	0.974	0.040
4.00	0.951	0.065	0.991	0.072	0.928	0.040	0.928	0.040

4.3.4. Reliability Analysis

Load and resistance factor design (LRFD) is capable of including uncertainty of both load and resistance using different factors. Once all the statistical parameters are

determined, the limit state function is defined as the difference between resistance and applying loads (Eq. 4-8). It should be noted that strength limit state function reflects the loss of the load carring capacity of structural members. Taking R and Q as the capacity of the member and applying loads, the limit state function, g, can be defined as:

$$g = R - Q \tag{4-8}$$

If $g>0$, the member is in the safe margin. This means that the capacity is greater than the load effect. In contrast, if $g<0$, the member fails. The probability of occurence of this event is called *probability of failure* (P_f).

In the current study, Monte Carlo simulation technique was used to evaluate the reliability of axially loaded steel members (Nowak 2000). This technique can be applied in most cases including those without a closed form solution. In this technique, all parameters in the limit state function are generated randomly considering their statistical parameters and distribution functions. Next, the value of the limit state function will be calcualetd to observe possible failure in the designed member. The process repeats until a number of failures occur. The accuracy of the Monte Carlo technique increases by increasing the number of cycles in the procedure. In this study, the results are based on 100 failures to obtain sufficiently smooth curves. The probability of failure and corresponding reliability index are estimated as:

$$P_f = N_f / N \tag{4-9}$$

$$\beta = \varphi^{-1}(-P_f) \tag{4-10}$$

where P_f expresses the probability of failure, N_f is the number of failures, and N is the total number of simulatios. Also, β represents the reliability index, and φ^{-1} is the standard normal inverse function. Higher values for β indicate lower probability of failure and therefore higher safety level for designed members.

To achieve the optimum safety level, or the optimum reliability index, code parameters including load and resistance factors should be adjusted (Ditleysen & Madsen, 2005). The ideal condition is having a uniform reliability index for different conditions and as close to *target reliability*, β_T, as possible. This target value will be applicable for the basic load modification factor, $\eta = 1.0$. According to AASHTO LRFD specifications (AASHTO 2007), to adjust the safety level for different bridges -based on redundancy, ductility and importance of the bridge- the total factored load in each limit state should be multiplied by calculated η. Higher and lower values of η are expected to decrease and increase the reliability of designed structure, respectively.

4.3.4.1. Tension members

For yielding mode, where the failure is specifying a ductile behavior, a minimum reliability index equal to 3.0 can be adequate. However, a higher target reliability should be taken for fracture mode due to the undesirable brittle failure. Considering target reliability index equal to 4.5 maintains the probability of fracture failure securely low enough.

Figure (4-1) shows the reliability analysis results for yielding equation in current AASHTO criteria. In presented diagrams, the horizontal axis shows the dead load to total load ratios, *r'*, and the vertical axis declares the calculated reliability index, β, for the

specific section and different load modification factors, η. For all sections, the applicable range of loading ratio is considered from 0.2 to 0.8. Lower and higher values correspond to too short and too long spans, respectively, with limited applications. Hence, the reliability analysis and any possible justification should be based on calculated values for this range.

Rolled W sections with the lowest resistance bias factor (Table 4-3) experience the least reliability indices. For all four monitored sections, reliability indices in dominant *r'* range (0.2-0.8) are fairly greater than 3.0. It should be noted that the reliability curves for $\eta=1.0$ should be compared with the target value. Minimum reliabilities are observed for Rolled W sections with β equal to 3.72. For HSS-C and HSS-H sections, reliability indices are even greater than 4.8.

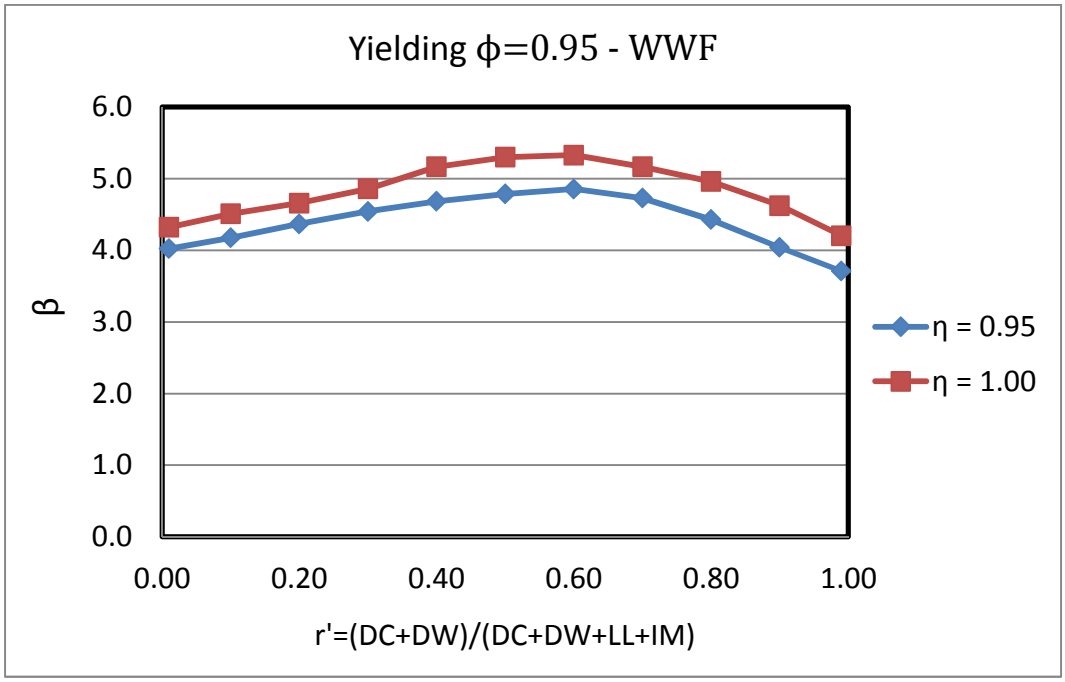

Figure 4-1a. Reliability curves for yielding of steel tension members using current AASHTO criteria: WWF sections

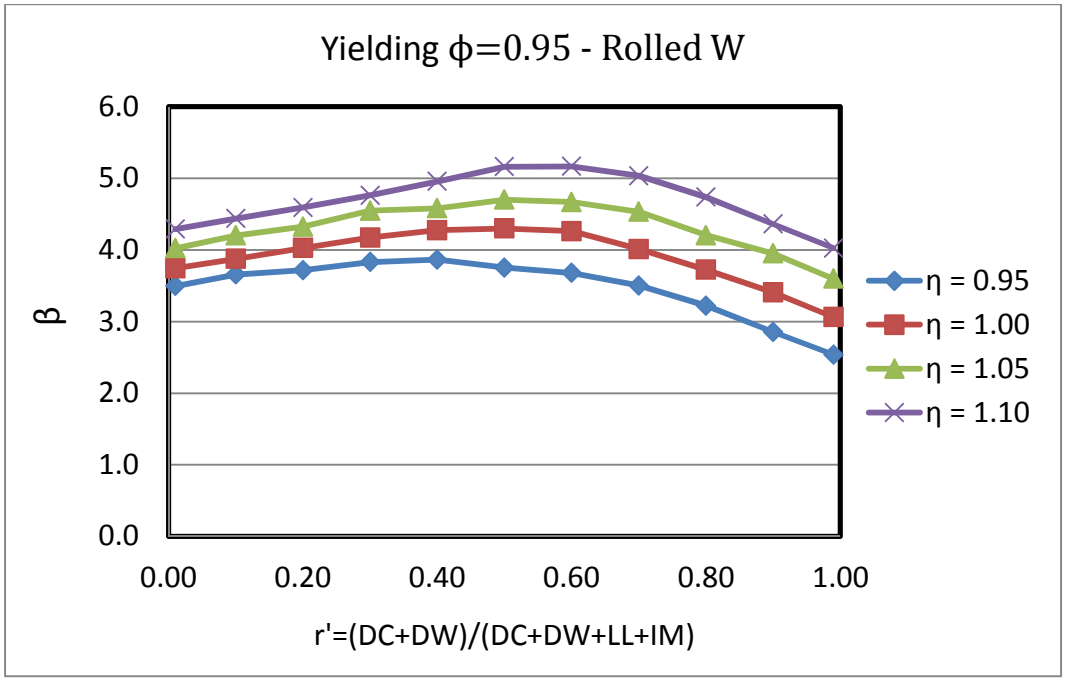

Figure 4-1b. Reliability curves for yielding of steel tension members using current AASHTO criteria: Rolled W sections

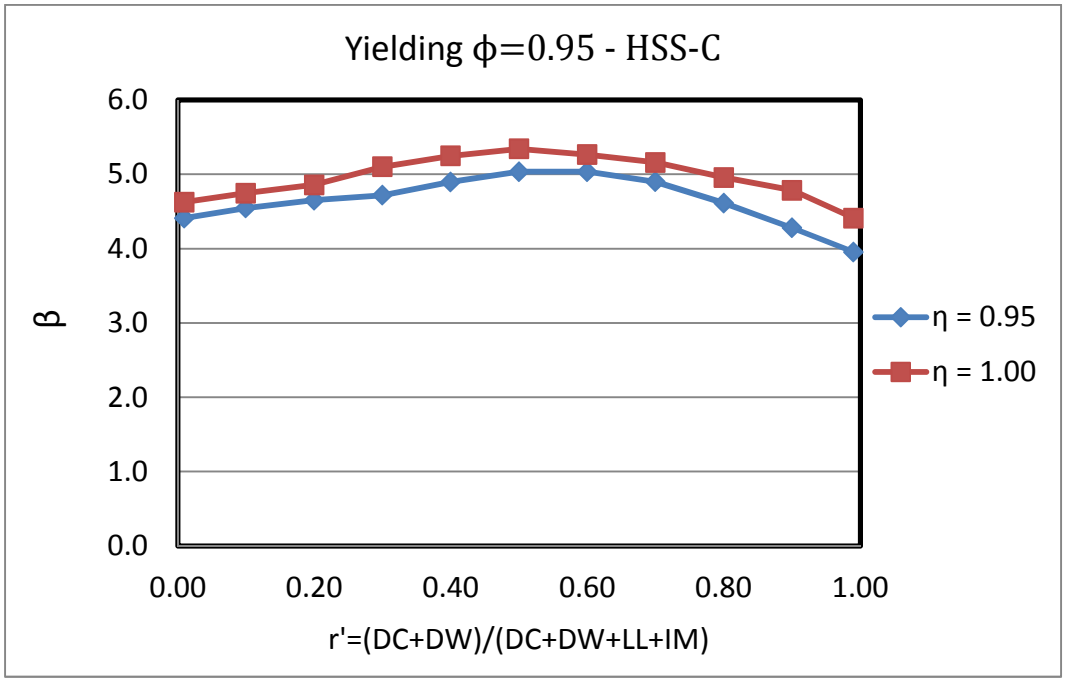

Figure 4-1c. Reliability curves for yielding of steel tension members using current AASHTO criteria: HSS-C sections

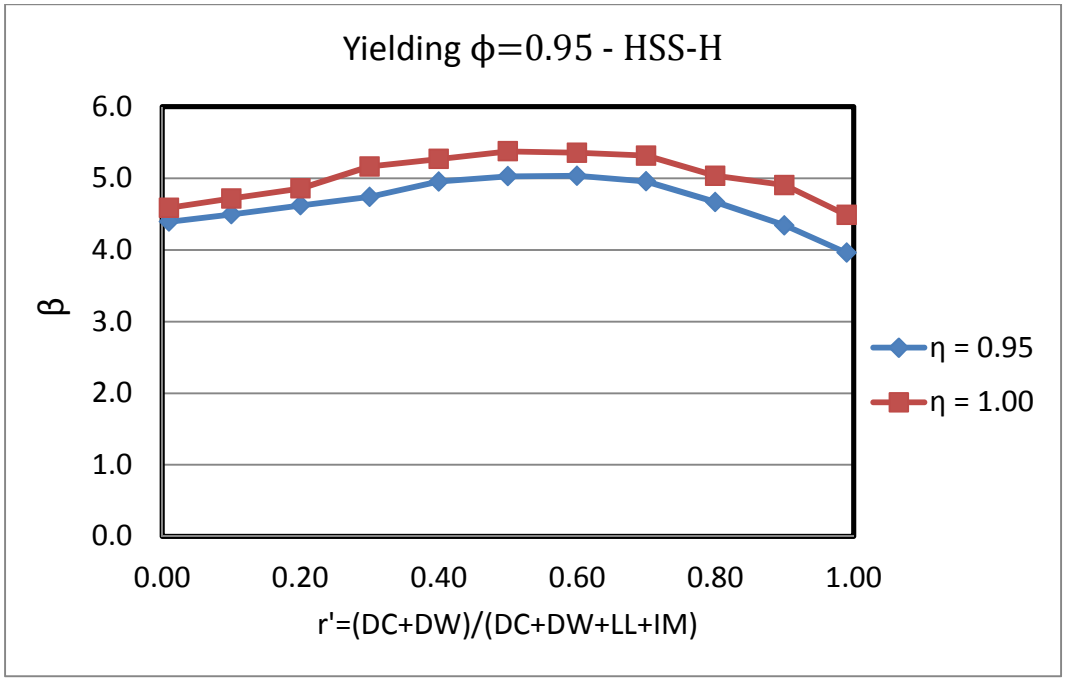

Figure 4-1d. Reliability curves for yielding of steel tension members using current AASHTO criteria: HSS-H sections

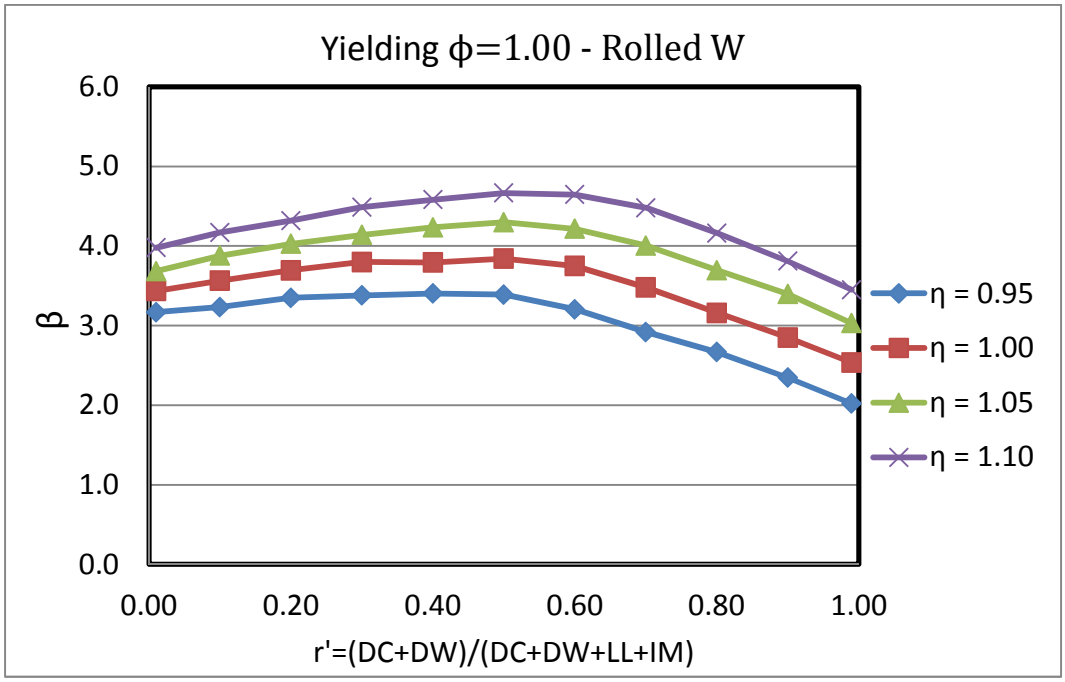

Figure 4-2. Reliability curves of Rolled W steel tension members designed for yielding with adjusted resistance factor φ_y=1.00

Figure (4-2) shows reliability curves for Rolled W sections with adjusted yielding resistance factor ($\varphi_y=1.00$). The resulting diagram shows that by increasing the resistance factor from 0.95 to 1.00, a safe enough behavior can still be provided for studied steel sections.

Calculated reliability indices, for fracture of the net section, in all monitored section were more than 5.2, which is considerable higher than the target reliability index, $\beta_T=4.5$. To adjust existing reliability of steel tension members for fracture, a greater resistance factor ($\varphi_u=0.90$ rather than current resistance factor: $\varphi_u=0.80$) has been examined for the weakest section in fracture (HSS-C). By accepting new resistance factor for fracture of the net section ($\varphi_u=0.90$), all monitored sections will experience a more reasonable safety level with reliability indices closer to the target reliability index: $\beta_T=4.5$.

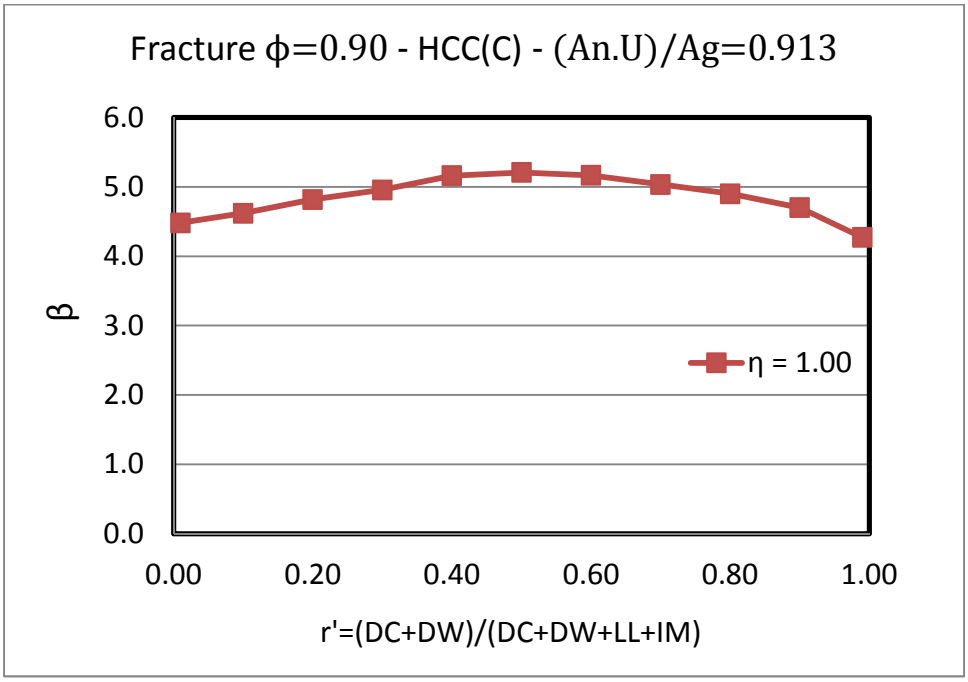

Figure 4-3. Reliability indices for HSS-C sections designed for fracture of net section with adjusted resistance factor: $\varphi_u=0.90$

4.3.4.2. Compression members

For compression members, a minimum reliability index equal to 3.0 was offered by the previous researchers (Schmidt & Bartlett, 2002-b). This target reliability index corresponds to a probability of failure equal to $P_f=1.35E-3$.

Figures (4-4a to 4-4d) show the reliability curves for different sections. The calculated reliability indices are based on the load modification factors $\eta= 1.0$. In AASHTO LRFD code, based on the importance of the structure, redundancy and achievable ductility, the reliability of the designed member will be adjusted by changing η.

Figure (4-4a) indicates that the reliability of designed Rolled W sections is slightly sensitive to the slenderness ratios, λ. Depending on the load ratio (r') and slenderness (λ), the reliability indices varies from 2.85 to 4.6 (3.3 to 4.6 for $0.20<r'<0.80$). As it can be seen in this figure, the reliability indices experience their maximum and minimum values for slenderness ratios equal to 0.16 and 4.0, respectively. However, this section is less sensitive to λ values with respect to three other sections.

Designed WWF sections achieve higher reliabilities (β) distributed from 3.1 to 5.1 (Fig. 4-4b). More slender members ($\lambda=4.00$ and $\lambda=3.24$) have the least β values, while other members with slenderness values changing from 0.04 to 2.56 experience closer reliability indices. HSS-C and HSS-H sections show similar behavior with high β values for $\lambda<1.96$ (Fig. 4-4c & 4-4d). By increasing slenderness ratio, reliability indices decrease to 2.6 in the worst case. It can be observed that the reliability of HSS members is more dependent on λ values. All calculated reliabilities for the practical range of the load ratio ($0.2<r'<0.8$) are higher than assumed target reliability for steel compression members ($\beta_T=3.0$).

Figures (4-4c) and (4-4d) indicate that Equation (4-6a) provides a uniform reliability for different slenderness ratios while Equation (4-6b) leads to lower reliability values for higher λ ratios. Some justifications in the resistance model (Eq. 4-6a & 4-6b) might provide more uniform designed compression members.

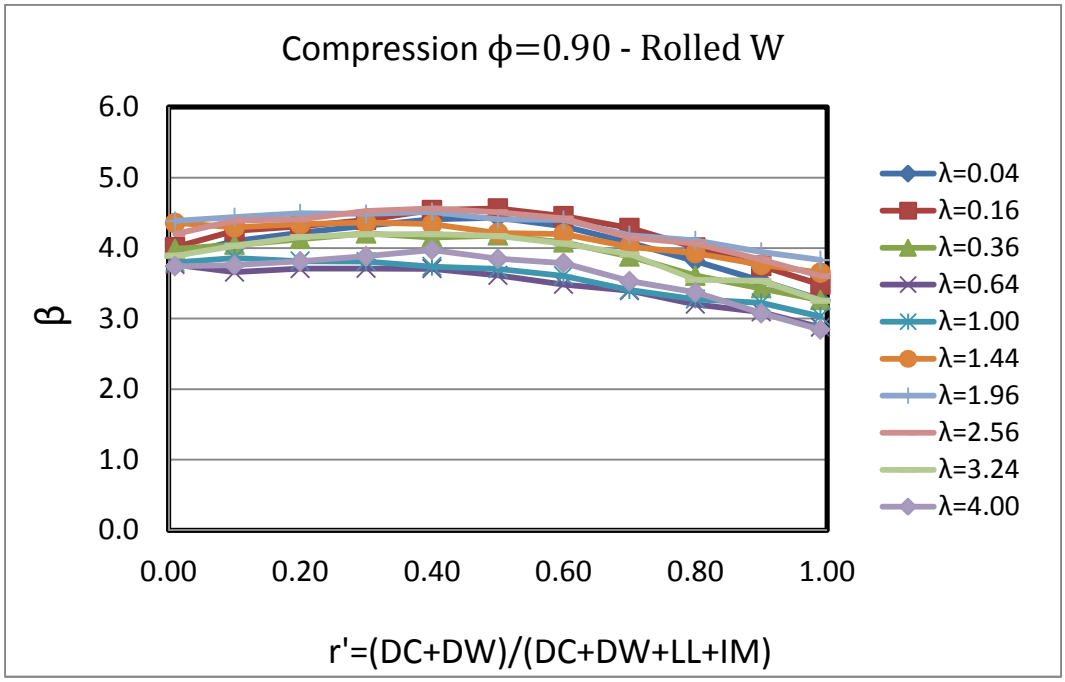

Figure 4-4a. Reliability curves for compression members designed with current AASHTO criteria, (a) Rolled W sections

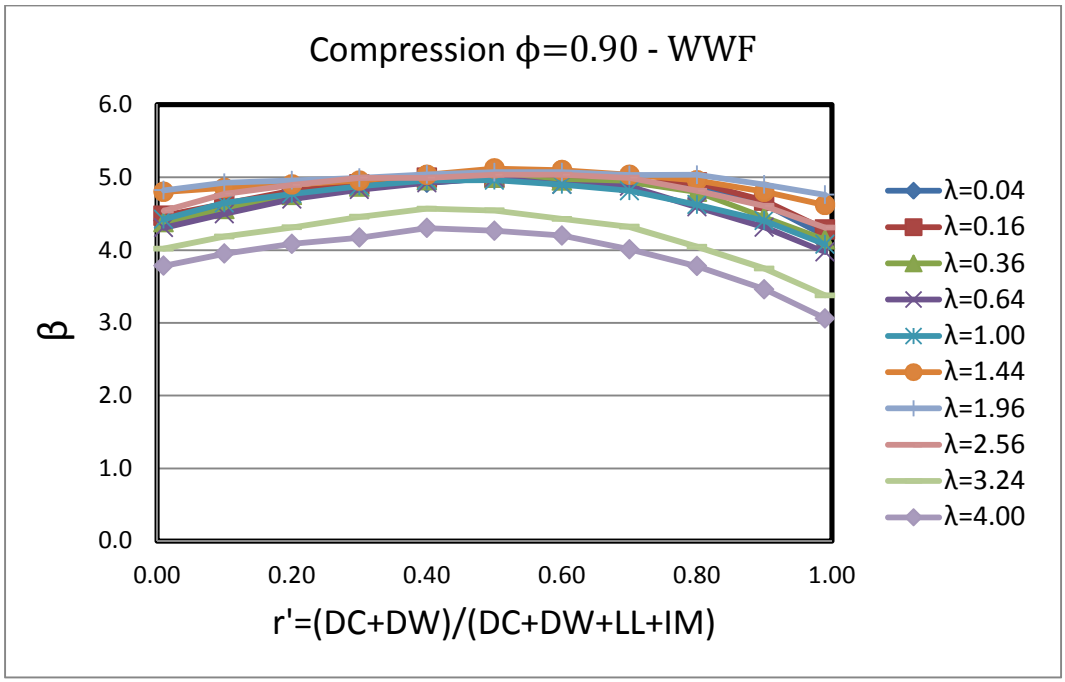

Figure 4-4b. Reliability curves for compression members designed with current AASHTO criteria, (b) WWF sections

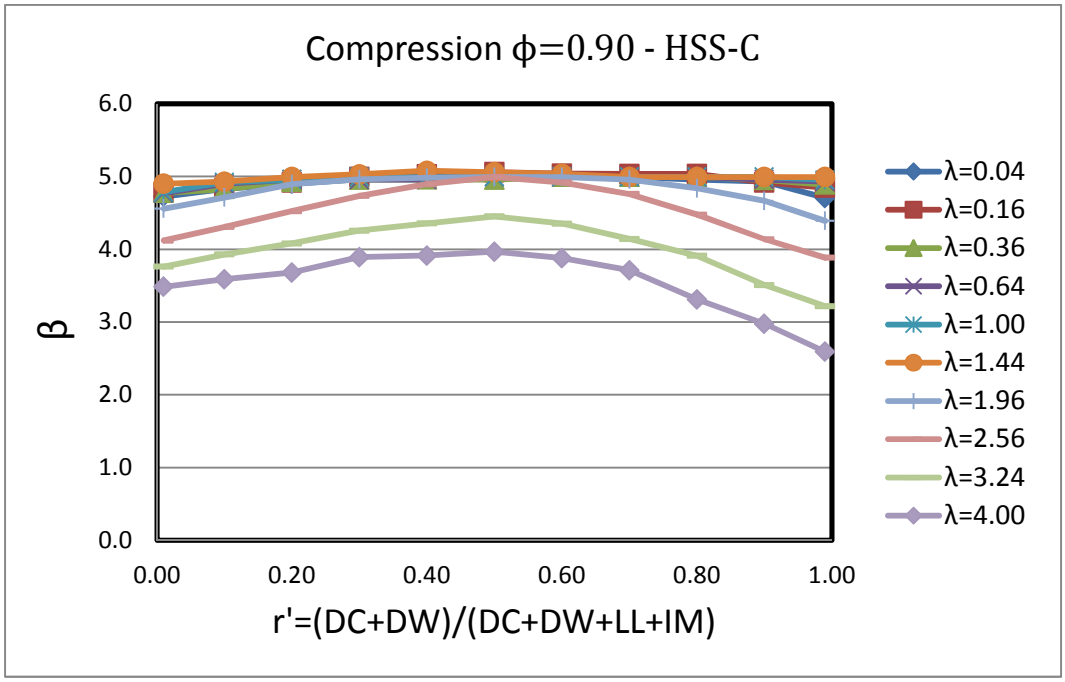

Figure 4-4c. Reliability curves for compression members designed with current AASHTO criteria, (c) HSS-C sections

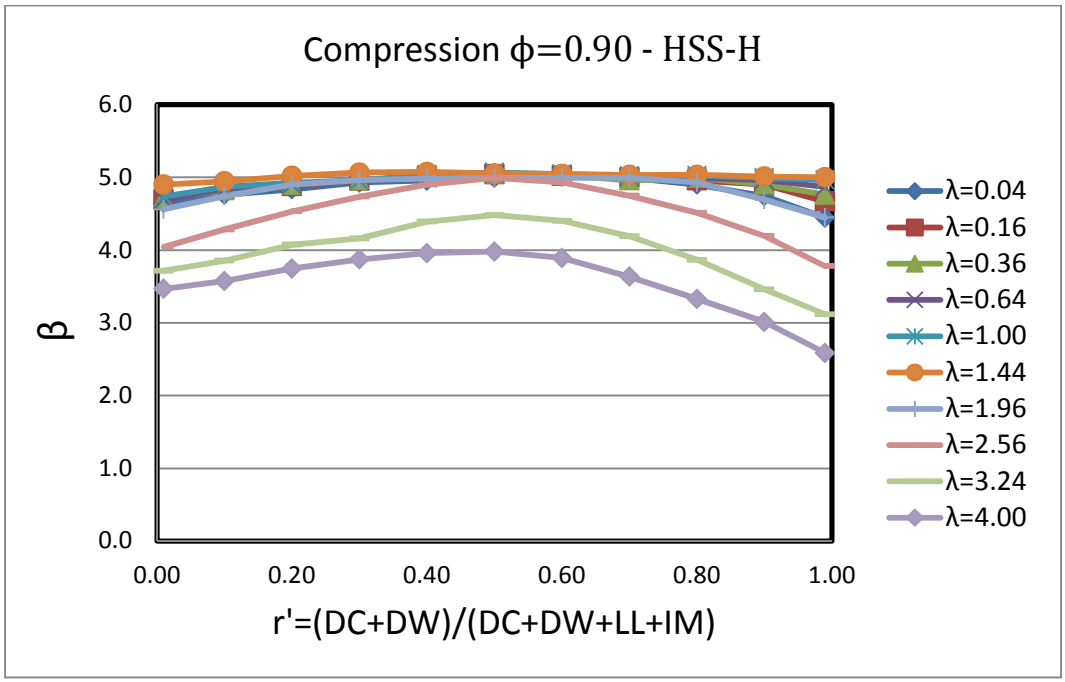

Figure 4-4d. Reliability curves for compression members designed with current AASHTO criteria, (d) HSS-H sections

In Figure (4-5), average reliability indices for different sections are plotted versus slenderness for load ratios changing from 0.2 to 0.8. In Rolled W and WWF sections, the calculated reliabilities reach their minimum value at $\lambda=0.70$, and then goes up to the peak values at nearly $\lambda=2.0$, and decreases rather linearly thereafter. In contrast, HSS sections indicate a different trend. These sections maintain almost consistent values with high averages up to $\beta=5.0$, and decrease linearly thereafter. It appears that the difference between the equations given for different slenderness ratios cause the variation in β values (Eq. 4-6a & 4-6b). It can be concluded that the first equation for $\lambda \leq 2.25$ offers higher reliability indices for most cases, and more than required safety. Using Equation (4-6b), β values decrease constantly by increasing λ values.

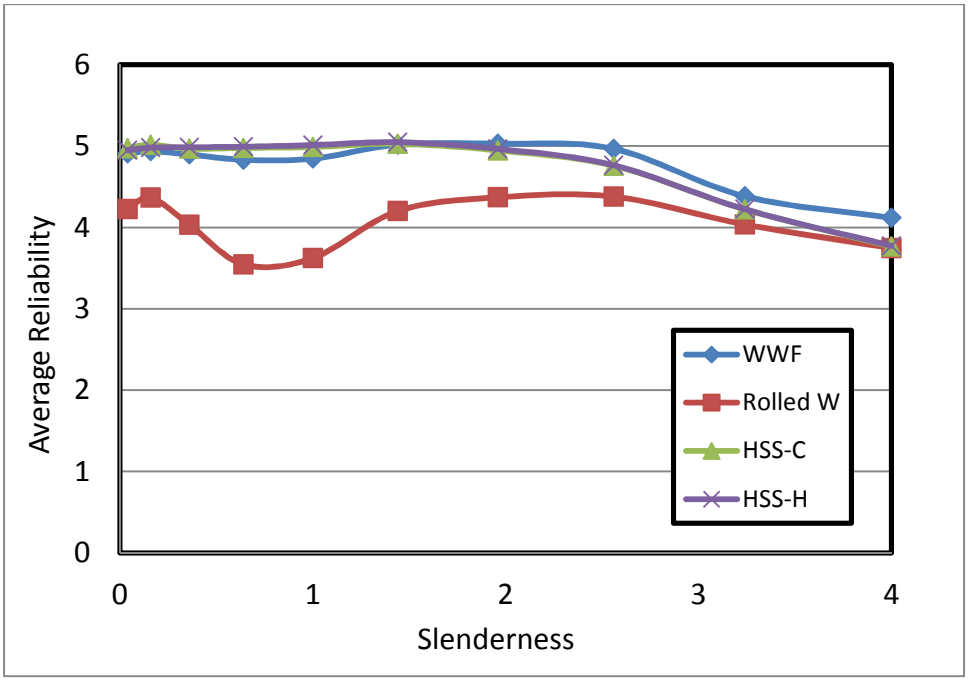

Figure 4-5. Average reliability curves for different sections

4.4. Conclusion

Structural cost optimization requires code developers to maintain a reasonable balance between safety and cost. In new generation of design codes, reliability analysis has been applied to keep an adequate safety level for different conditions. However, to decrease possibility of human errors in design phase, and maintain a simple design code, perfectly optimized criteria cannot be applicable everywhere. As an example, by accepting current load factors in AASHTO LRFD code, due to their verification for majority of bridge structures (girder-type bridges) a uniform reliability level could not be achieved for steel tension members in truss and arc bridges.

Results of the executed reliability analysis on current yield and fracture design equations for tension members display a conservative design for yielding and fracture of steel tension members. By increasing current resistance factor for yielding in gross section from $\varphi_y=0.95$ to $\varphi_y=1.00$, the reliability indices for the worst section are adjusted just above the target value $\beta_T=3.0$. Also, by suggesting $\varphi_u=0.90$ instead of current resistance factor, $\varphi_u=1.00$, the reliability indices are decreased to the target reliability index $\beta_T=4.5$ for fracture of the net section.

In addition, the analysis results indicated safe behavior of all monitored steel sections, designed for axial compression. However, in practical span length ratios ($0.2<r'<0.8$), AASHTO criteria produce extremely conservative design in some cases, with β values up to 5.1 for HSS compression members. According to this study, AASHTO LRFD resistance models for compression steel members (Eq. 4-6a & 4-6b) can be adjusted to achieve a more uniform safety, for different slenderness values. For example, for

slenderness values equal 2.0, the average reliability index for all sections is greater than 4.37 (compared to the target reliability index $\beta_T=3.0$).

By using new collected data for axially loaded steel members, evaluation of steel compression members along with evaluation of tension members designed in accordance with the latest AASHTO LRFD code (AASHTO 2007) has provided a superior understanding of safety level for these elements. Utilizing reliability analysis results in evaluation of the current design criteria, insures a safe performance for structural elements and therefore the bridge system. For further research it can be advantageous to use the desired safety level for bridge systems to develop/evaluate members' design criteria.

Chapter 5

Part III: High-Speed Passenger Train Loads

5.1. High-Speed Rail Programs in the United States

Future developments in the US transportation network intend to reduce dependency on oil and apply other sources of energy. High-speed passenger rail program has been discussed in the Unites States in the past few years. This program is expected to have an efficient contribution to the transportation network in the US mega regions (Todorovich et al., 2011). High-Speed Rail (HSR) is a fast and reliable alternative with less dependency on weather, which requires a huge amount of initial investment. Infrastructure, technology and land acquirement are critical parts of HSR development which needs federal, state

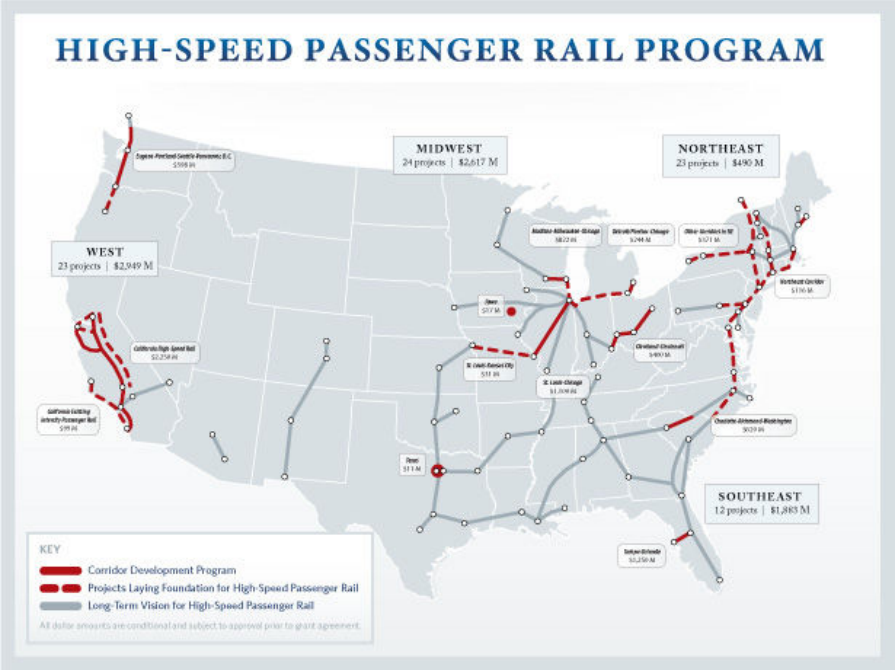

Figure 5-1. High-speed passenger rail programs in the United States (http://www.wikipedia.org/, Image credit: United States Department of Transportation)

and private party investments. In the fiscal year 2010, the US Congress allocated $2.5 billion to spend on high-speed rail. Figure (5-1) shows planned HSR programs in the United States with almost isolated divisions and corridors. The only in operation HSR in the US at the moment is Amtrak's Acela Express which connects Boston to Washington, DC with the maximum speed of 240 km/hr (150 mph).

5.2. Dynamic Response of High-Speed Railway Bridges and Resonance

Successful high-speed passenger rail projects in Europe and East Asia can be a valuable source of knowledge for the US decision makers in both strategic and technical development. The European code for traffic loads on bridges (Eurocode, 2002) has been widely used in the past two decades. Real trains and simulated load models are categorized in this code and suggestions for choosing the critical train, verifying design limit states, and requirements for dynamic analysis of brides are provided. However, due to the complexity of the bridge response to high-speed trains and high dependency of the results to the structure and moving load properties, dynamic analysis is inevitable in most cases.

In practice, two different techniques can be used in dynamic analysis of bridges: analytical methods with application of Eigen modes of vibrations, and numerical techniques such as finite element method with the capabilities of modeling specific structures and possible nonlinear responses through a step-by-step analysis (Goicolea et al., 2002). In general, the first mode of vibration has often been considered in analytical closed-form solutions. By neglecting higher modes of vibration, the equation of motion can be simplified. Museros and Alarcon (2005) have studied the influence of the second

bending mode on the dynamic response of simply supported bridges with different span length to passenger car length ratios. The results of their study indicate neglecting the higher modes of vibration does not affect the deflection response and bending moment in the bridge superstructure. However, it has been shown that the second bending mode should be considered in determining maximum acceleration for the simply supported girders. More investigation can be accomplished on the response of continuous girders and the influence of higher modes of vibration in shear response. Yau (2001) applied the finite element method to examine the response of continuous bridges under high-speed train loads. Considered samples in his study include 1-span to 7-span bridges with uniform span lengths. Based on the analysis results, the calculated impact factor for the superstructure displacement decreases by increasing the number of spans.

Goicolea et al. (2002) showed that vehicle-structure interaction has a deductive effect on girder displacements and accelerations. Compared to simple moving load models, their analysis results declare up to 45% reduction in maximum accelerations. It can be observed that this dynamic response reduction is more considerable for accelerations rather than displacements. This reduction effect was increased by increasing the train speed. In addition, short spans showed more sensitivity to vehicle-structure interaction by experiencing more reduced responses. It should be noted that results are based on evaluating simply supported bridges with consideration of the first mode of vibration with no shear deformation.

More detailed numerical studies have been done for specific bridges designed for high-speed rails (Xia & Zhang, 2005; Dinh et al., 2009; Martinez-Rodrigo et al., 2010). In some cases, theoretical results have been verified with field recorded data for a

specific bridge (Xia & Zhang, 2005). Martinez-Rodrigo et al. (2010) have evaluated possible solutions for strengthening vulnerable existing bridges. In their study, the influence of passive control retrofitting techniques for short simply supported bridges has been investigated and fluid viscous dampers with feasibility considerations are proposed. However, a comprehensive study using the multimode solution with considerations for bridge-train interaction for different types of bridges can be advantageous in designing railway bridges. In this study, a series of diagrams are proposed to determine dynamic load factors for bending moment in bridge superstructures. For this reason, conventional high-speed load models in Europe are applied in analysis and maximum responses are presented in terms of envelope diagrams. A range of span lengths, superstructure vibration frequencies and train speeds are considered in calculations. In addition, three different support conditions such as simple, simple-continuous and continuous are investigated. The effects of the superstructure damping ratio is considered to study different bridge systems. The proposed diagrams provide an inclusive database for bridge designers to initially estimate the dynamic response and avoid the possible resonance phenomenon for different types of railway bridges.

5.3. High-Speed Load Models

Train configuration and its load distribution is an important term in determining bridge response and the possibility of resonance. Train specifications such as power car characteristics, number of intermediate coaches, coach length, axle spacing, the associated weight at each axle location and train speed define the dynamic load for each specific rail project. Due to the extensive amount of investment in rail programs, it is

desirable to keep the railway bridge designs independent of train types. This fact necessitates considering a wide range of possible passing trains in designing brides and taking into account the possibility of higher traveling speeds.

By implementing the broad experience from successful high-speed rail programs in Europe, a specific European Standard publication was developed for traffic load considerations on bridges (Eurocode, 2002). In this code, different load models for static and dynamic analysis, short-span to long-span bridges and simply supported or continuous bridges are recommended. Load Model 71 (Fig. 5-2) and Load Model SW/0 (Fig. 5-3) are proposed as normal rail traffic on mainline bridges for static analysis. Load Model SW/0 is only applicable for continuous bridges. Suggested loads for static analysis can be replaced with real train loads in any particular project if applicable.

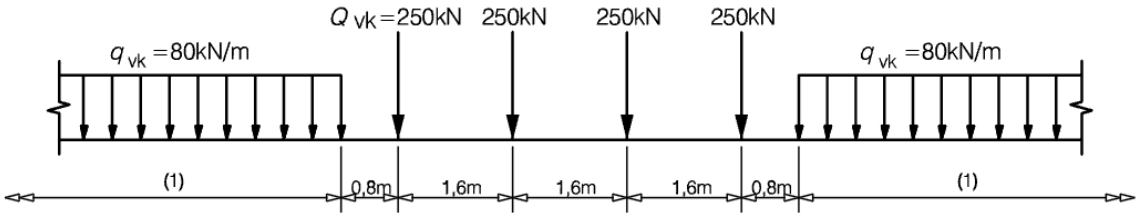

Figure 5-2. Load Model 71 (Eurocode, 2002)

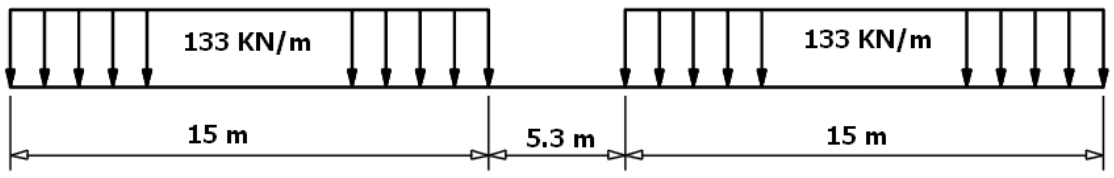

Figure 5-3. Load Model SW/0 (Eurocode, 2002)

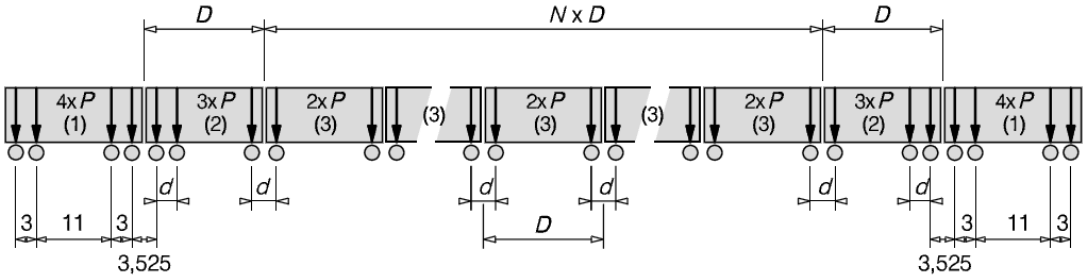

Key

(1) Power car (leading and trailing power cars identical)
(2) End coach (leading and trailing end coaches identical)
(3) Intermediate coach

Figure 5-4. HSLM-A applicable for continuous bridges and simple spans equal to or longer than 7m (Eurocode, 2002)

Table 5-1. Corresponding parameter for HSLM-A (Eurocode, 2002)

Universal Train	Number of intermediate coaches (N)	Coach length D(m)	Bogie axle spacing d(m)	Point Force P(kN)
A1	18	18	2.0	170
A2	17	19	3.5	200
A3	16	20	2.0	180
A4	15	21	3.0	190
A5	14	22	2.0	170
A6	13	23	2.0	180
A7	13	24	2.0	190
A8	12	25	2.5	190
A9	11	26	2.0	210
A10	11	27	2.0	210

To include the induced dynamic effects, the static analysis results should be multiplied by a dynamic factor, Φ. However, this factor does not consider resonance effects. To predict any possible resonance due to the passing high-speed trains, proposed High Speed Load Models (HSLM) with a variety of simulated trains should be considered in the dynamic analysis (Figs. 5-4 to 5-6 and Table 5-1). These virtual trains

are designed to simulate the dynamic effects of all conventional train models and real trains in Europe. These load models weight about 40% of real trains and therefore should not be applied for static analysis purposes. Bridge structures along high-speed rails (with design speed varying from 55 m/s to 100 m/s) should satisfy corresponding service and strength limit states. The maximum response from the dynamic analysis and static analysis (including dynamic factor Φ) should be used for design purposes.

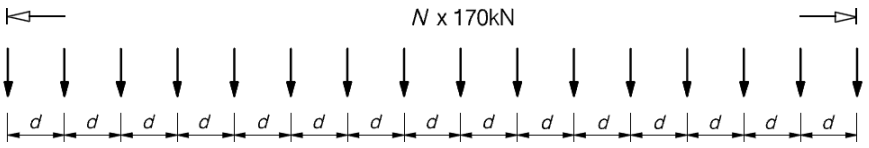

Figure 5-5. HSLM-B applicable for simple spans shorter than 7m (Eurocode, 2002)

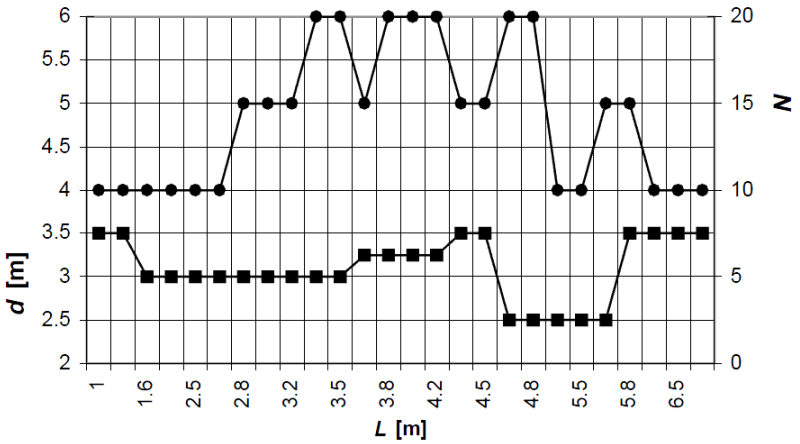

Figure 5-6. Corresponding parameter for HSLM-B (Eurocode, 2002)

5.4. Methodology

5.4.1. Superstructure Modeling

Railroad bridge superstructures are modeled as a 2-dimensional Bernoulli-Euler beam. Non-prismatic cross section and uniform mass distribution is assumed. The governing differential equation of vibration for this model is as follows (Chopra, 2007):

$$EI\frac{\partial^4 u(x,t)}{\partial x^4}+m\frac{\partial^2 u(x,t)}{\partial t^2}+C\frac{\partial u(x,t)}{\partial t}=p(x,t) \tag{5-1}$$

where m and C is the mass and viscous damping per unit length; E is the modulus of elasticity; I is the moment of inertia of the superstructure section; $u(x,t)$ is transverse displacement of the beam at point x and time t; and $p(x,t)$ is the load per unit length of the beam. Solving the equation requires the boundary and initial condition information. The initial condition is often expressed as zero deflection and velocities at time zero where the bridge superstructure is at rest. Zero deflections at the supports can also be applied to the equation of motion as boundary conditions. The solution to partial differential Equation (5-1) can be expressed as the superposition of individual mode effects as follows (Chopra, 2007):

$$u(x,t)=\sum_{n=1}^{\infty}\phi_n(x)q_n(t) \tag{5-2}$$

where $\phi_n(x)$ is the nth mode spatial function or mode shape and $q_n(t)$ is the time function. For the circumstance of constant EI and mass, $\phi(x)$ can be derived solving the ordinary differential Equation (5-3) with the application of boundary conditions.

$$EI\phi^4(x)-\omega^2 m\phi(x)=0 \tag{5-3}$$

in which ω represents the natural circular frequency. An infinite number of mode shapes and corresponding frequencies associated with the eigenvalue problem can be obtained

solving this equation. The natural frequency at the nth mode of vibration of a simple span, two-span and 3-span continuous beam can be formulated as:

$$\omega_n = \frac{\lambda_n^{\,2}}{L^2}\sqrt{\frac{EI}{m}} \tag{5-4}$$

in which n is the mode number; ω_n is the nth mode natural frequency; L is the span length; and λ_n is the nth mode frequency related parameter represented in Table (5-2) for the first five modes of vibration.

Table 5-2. Frequency related parameter (λ_n) for simple span, two span and three span bridges

	Mode number				
	1	2	3	4	5
1-span	3.142	6.283	9.425	12.566	15.708
2-span	3.142	3.927	6.283	7.069	9.425
3-span	3.142	3.550	4.303	6.283	6.692

Dynamic analysis of bridge superstructures can disclose possible resonance in responses. A group of regularly spaced axel loads moving at a particular speed generates a specific loading frequency. Depending on how close the loading frequency is to the natural frequencies of the bridge superstructure, different levels of response can be recorded. Resonance is likely to occur when the loading frequency coincides with one of the modal natural frequencies of the bridge, causing the dynamic responses to be magnified. There are infinite numbers of natural frequencies in continuous mass and stiffness problems, each referring to a specific mode of vibration. Lower modes corresponding to lower frequencies of vibration practically comprise a major portion of the overall response. As the structural reaction amplifies at its natural frequencies, only

first few modes of vibration, within the possible spectrum of loading frequency, are required to be considered.

A simple practical procedure is employed to consider vehicle-bridge interaction effect in the analyses. Each train axle is modeled as a single degree of freedom moving load on the bridge with a suspension system composed of a spring and a viscous damper (Fig. 5-7). An iterative calculation is then used to determine the exact responses of the bridge. At the first step it is assumed that there is no train-interaction effect and the deflections are calculated at each time step. These responses are then applied to single degree of freedom systems of train axles and their resulting force are calculated solving their single degree of freedom equation of motion. The updated forces are then applied to bridge system and responses are calculated again. The computation cycle requires to be repeated several times until the change in forces in two consecutive steps is negligible.

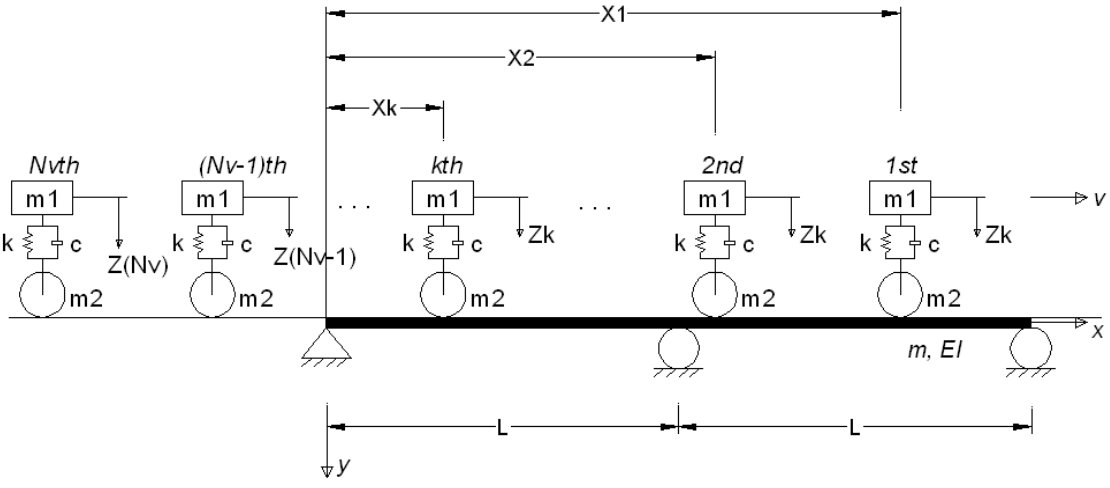

Figure 5-7. Vehicle-bridge interaction model

5.4.2. Superstructure Frequency Range

Superstructure fundamental bending frequency can be defined as a function of bridge span length (or an equivalent parameter as described in Eurocode (2002)) in terms of upper and lower bounds. Fryba (1996) has suggested the upper and lower bounds for the fundamental frequency of railway bridges as illustrated in Figure (5-8). For each span length value, fundamental bending frequency depends on several parameters such as superstructure, materials, girder spacing, support conditions, bridge age, etc. In calculating bending DLFs, main focus should be on the practical range for each span length value. However, irregular or innovative bridge structures may experience an out of range natural frequency.

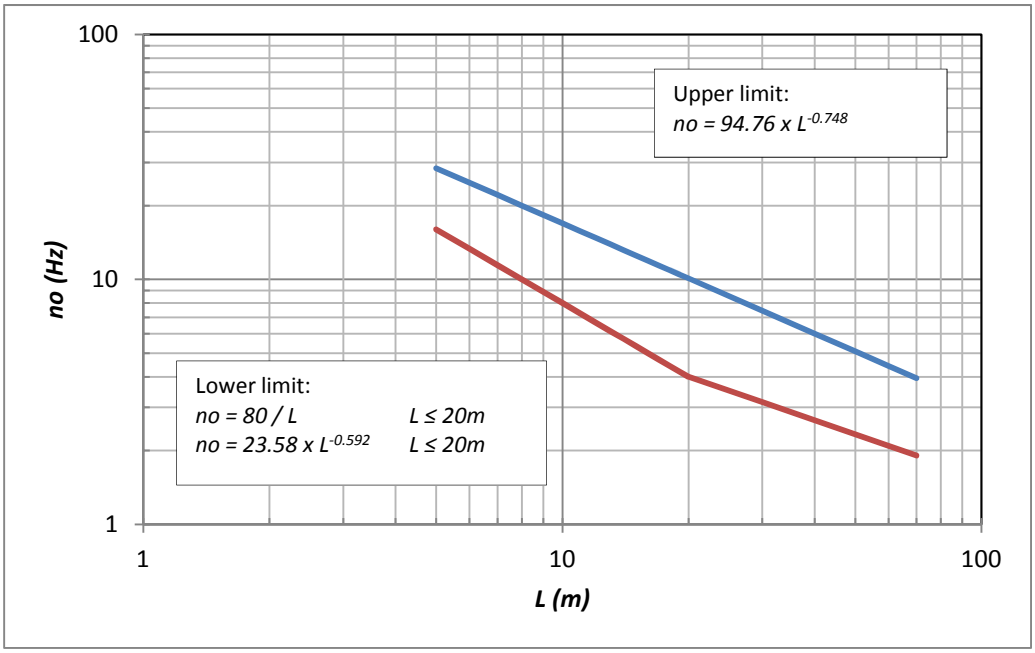

Figure 5-8. Practical range of bridge superstructure fundamental frequency versus span length

5.4.3. Damping

Damping of the superstructure system can significantly change dynamic analysis results and determined dynamic load factors. Eurocode (2002) requires using the lower bound of structural damping in the vibration analysis. Equations (5-5) to (5-7) summarize suggested lower bounds for bridge structural damping (Eurocode, 2002):

Steel and composite:

$$\zeta=0.5+0.125(20-L) \quad \text{for } L<20m \quad \text{and} \quad \zeta=0.5 \quad \text{for } L\geq 20m \tag{5-5}$$

Prestressed concrete:

$$\zeta=1.0+0.07(20-L) \quad \text{for } L<20m \quad \text{and} \quad \zeta=1.0 \quad \text{for } L\geq 20m \tag{5-6}$$

Filler beam and reinforced concrete:

$$\zeta=0.5+0.125(20-L) \quad \text{for } L<20m \quad \text{and} \quad \zeta=0.5 \quad \text{for } L\geq 20m \tag{5-7}$$

Estimated percentage of critical damping for different bridge systems are shown in Table (5-3) for each examined span length (L).

Table 5-3. Damping values for different bridge systems suggested by Eurocode (2002)

L (m)	Steel and composite (%)	Prestressed concrete (%)	Filler beam and reinforced concrete (%)
3	2.63	2.19	2.69
5	2.38	2.05	2.55
7	2.13	1.91	2.41
10	1.75	1.70	2.20
15	1.13	1.35	1.85
20 ~ 50	0.50	1.00	1.50

5.4.4. Dynamic Effects

In addition to the mass and suspension characteristics of the vehicle, the traffic speed, span length, girder supports, natural frequency of the structure, damping, number of train axles, axle loads and their spacing are key factors in determining the dynamic response of bridge superstructures. Past concluded studies have been utilized to determine whether a vibration analysis is required for each specific superstructure (Eurocode, 2002). If a dynamic analysis is necessary, modified static analysis results should be compared with the dynamic analysis responses for both service and strength limit states. Service limit state design for passenger rail bridges limits the maximum deck acceleration, while strength limit states ensure acceptable stresses in structural components such as main girders.

When using HSLM in dynamic analysis, the maximum obtained value from following equations should be considered in the design of the superstructure (Eurocode 2002):

$$LL = max\left(\frac{y_{dyn}}{y_{stat}}\right) \times (LM71) \qquad \textit{for simple girders} \qquad (5\text{-}8a)$$

$$LL = max\left(\frac{y_{dyn}}{y_{stat}}\right) \times Max(LM71, SW/0) \qquad \textit{for continuous girders} \qquad (5\text{-}8b)$$

$$LL = \Phi \times (Real\ Train\ or\ equivalent) \qquad (5\text{-}9)$$

where LL is the design live load, and y_{dyn} and y_{stat} are maximum dynamic and static response at the specified section in the member, respectively. The ratio $\left(\frac{y_{dyn}}{y_{stat}}\right)$ is defined as the Dynamic Load Factor (DLF) which can be obtained from presented diagrams in Section (5.5). Additional considerations and modifications might be needed due to the track defects or vehicle imperfections which are not the main focus in this study.

Examined sections for determining positive and negative moment DLFs are shown in Figure (5-9).

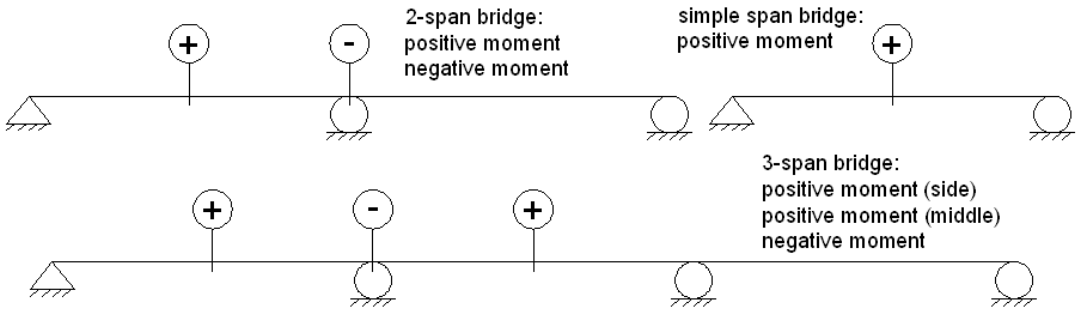

Figure 5-9. Examined sections for determining positive and negative moment DLFs

5.5. Vibration Analysis

The demonstrated closed form solution has been applied to calculate bridge responses in different situations. As recommended by Eurocode (2002), one particular high speed load model (HSLM-B) for simply supported spans shorter than 7m long and 10 different load models (HSLM-A) for all other simply supported and continuous spans are considered in the dynamic analysis. A computer code is utilized to perform the massive numerical analysis for each specific span length and damping ratio. For each particular velocity (40 m/s to 100 m/s), the bridge dynamic response is measured under all applicable trains. The highest produced bending moment from all applicable train loads is taken as the structural response for each velocity. It should be noted that Eurocode (2002) requires dynamic analysis for all rail bridges with the maximum line speed greater than 55 m/s (200 km/hr). In that case, dynamic analysis should be performed for a range of train

speeds from 40 m/s up to the maximum line speed times 1.2. Proposed High Speed Load Models are valid for simulations with speeds up to 100 m/s (360 km/hr).

In order to provide simplified DLF diagrams, only envelope curves are presented for each observed section in simply supported, 2-span continuous and 3-span continuous bridges. Figure (5-10) shows in detail the concluded responses for 20m long simply supported bridges with 1% damping ratio. A complete set of DLF diagrams in various train velocities along with the push curve is given against superstructure frequency. The peak responses have shifted to the right side as the train velocity increases. These values are the peak points at which the train velocity causes the loading frequency to coincide with superstructure natural frequency. For each structural frequency of vibration, one specific velocity may cause the most undesired dynamic response. Proposed push diagrams can be used to determine structural response to passing high-speed passenger trains.

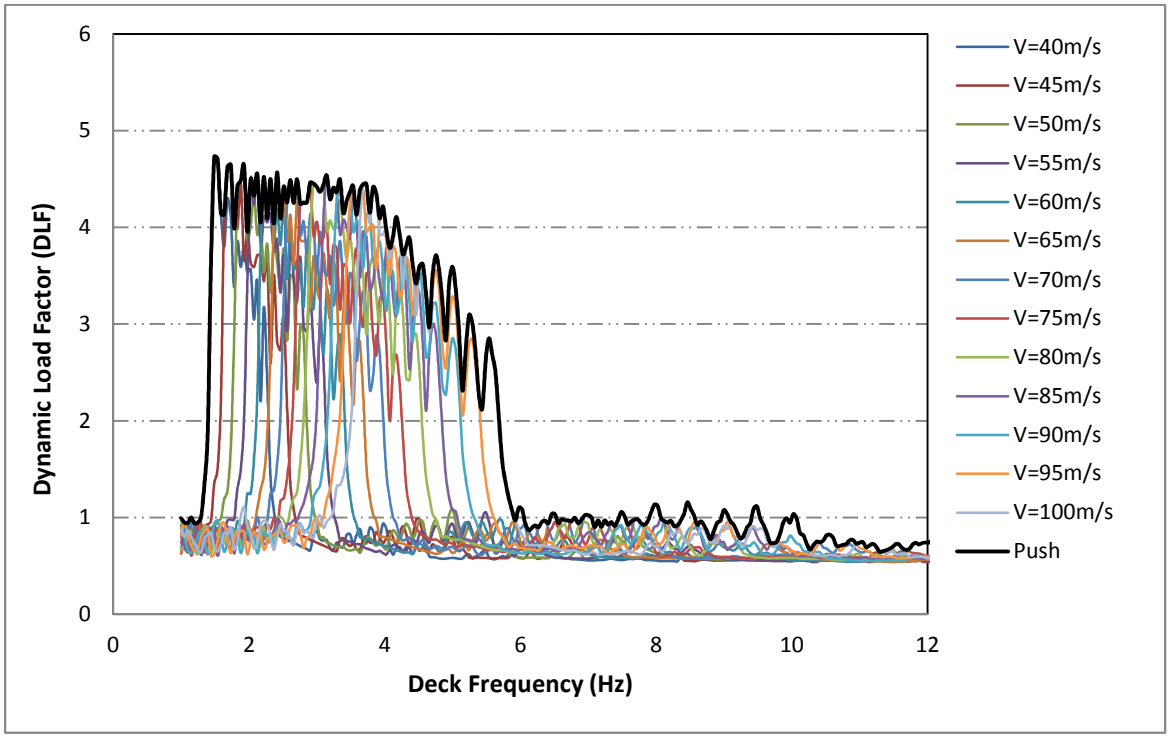

Figure 5-10. DLFs for bending moment in midspan, simple spans, L=20m, Damping=1%

Figures (5-11) to (5-20) show push DLF diagrams for different types of bridges such as steel and composite, prestressed concrete and reinforced concrete bridges with associated damping ratios as explained in Section (5.4.3). The span length changes from 3 to 50 meters in an appropriate increment. Superstructure frequency values are changed in a practical range of 1 to 40 Hz with 0.05 Hz intervals. In some figures, for a clearer display, the frequency range in horizontal axis is limited to a tighter range yet covering all frequencies delivering a DLF of greater than 1. Due to the fact that proposed high speed load models weigh about 40% of the real trains for static analysis, DLF values tend to eventually descend to a value about 0.4 for higher frequencies where no dynamic effect is predicted.

As mentioned before, HSLM-B which follows a different pattern is suggested for simple spans shorter than 7m. Dissimilar response diagrams for 3m and 5m simple spans are because of the difference in the dynamic load models. Comparing two closer simple spans, 5m long and 7m long spans in Figures (5-12) and (5-13) with different HSLMs (types A and B), the peak response values are obtained in different range of superstructure frequency. For 3m and 5m simple spans using HSLM-B maximum response is reflected in a broader range of frequency. More dissimilarity in shape and DLF values reveals a discontinuity in analysis results using HSLM-A and HSLM-B even for close span lengths.

Positive and negative moments for continuous spans have been considerably reduced for 3-span bridges with respect to 2-span models in all considered spans. However, DLF values for 1-span bridges are lower than DLFs for 2-span bridges in some cases such as 5m, 7m, 10m and 15m long spans. Similar response trends for positive and negative moments are also visible in most figures.

Another important factor is the practical range of the superstructure vibration frequency for each span length. As it was mentioned before, the practical range of the superstructure frequency depends on the bridge span length. As an example, for a 15m long bridge, superstructure vibration frequency would be most likely in the range of 5 to 12 Hertz. Using obtained diagrams in Figure (5-15), it can be concluded that low frequency bridges may experience resonance under passing high-speed trains. DLF values for steel and composite bridges with the least damping can be up to 5 for positive bending moments in simply supported and 2-span continuous bridges corresponding to 5 Hz frequency of vibration. This value is measured about 2.8 for positive moments in 3-

span bridges, up to 2 for negative moment in a 2-span bridge, and up to 1.2 for negative moments in a 3-span bridge.

One noticeable phenomenon in the diagrams is the stepped response peaks occurred in different frequency ranges. This is more obvious for long span bridges where a set of stepped peaks has consecutively occurred. For example, for the negative moment at the support of 2-span 15m long bridge shown in Figure (5-15), two peaks are clearly identifiable from the figure indicating the resonance occurrence in the first two modes of vibration. The second mode resonance has occurred in the low frequency range, where the next set of peak with lower DLF values is mostly due to the first mode resonance. This fact demonstrates the importance of considering higher modes of vibration even though the practical frequency range of bridge superstructures may not often allow its resonance.

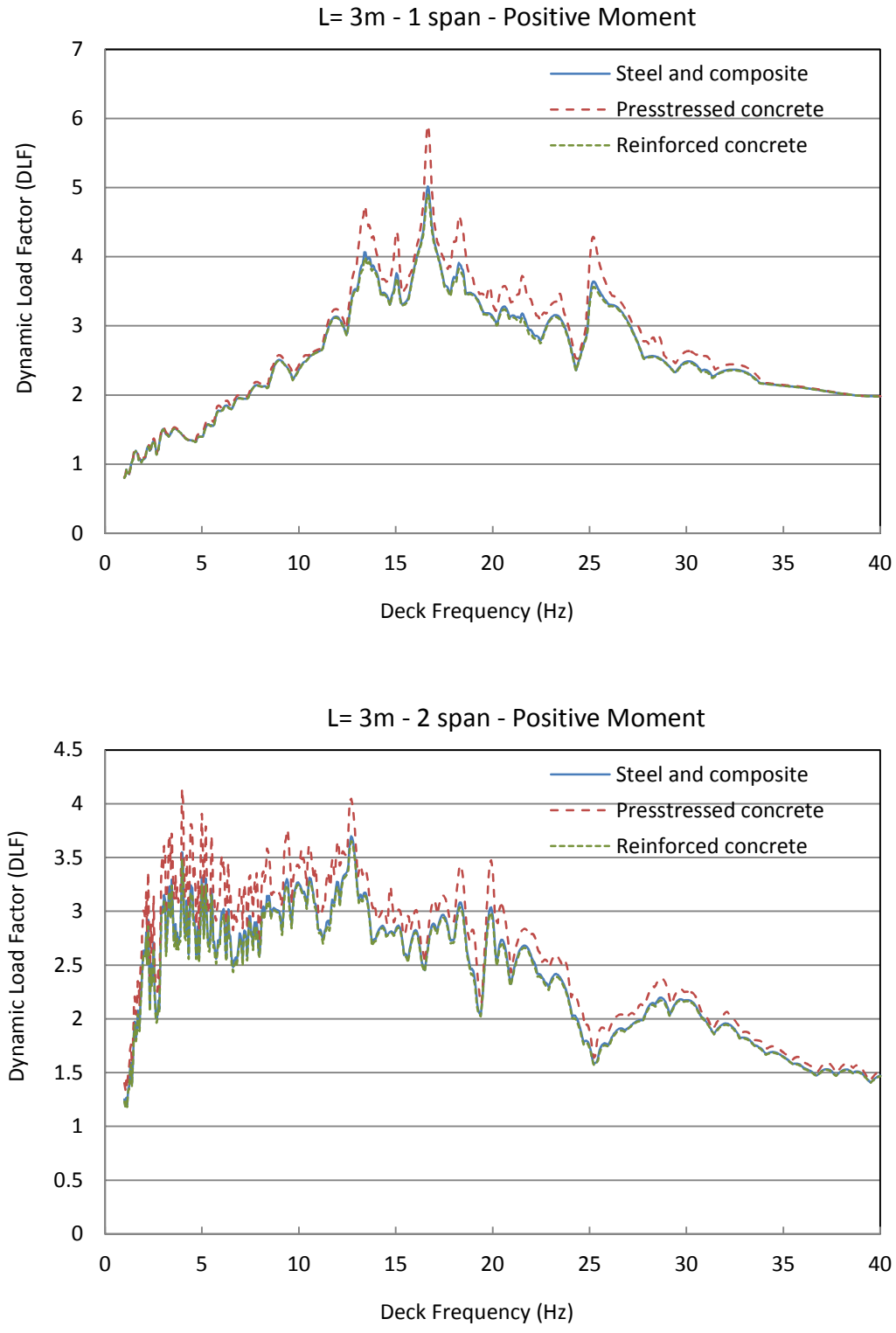

Figure 5-11. Dynamic Load Factors for bending moment in 1-span, 2-span and 3-span bridges, L=3m

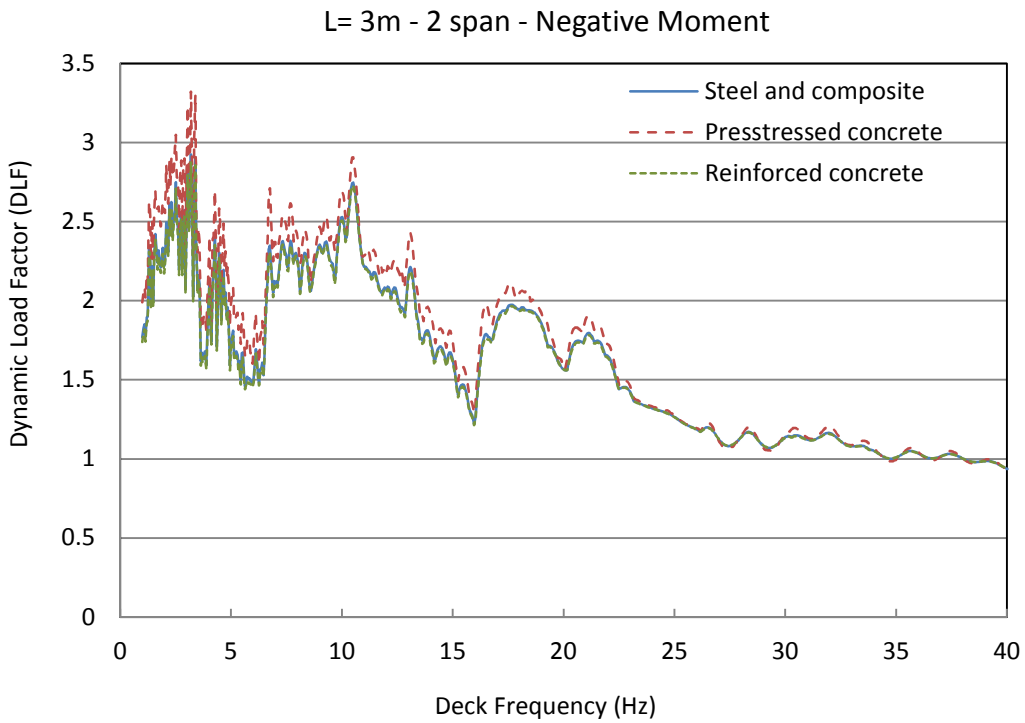

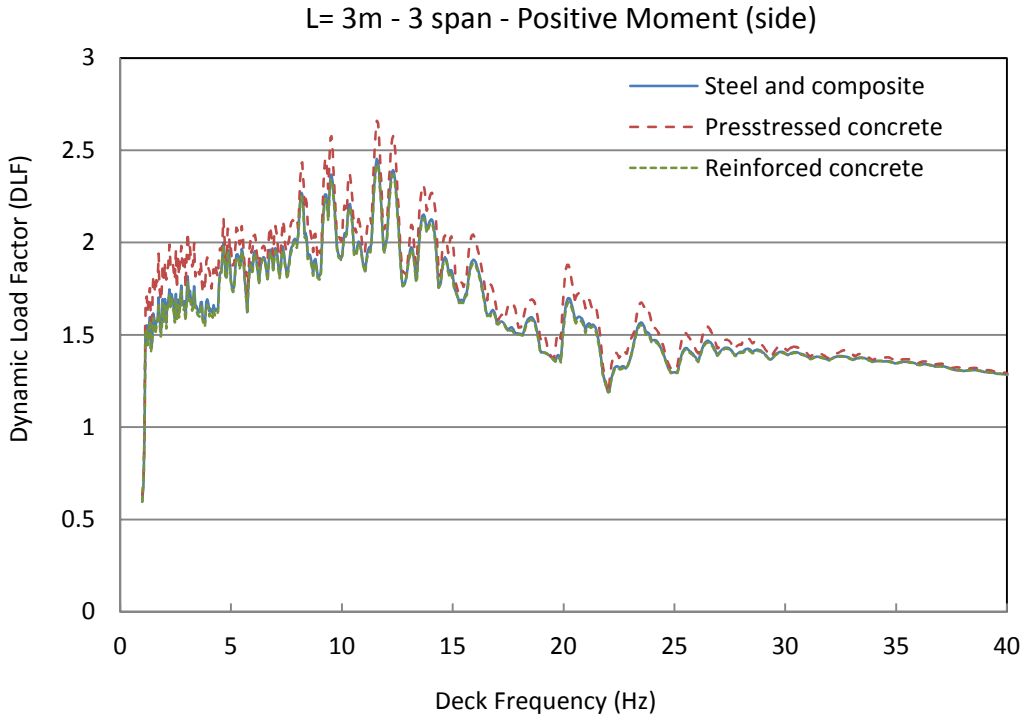

Figure 5-11(Cont.). Dynamic Load Factors for bending moment in 1-span, 2-span and 3-span bridges, L=3m

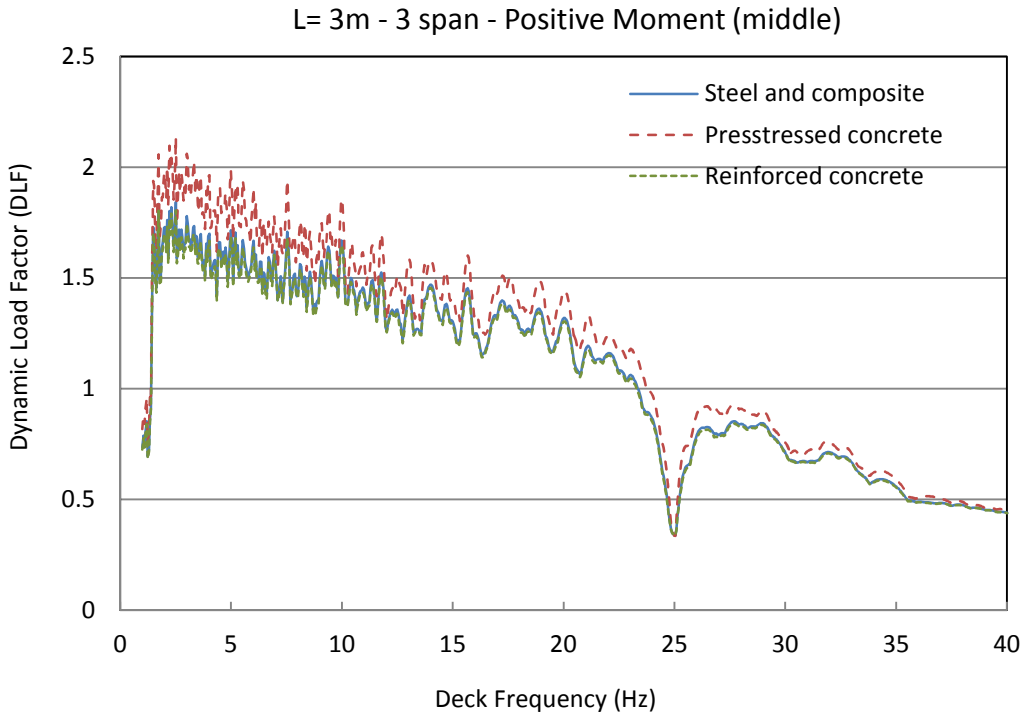

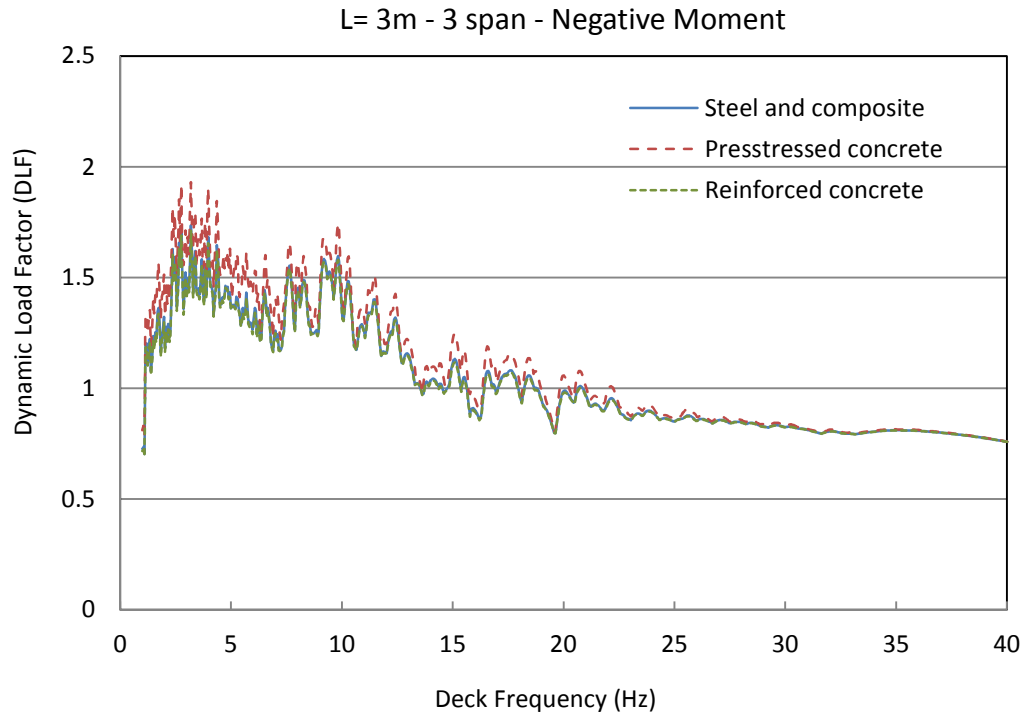

Figure 5-11(Cont.). Dynamic Load Factors for bending moment in 1-span, 2-span and 3-span bridges, L=3m

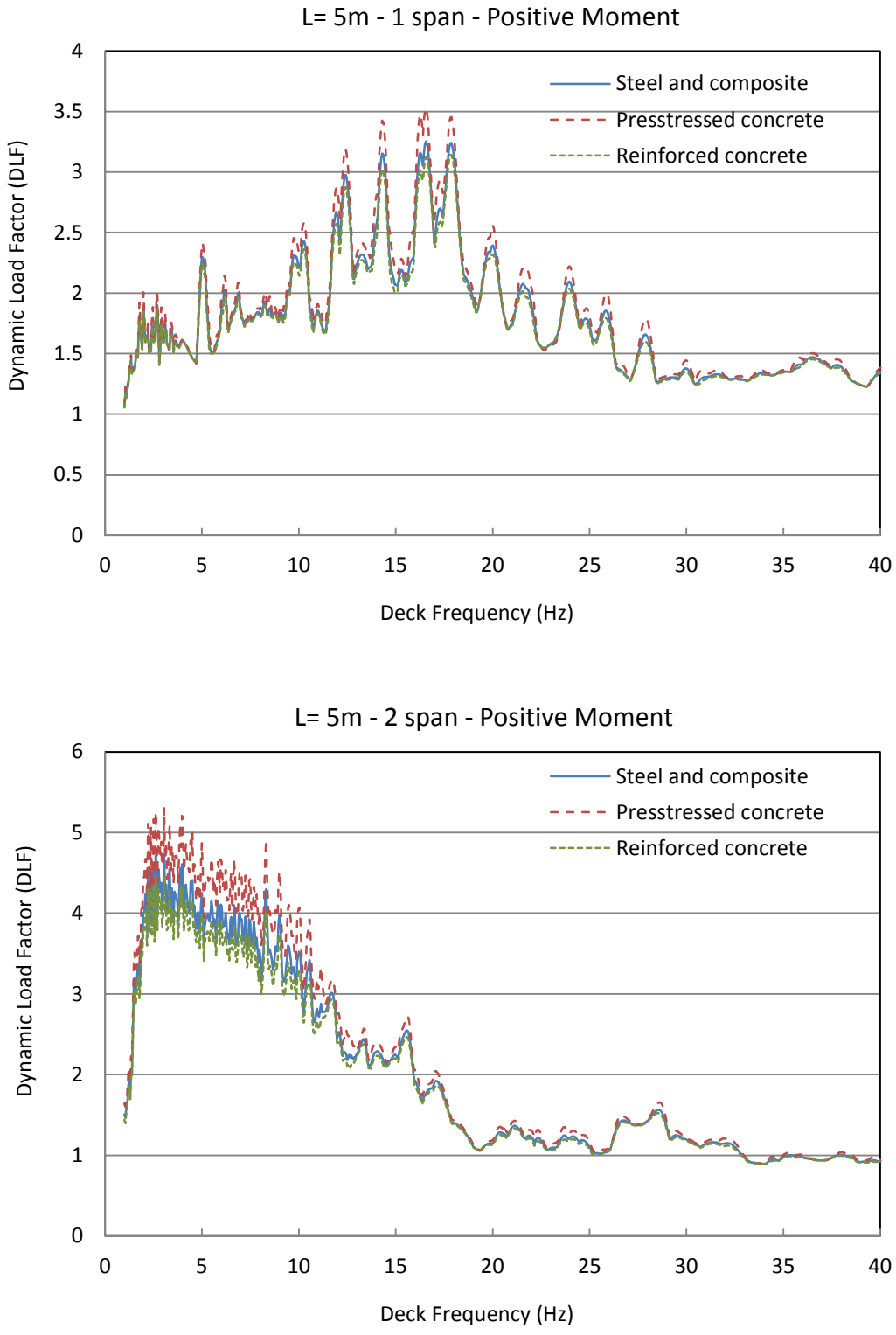

Figure 5-12. Dynamic Load Factors for bending moment in 1-span, 2-span and 3-span bridges, L=5m

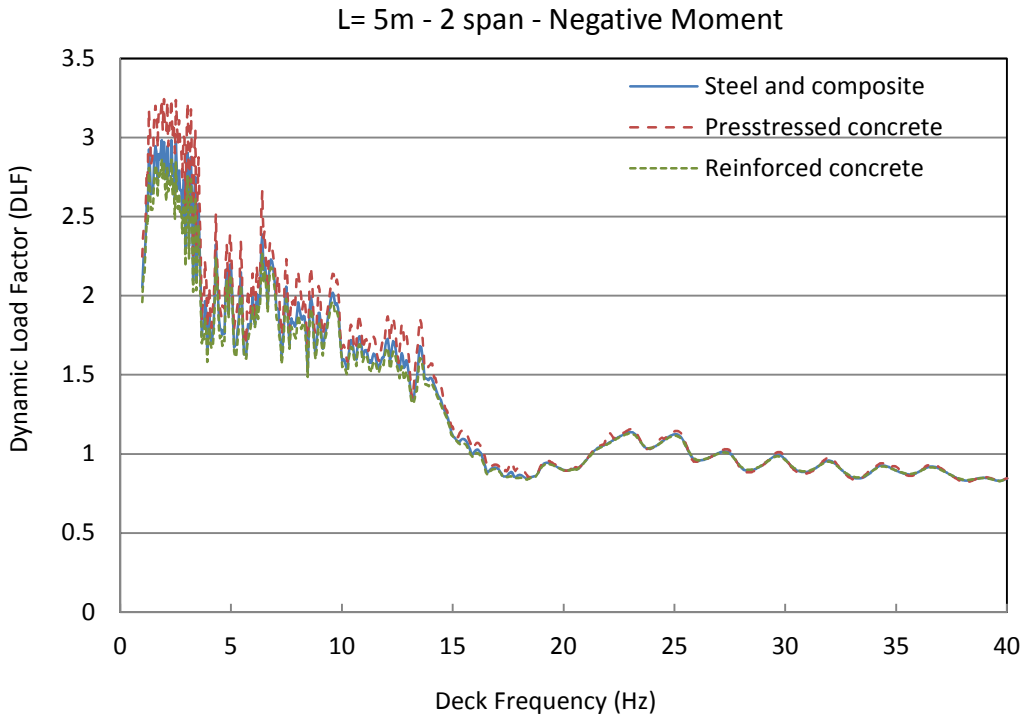

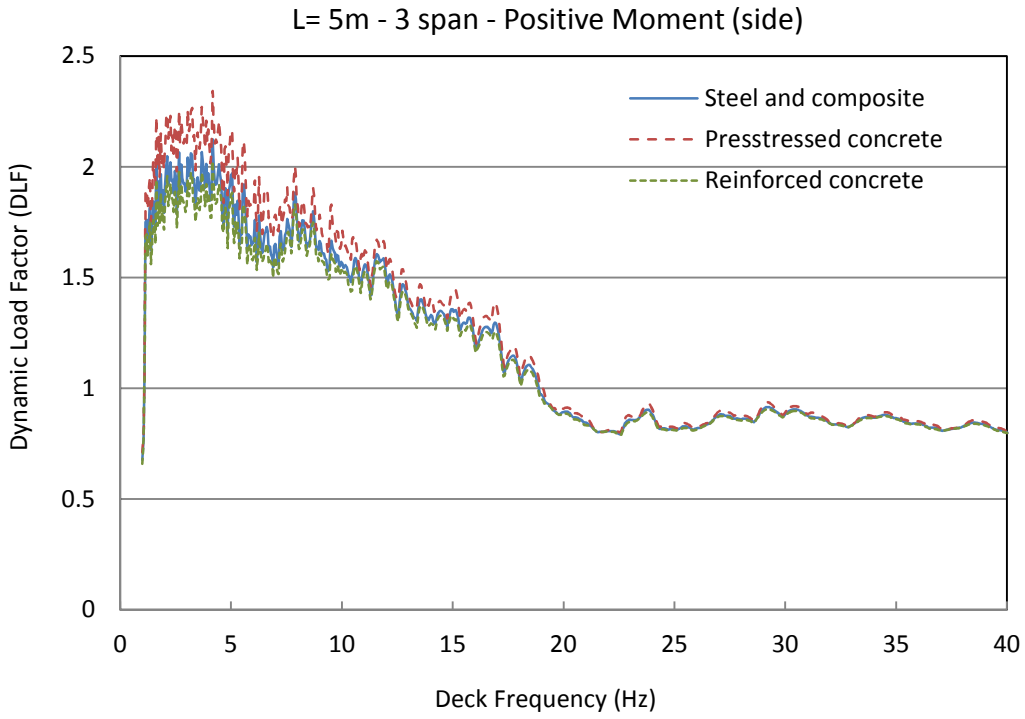

Figure 5-12(Cont.). Dynamic Load Factors for bending moment in 1-span, 2-span and 3-span bridges, L=5m

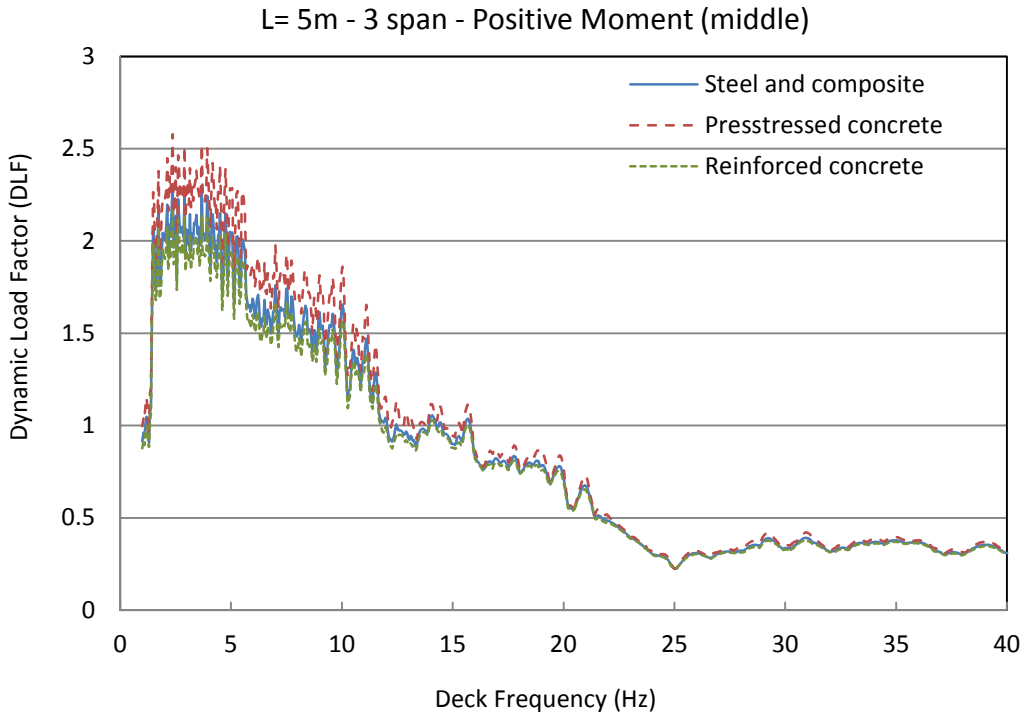

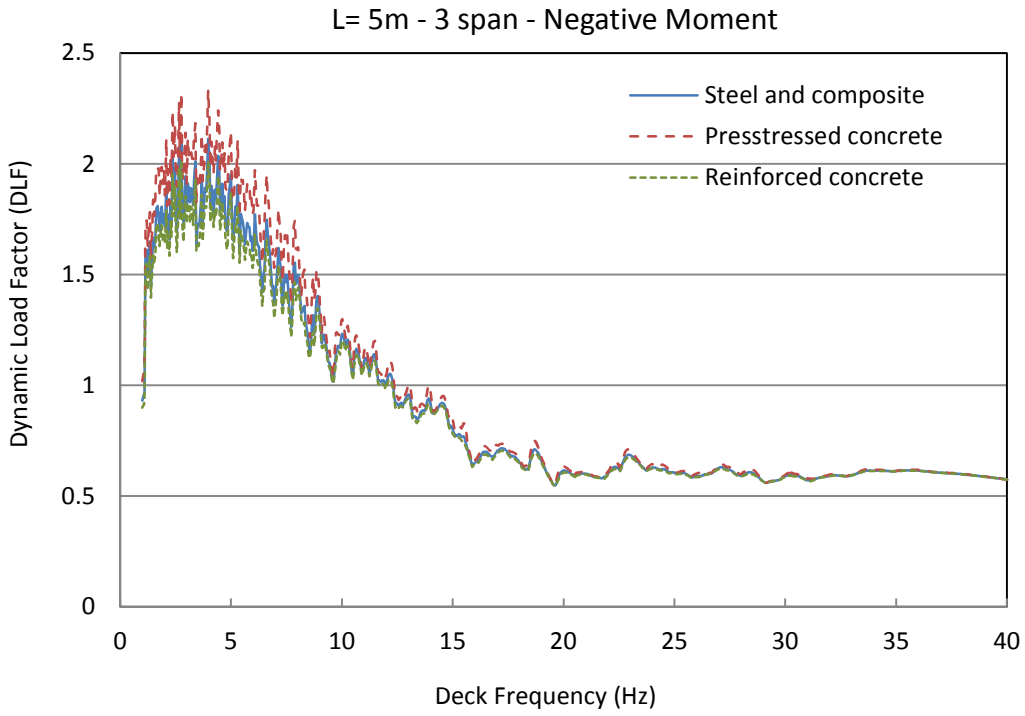

Figure 5-12 (Cont.). Dynamic Load Factors for bending moment in 1-span, 2-span and 3-span bridges, L=5m

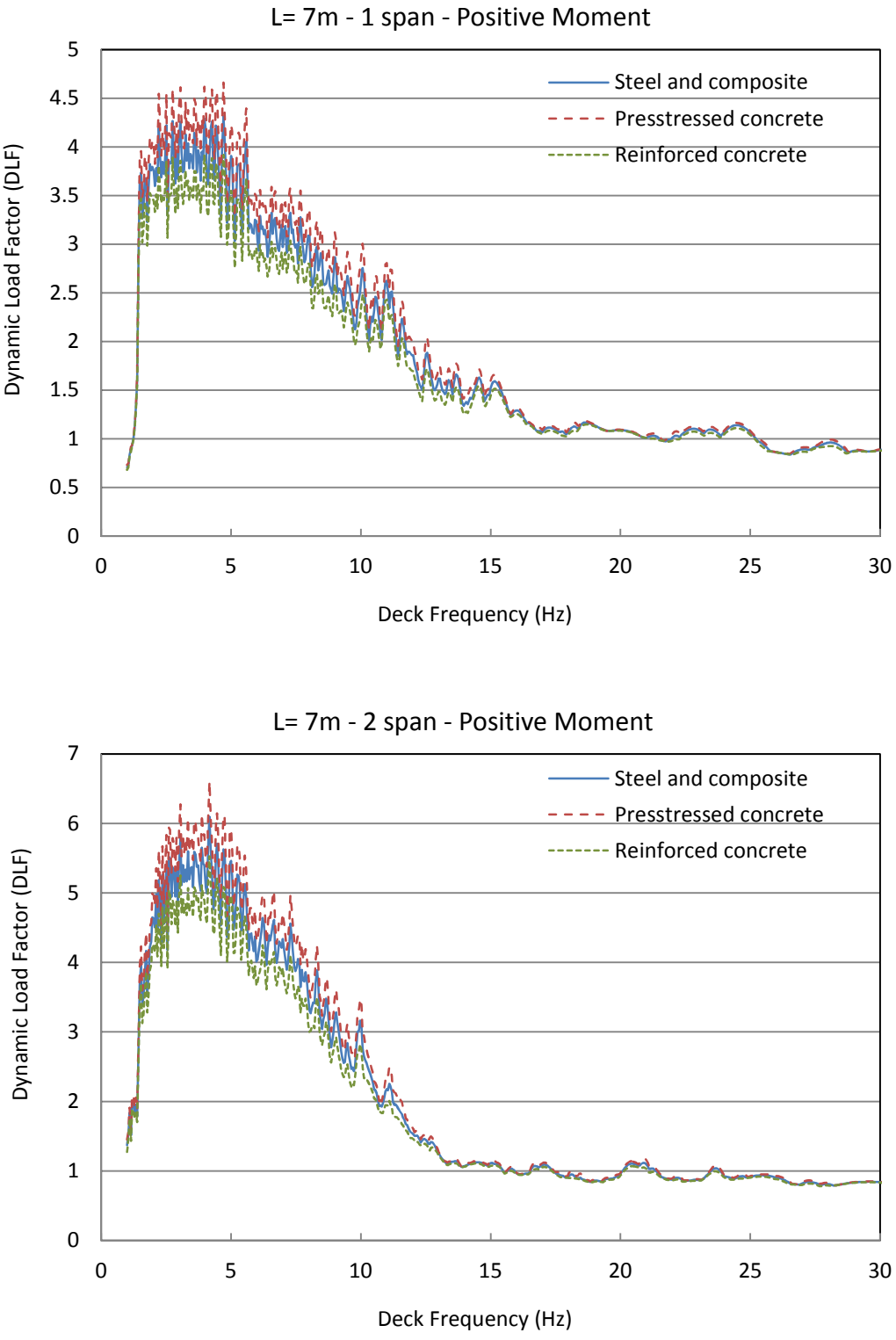

Figure 5-13. Dynamic Load Factors for bending moment in 1-span, 2-span and 3-span bridges, L=7m

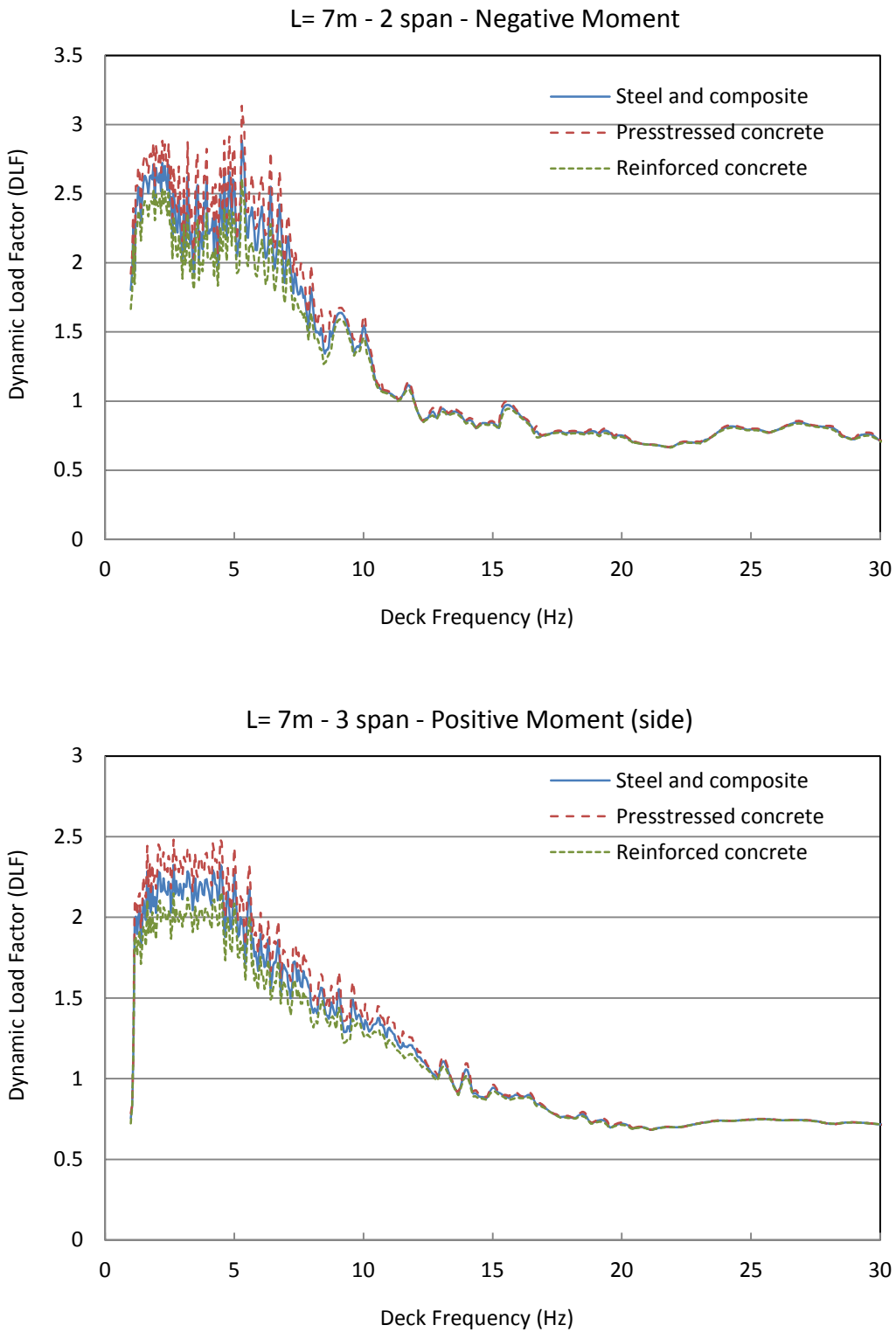

Figure 5-13 (Cont.). Dynamic Load Factors for bending moment in 1-span, 2-span and 3-span bridges, L=7m

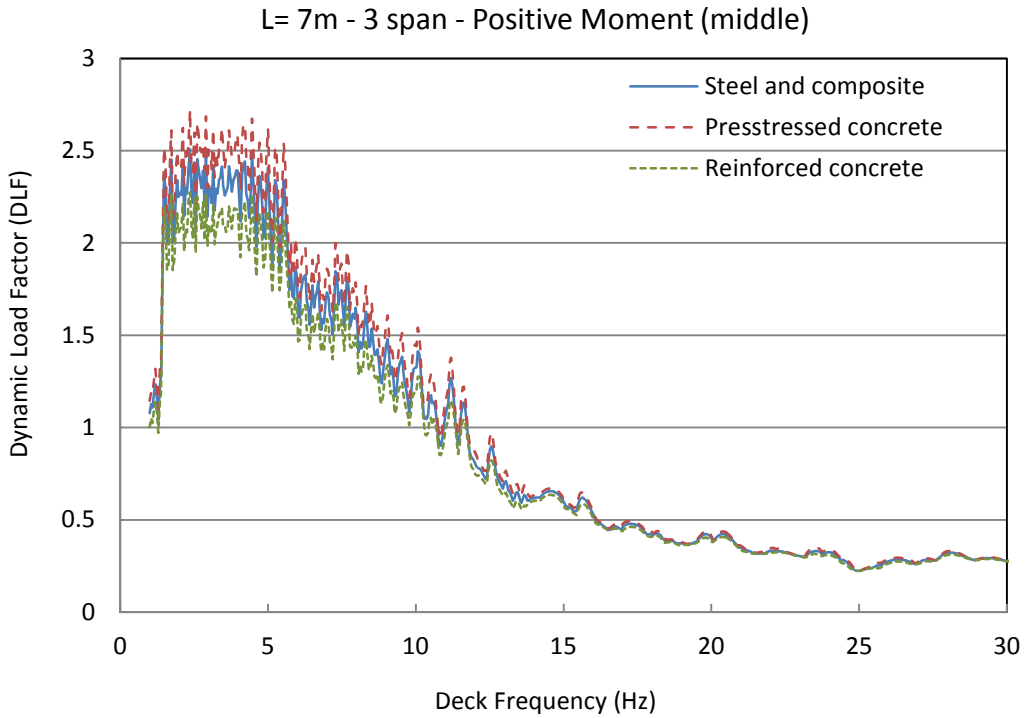

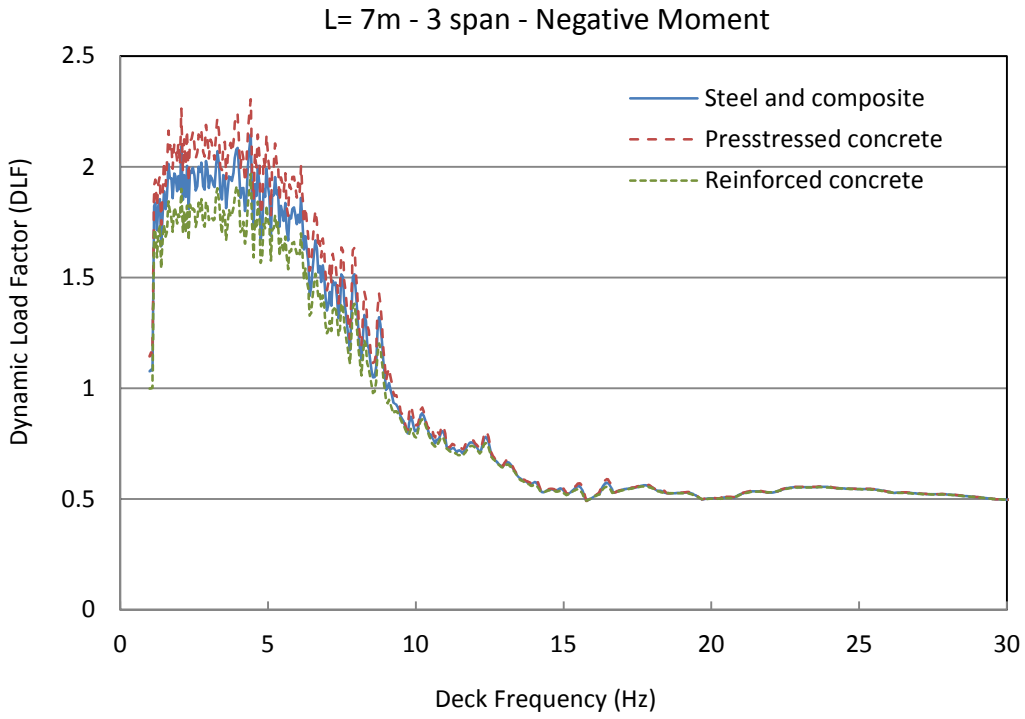

Figure 5-13 (Cont.). Dynamic Load Factors for bending moment in 1-span, 2-span and 3-span bridges, L=7m

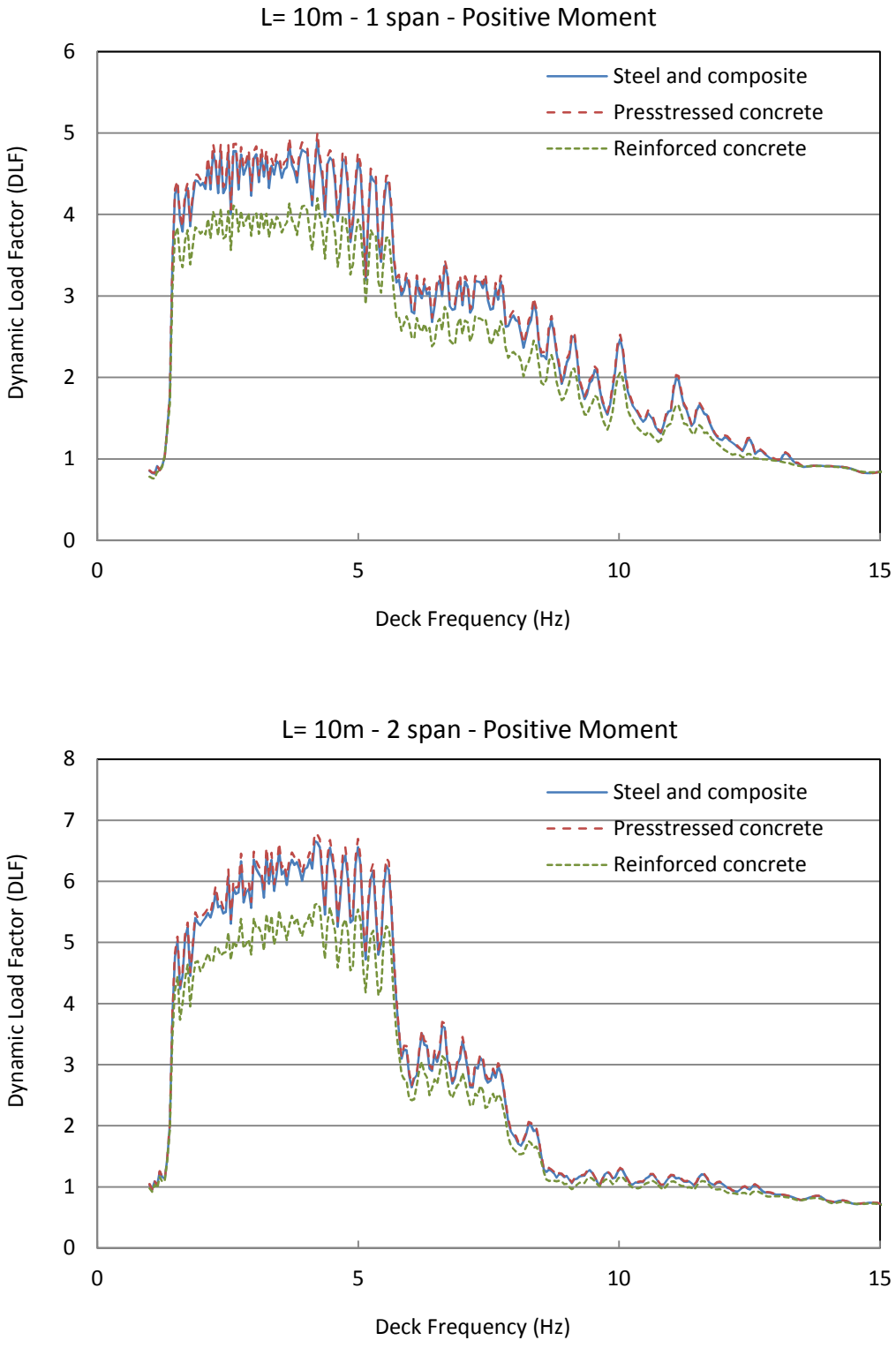

Figure 5-14. Dynamic Load Factors for bending moment in 1-span, 2-span and 3-span bridges, L=10m

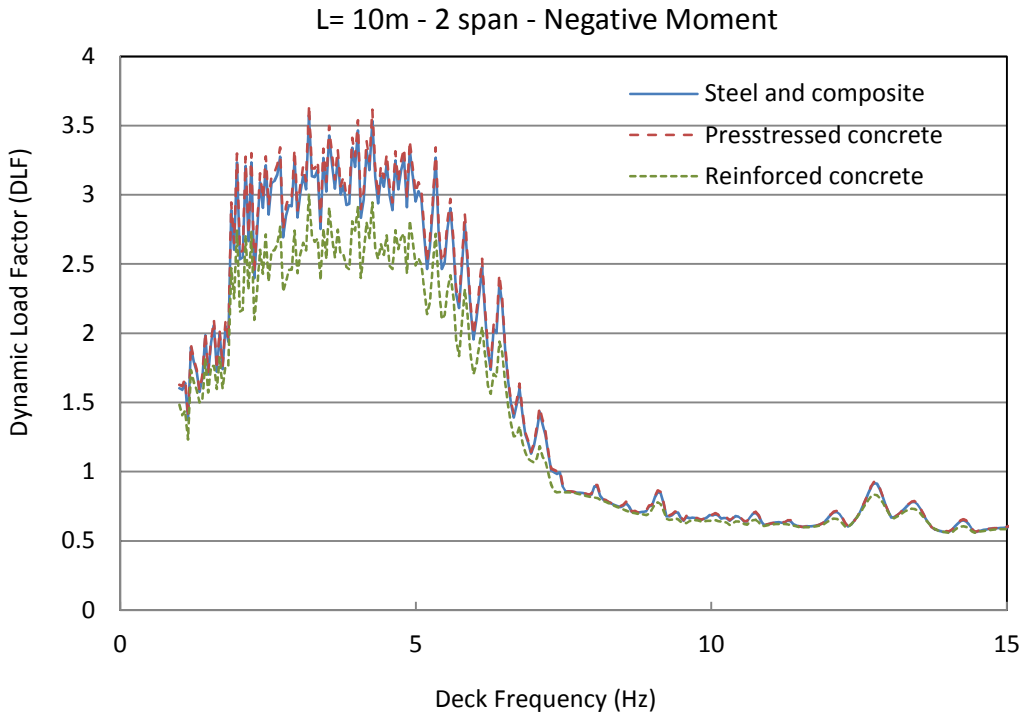

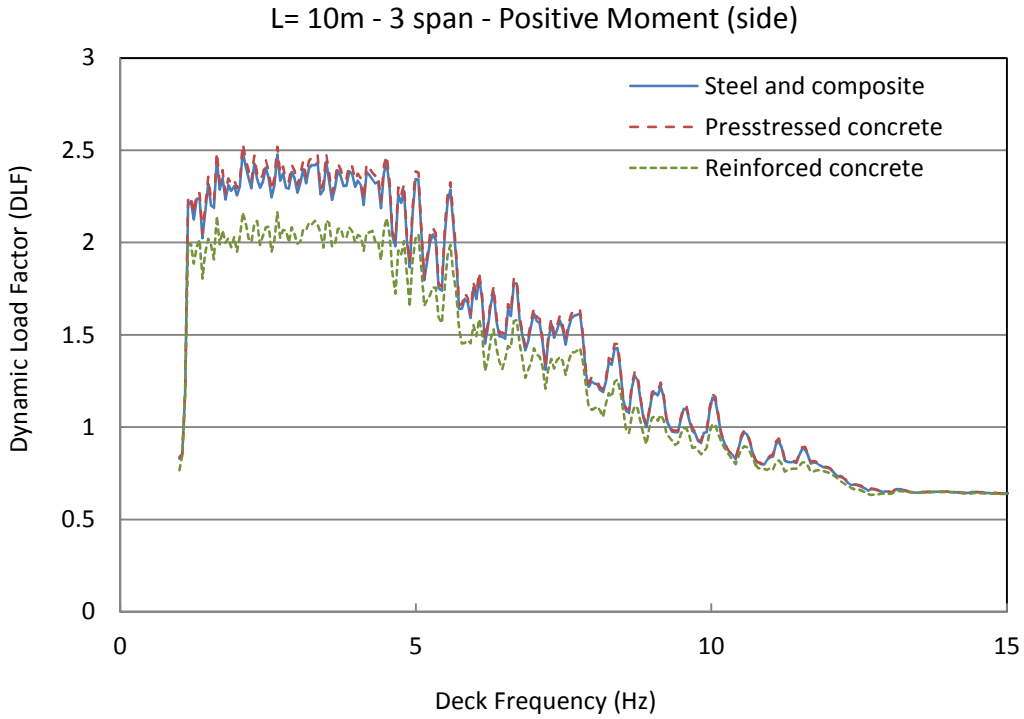

Figure 5-14 (Cont.). Dynamic Load Factors for bending moment in 1-span, 2-span and 3-span bridges, L=10m

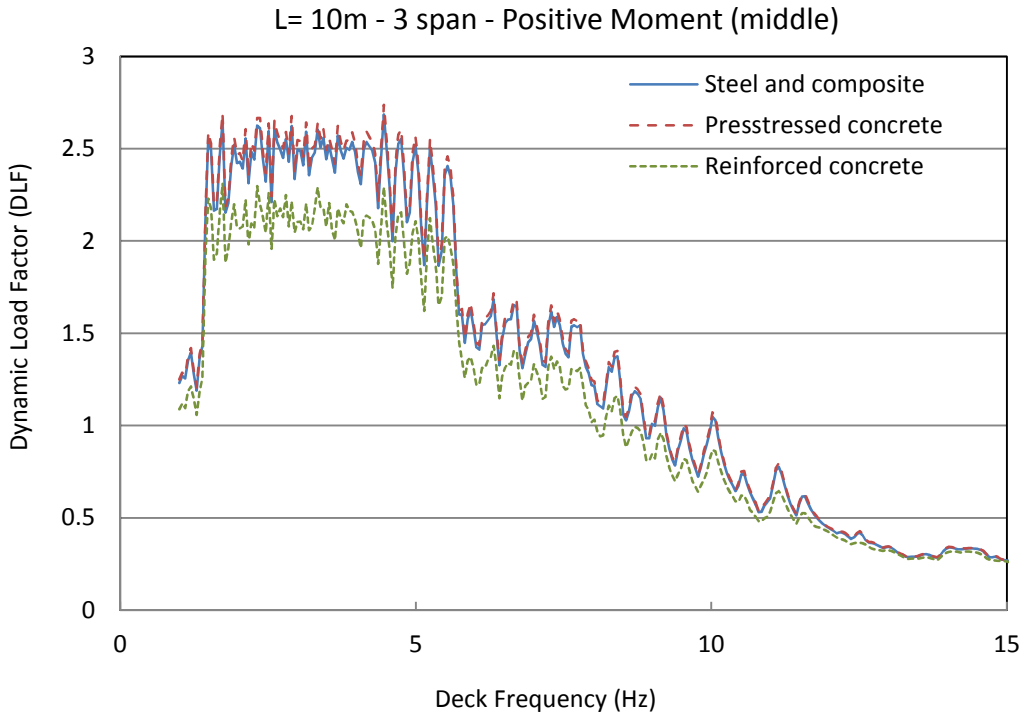

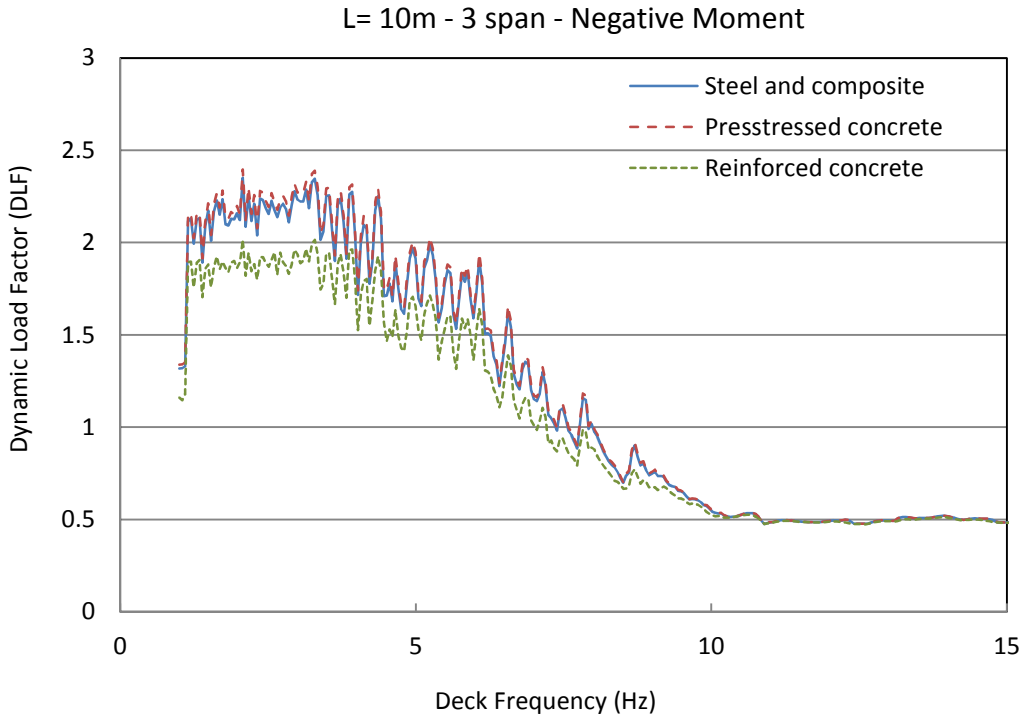

Figure 5-14 (Cont.). Dynamic Load Factors for bending moment in 1-span, 2-span and 3-span bridges, L=10m

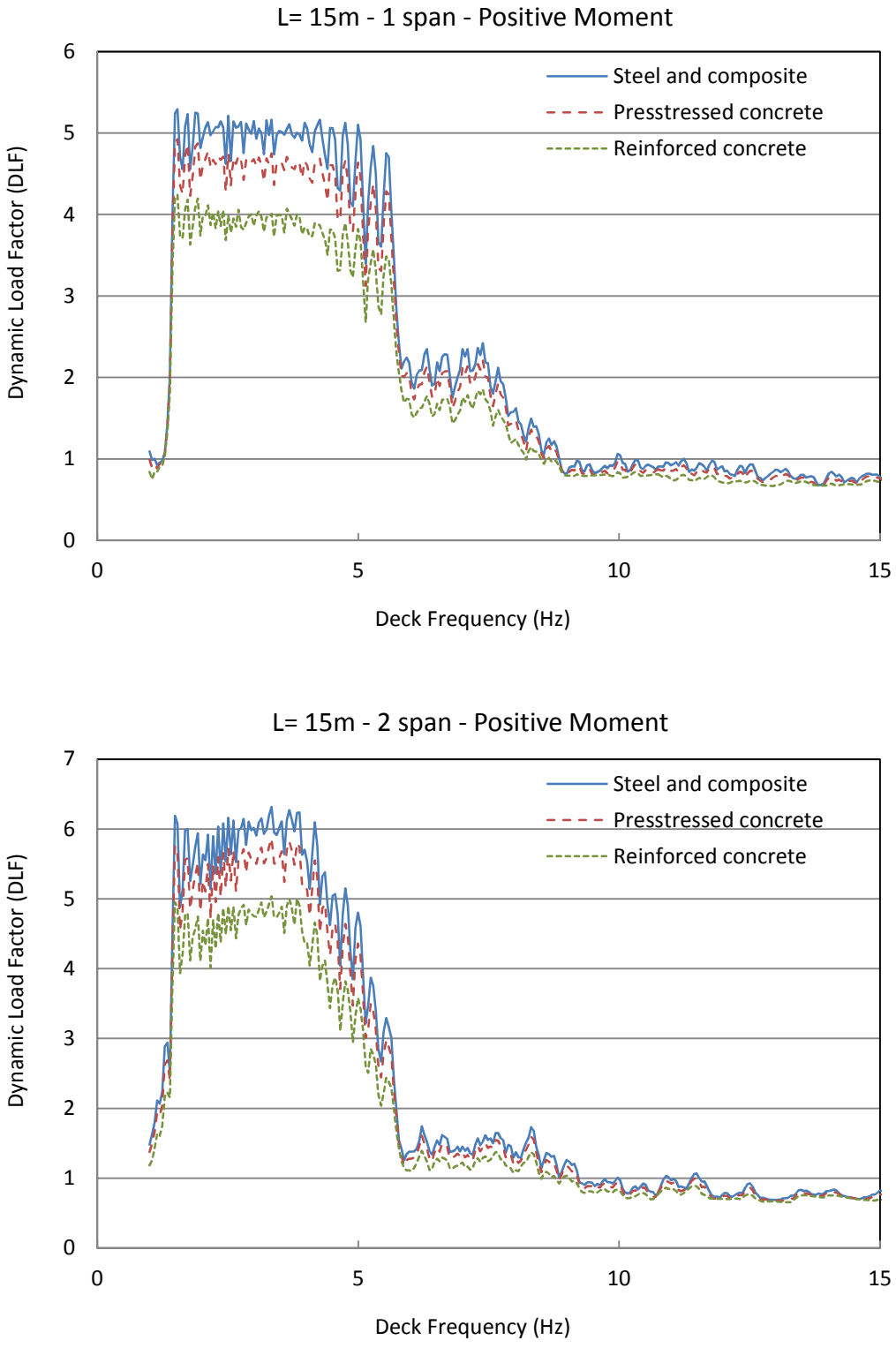

Figure 5-15. Dynamic Load Factors for bending moment in 1-span, 2-span and 3-span bridges, L=15m

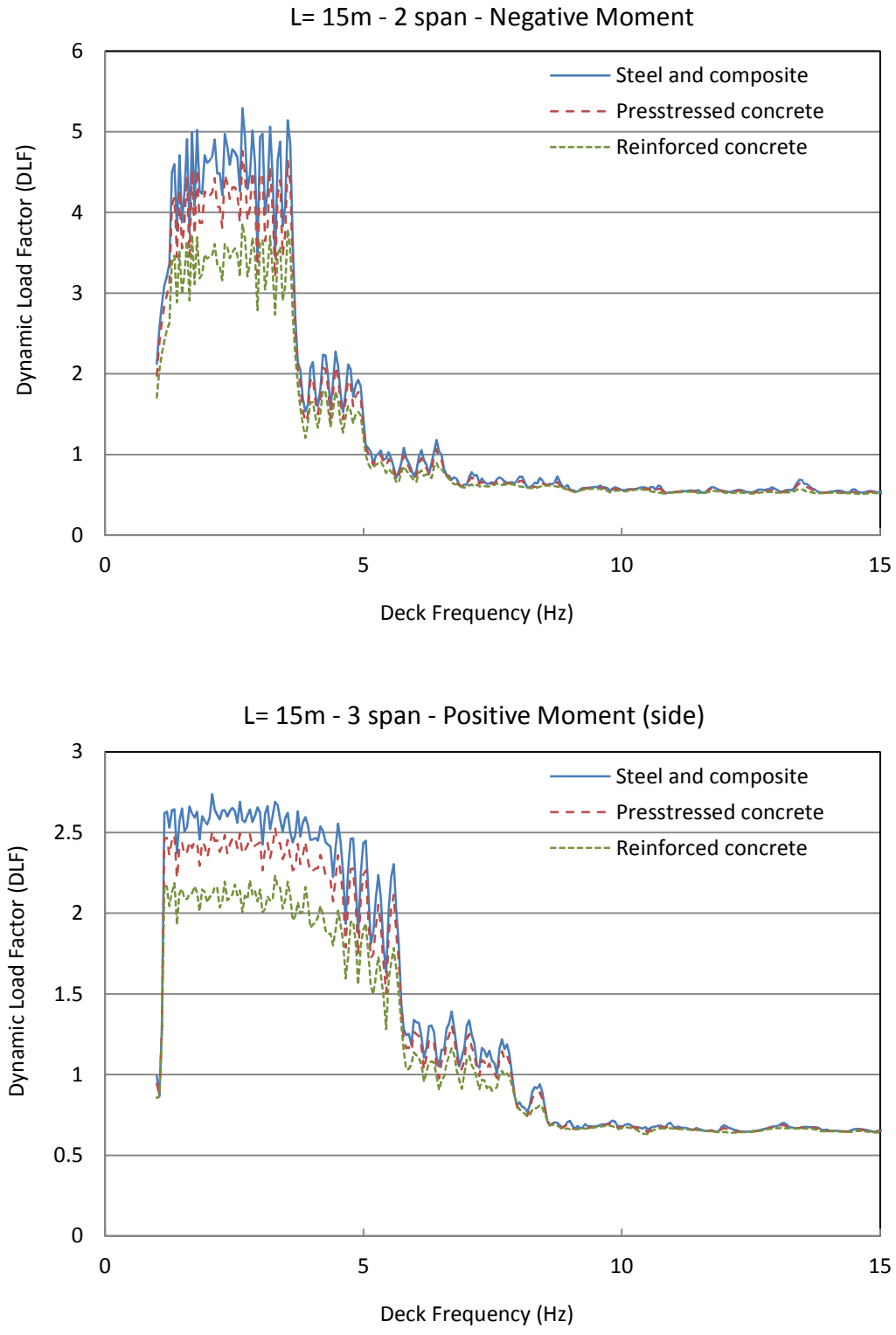

Figure 5-15 (Cont.). Dynamic Load Factors for bending moment in 1-span, 2-span and 3-span bridges, L=15m

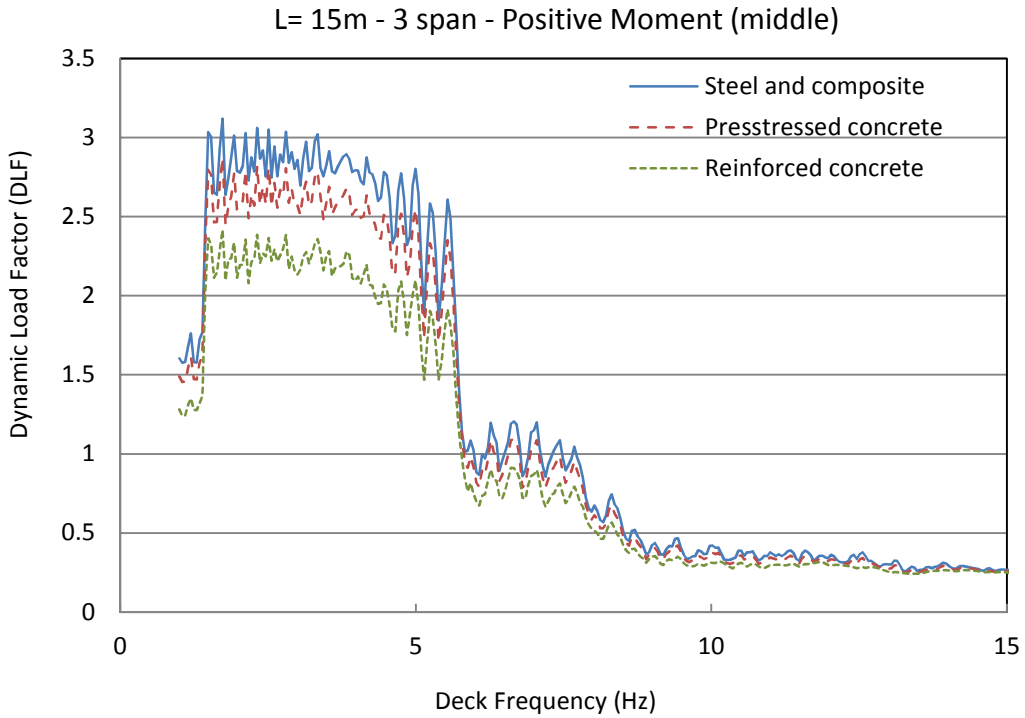

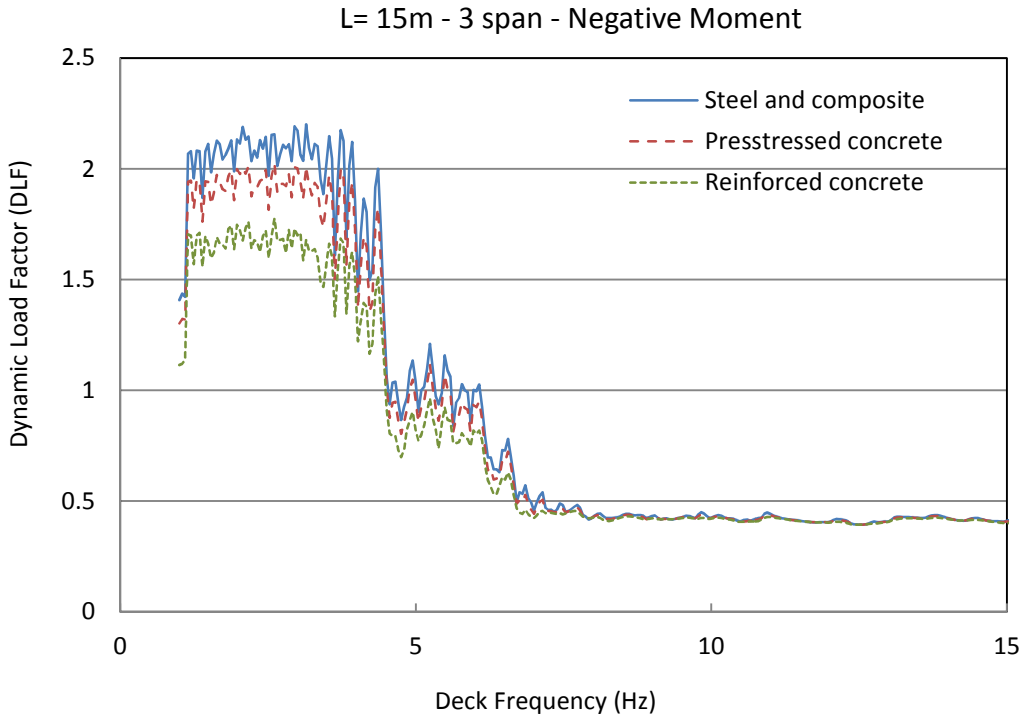

Figure 5-15 (Cont.). Dynamic Load Factors for bending moment in 1-span, 2-span and 3-span bridges, L=15m

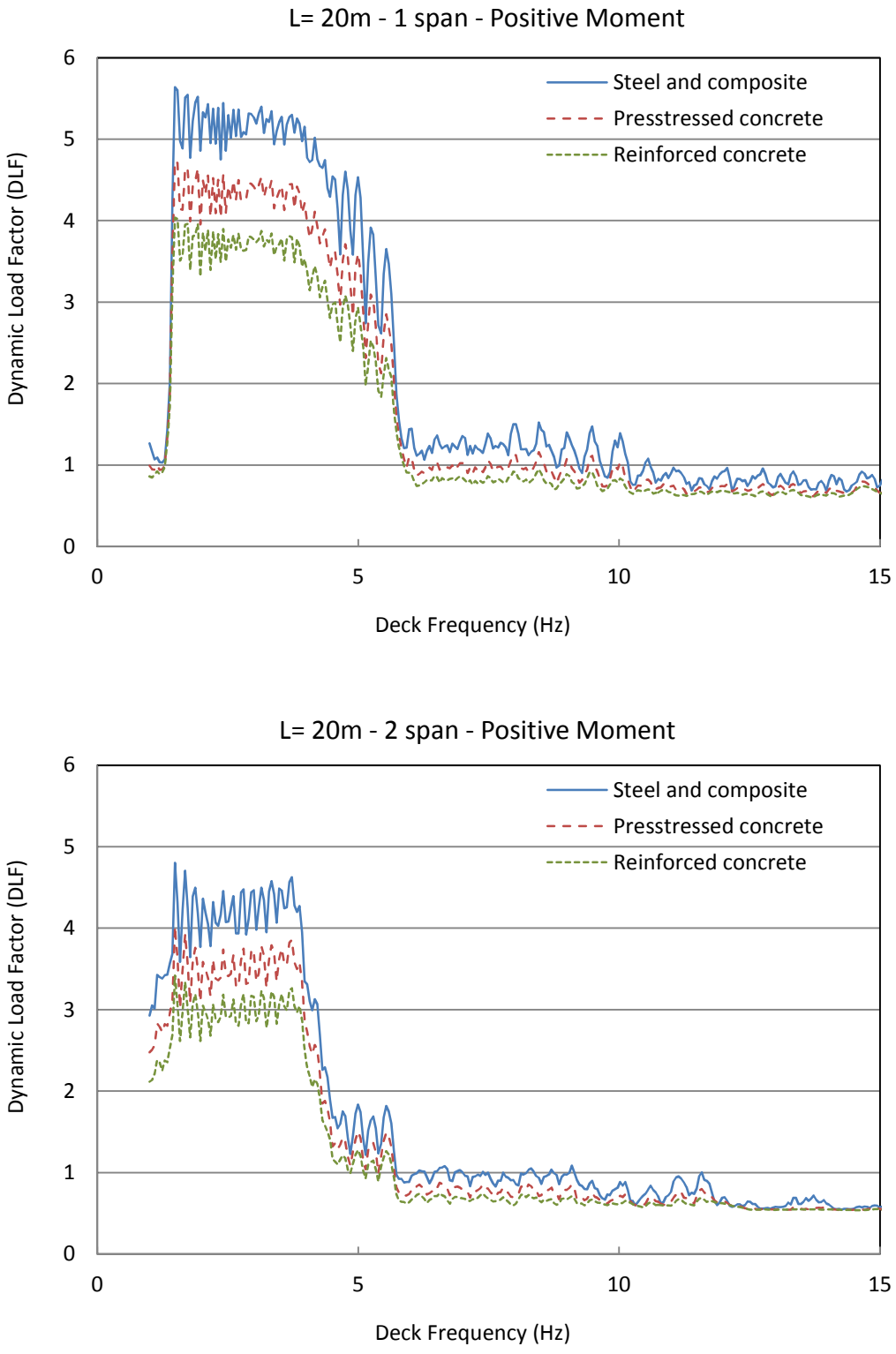

Figure 5-16. Dynamic Load Factors for bending moment in 1-span, 2-span and 3-span bridges, L=20m

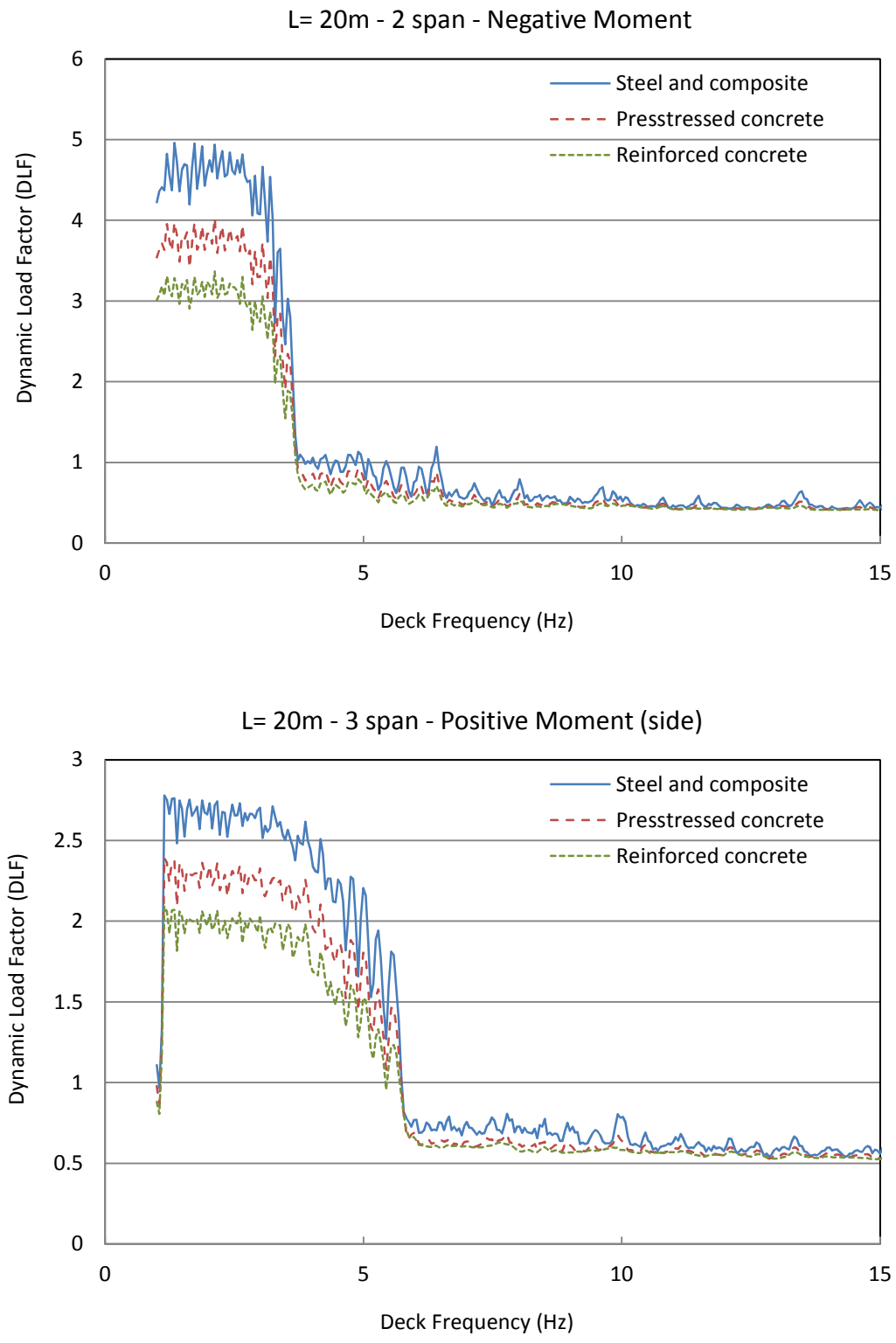

Figure 5-16 (Cont.). Dynamic Load Factors for bending moment in 1-span, 2-span and 3-span bridges, L=20m

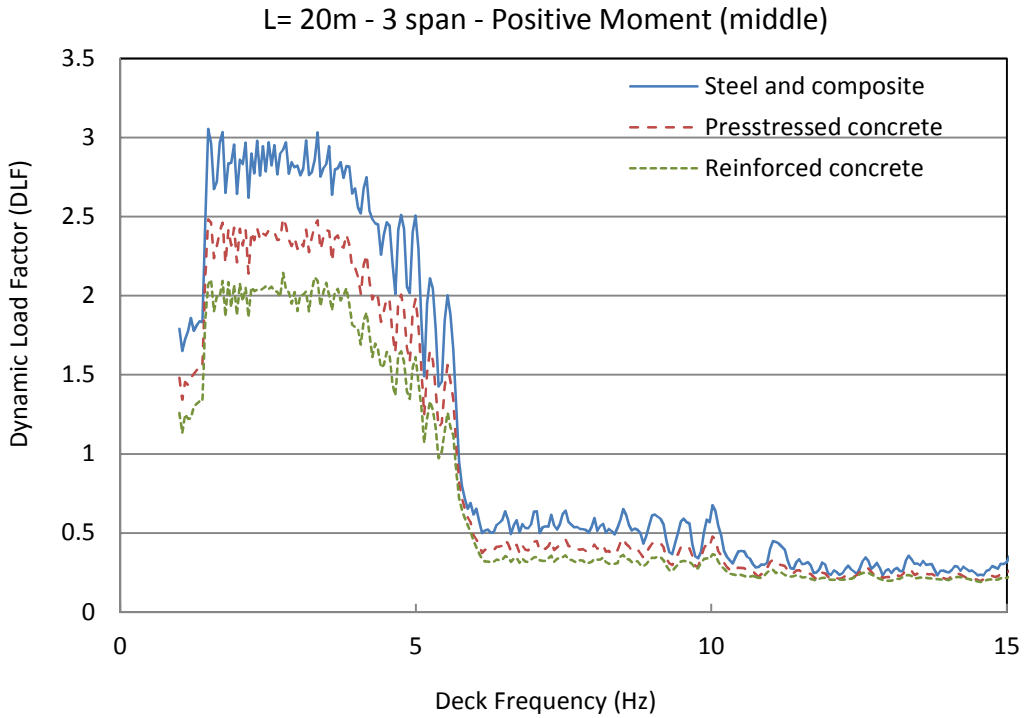

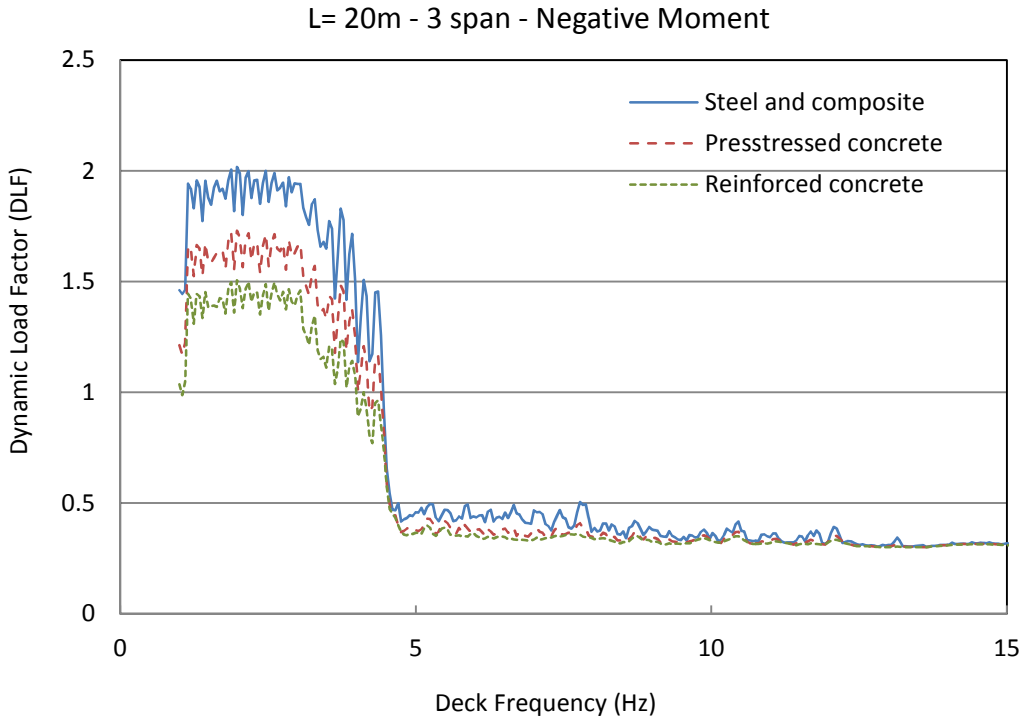

Figure 5-16 (Cont.). Dynamic Load Factors for bending moment in 1-span, 2-span and 3-span bridges, L=20m

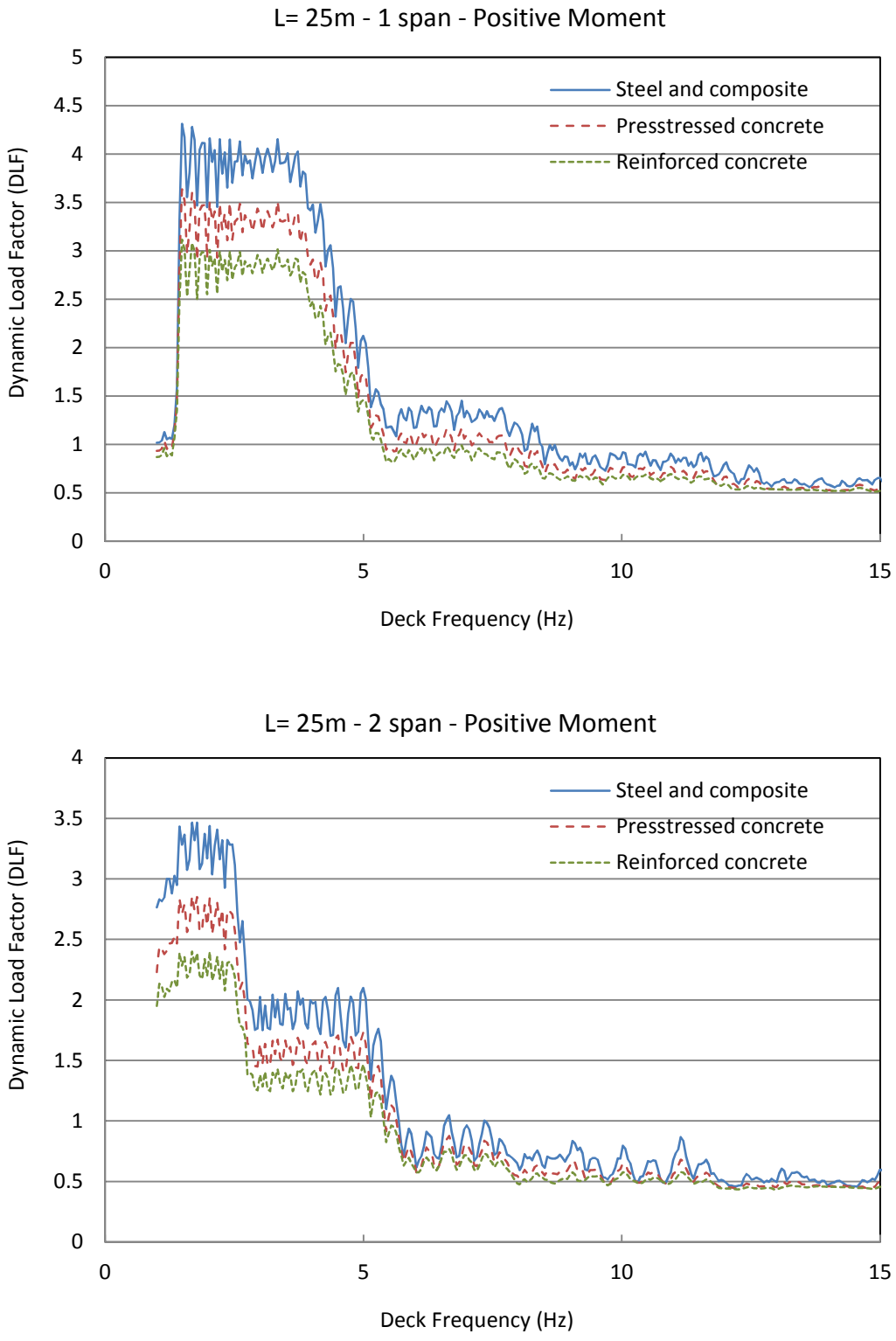

Figure 5-17. Dynamic Load Factors for bending moment in 1-span, 2-span and 3-span bridges, L=25m

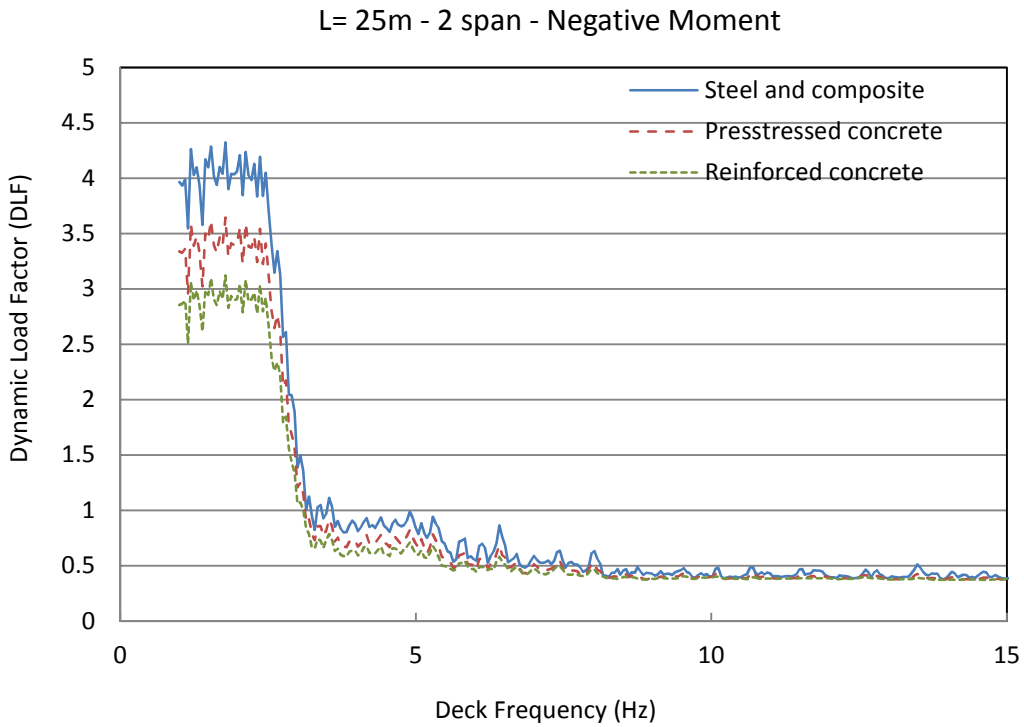

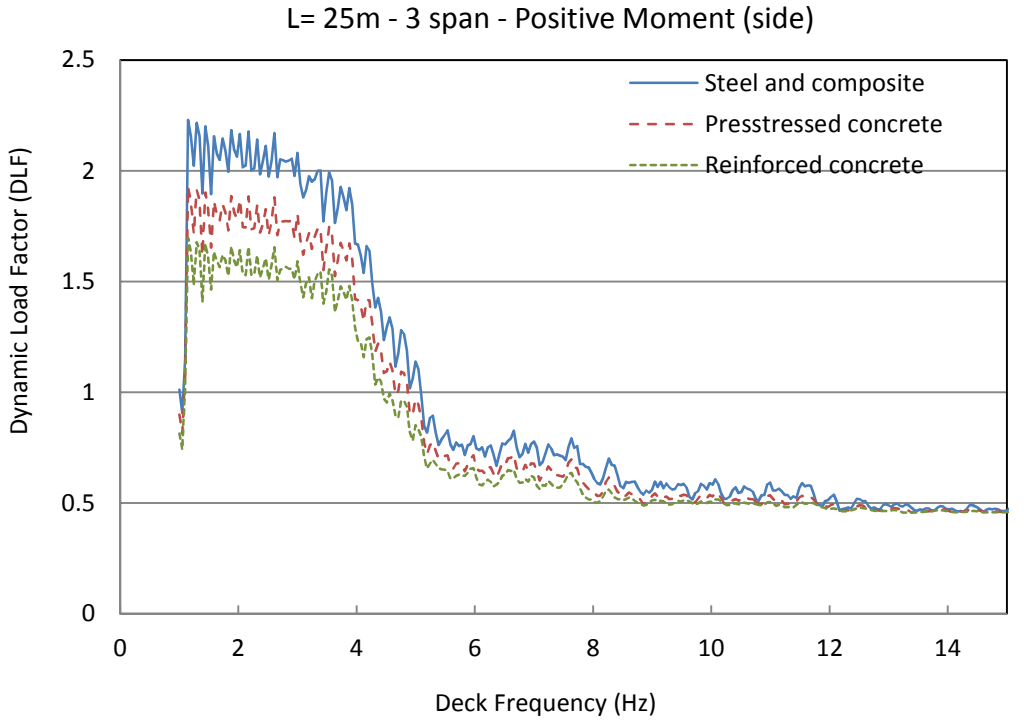

Figure 5-17 (Cont.). Dynamic Load Factors for bending moment in 1-span, 2-span and 3-span bridges, L=25m

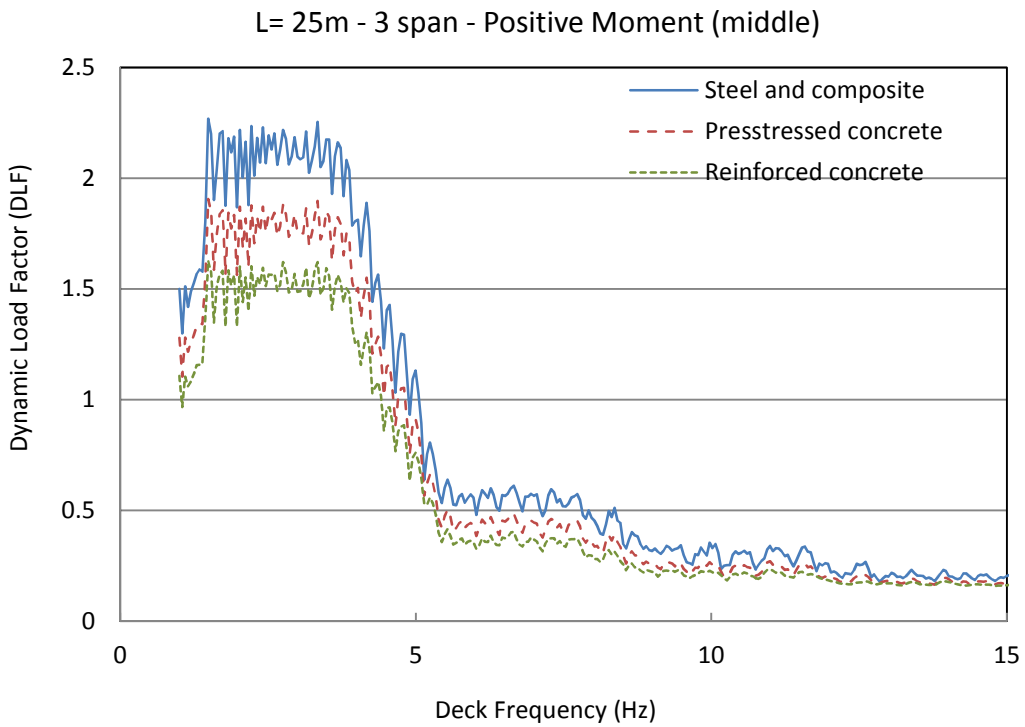

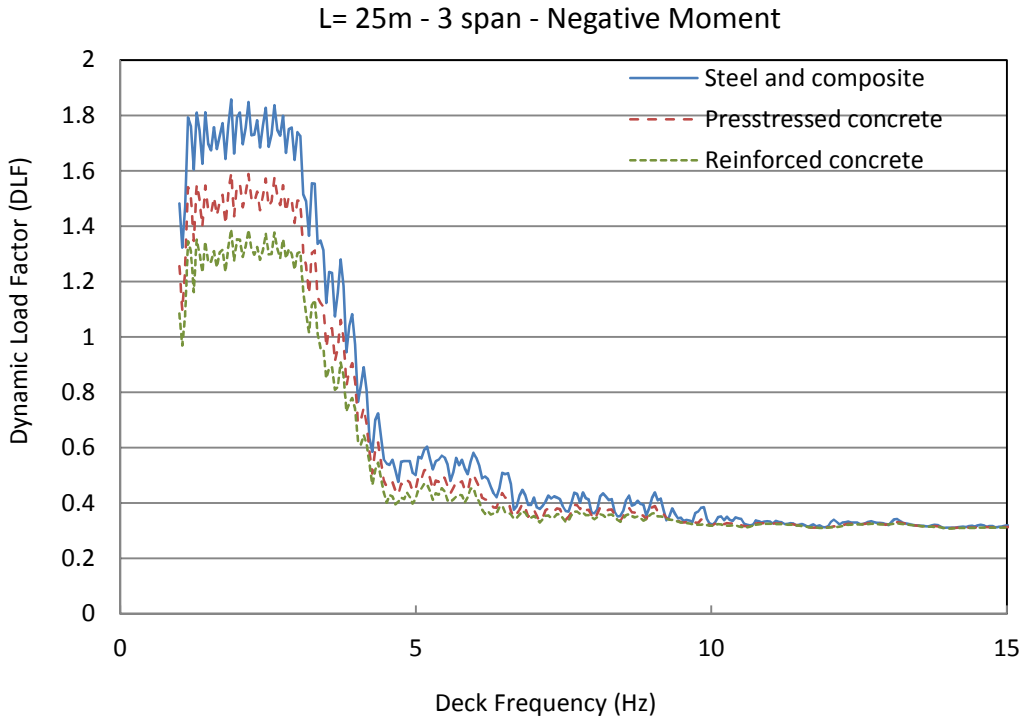

Figure 5-17 (Cont.). Dynamic Load Factors for bending moment in 1-span, 2-span and 3-span bridges, L=25m

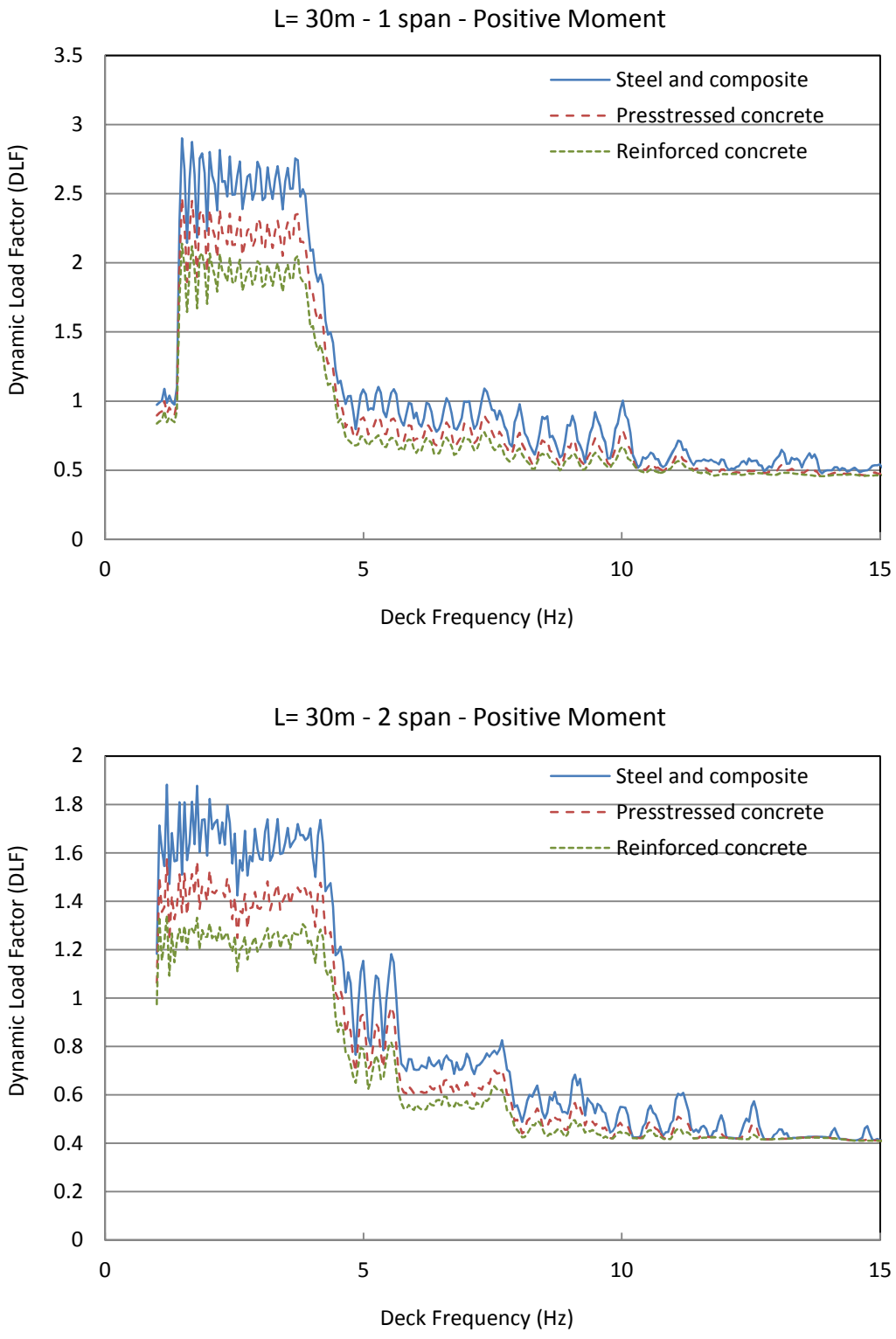

Figure 5-18. Dynamic Load Factors for bending moment in 1-span, 2-span and 3-span bridges, L=30m

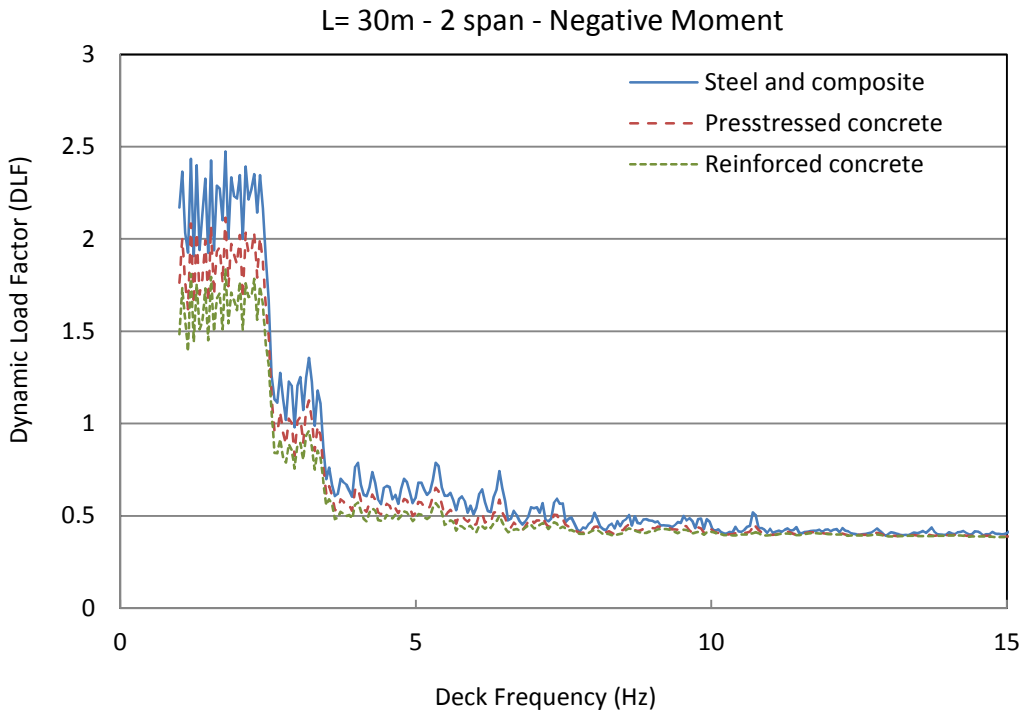

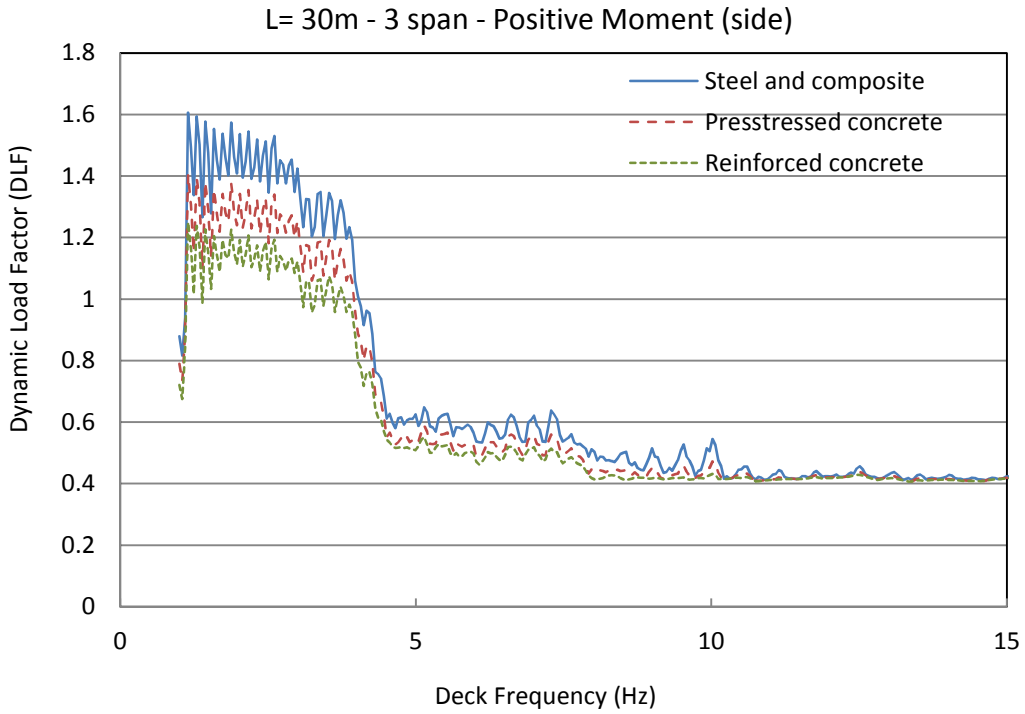

Figure 5-18 (Cont.). Dynamic Load Factors for bending moment in 1-span, 2-span and 3-span bridges, L=30m

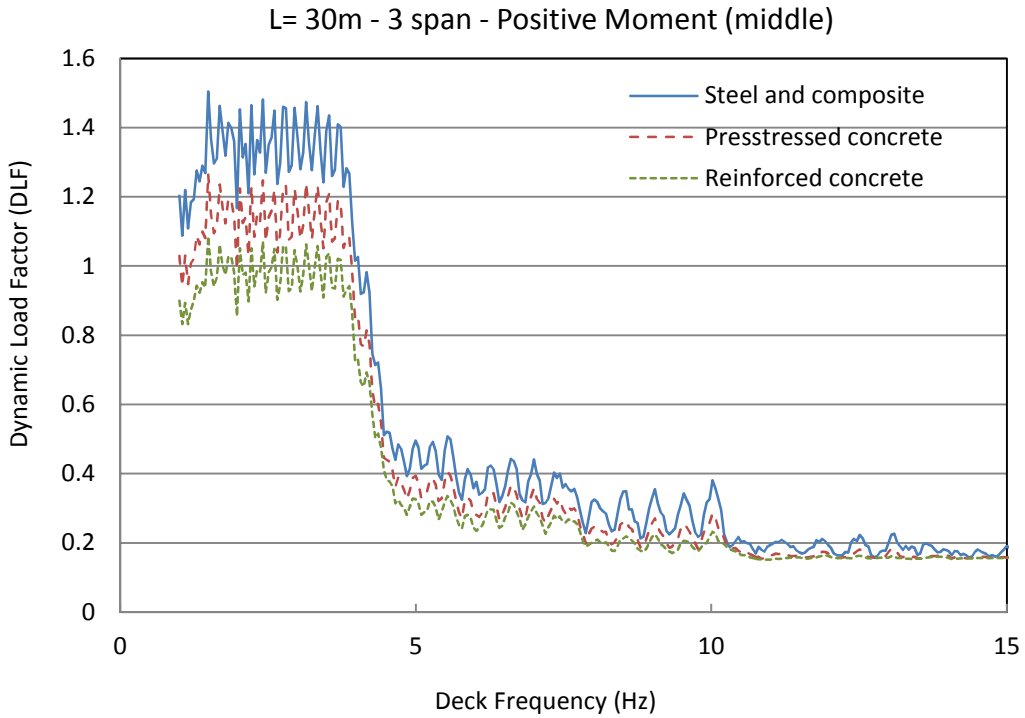

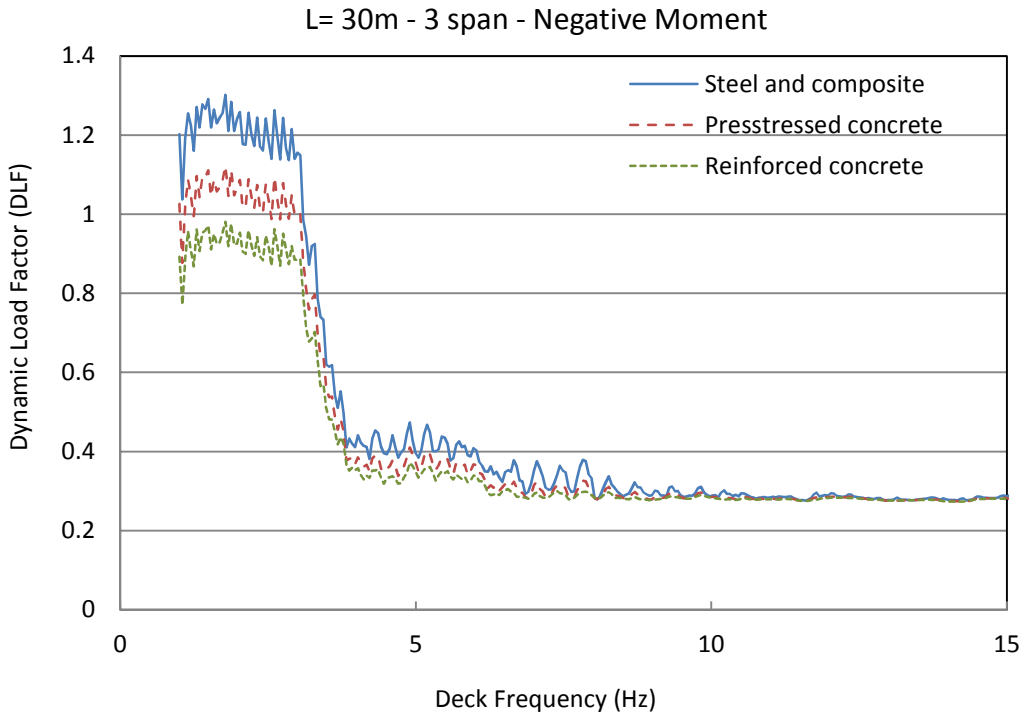

Figure 5-18 (Cont.). Dynamic Load Factors for bending moment in 1-span, 2-span and 3-span bridges, L=30m

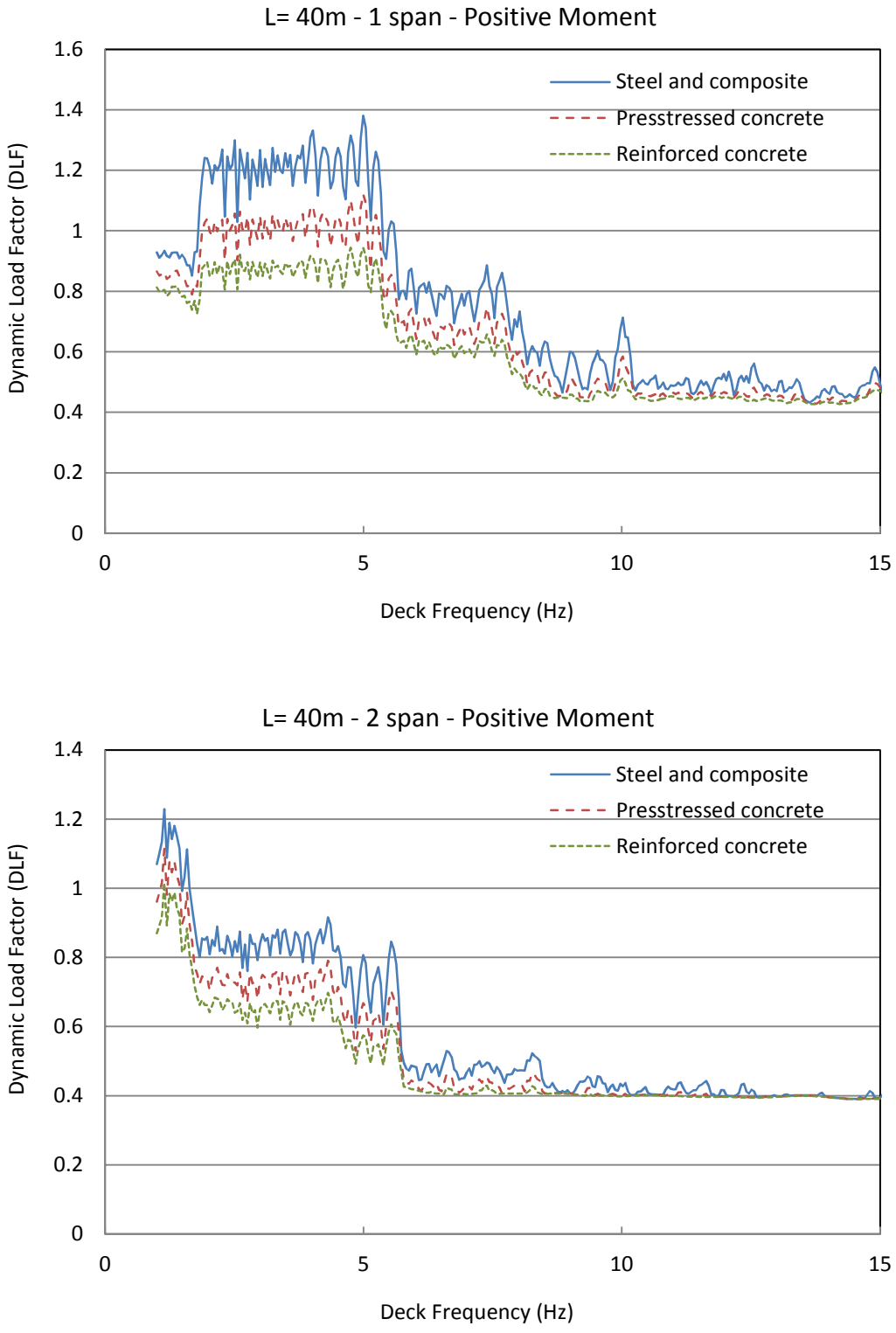

Figure 5-19. Dynamic Load Factors for bending moment in 1-span, 2-span and 3-span bridges, L=40m

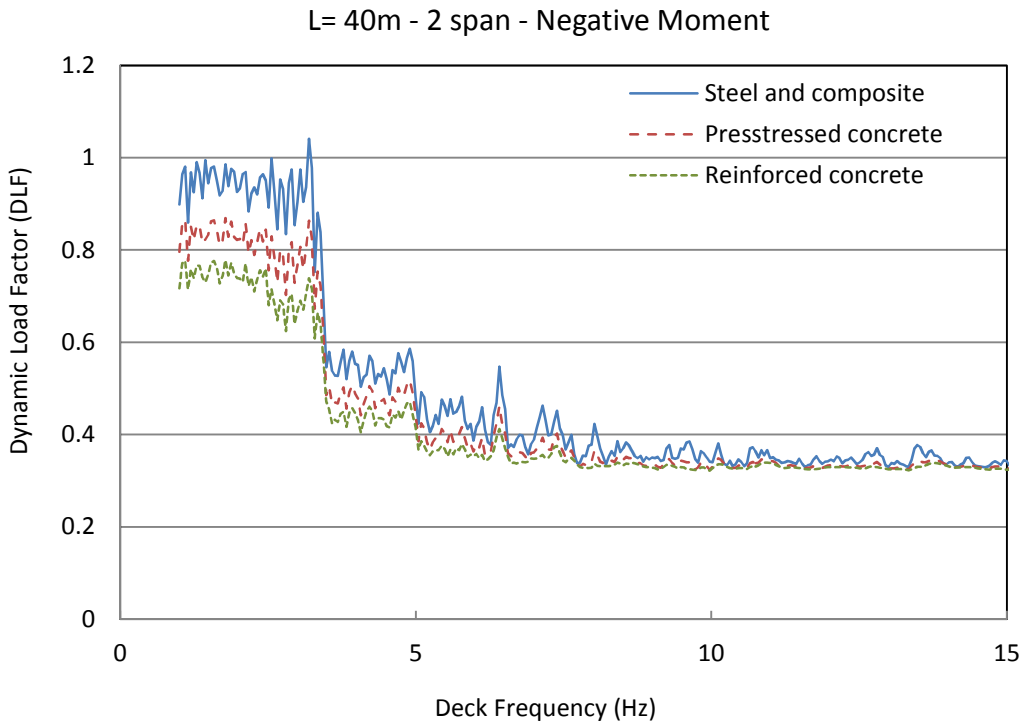

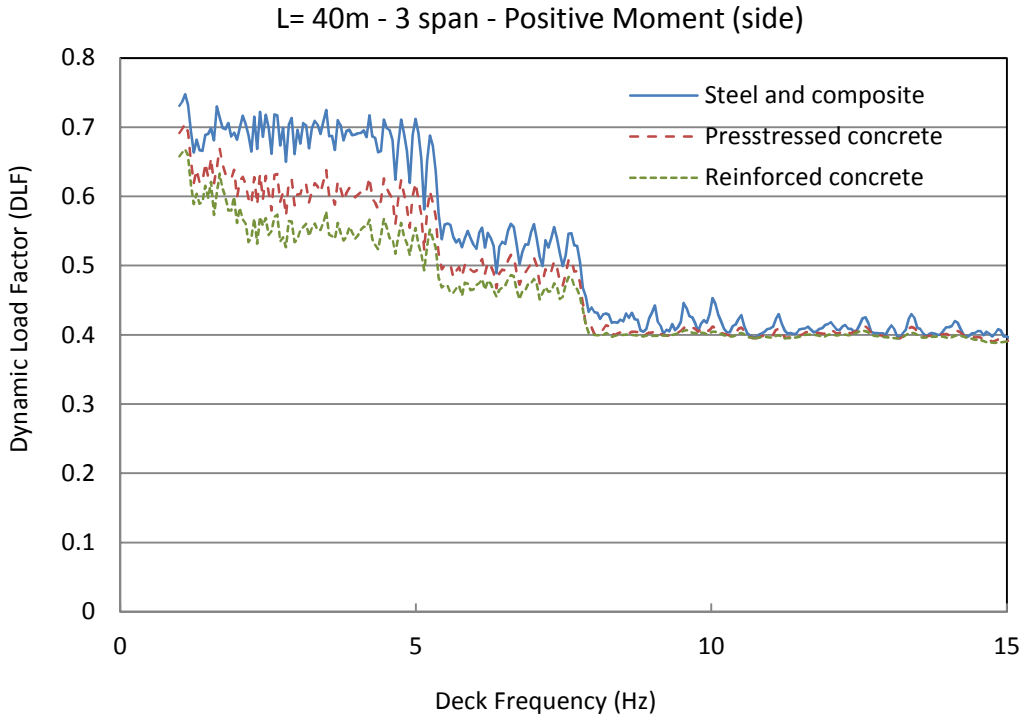

Figure 5-19 (Cont.). Dynamic Load Factors for bending moment in 1-span, 2-span and 3-span bridges, L=40m

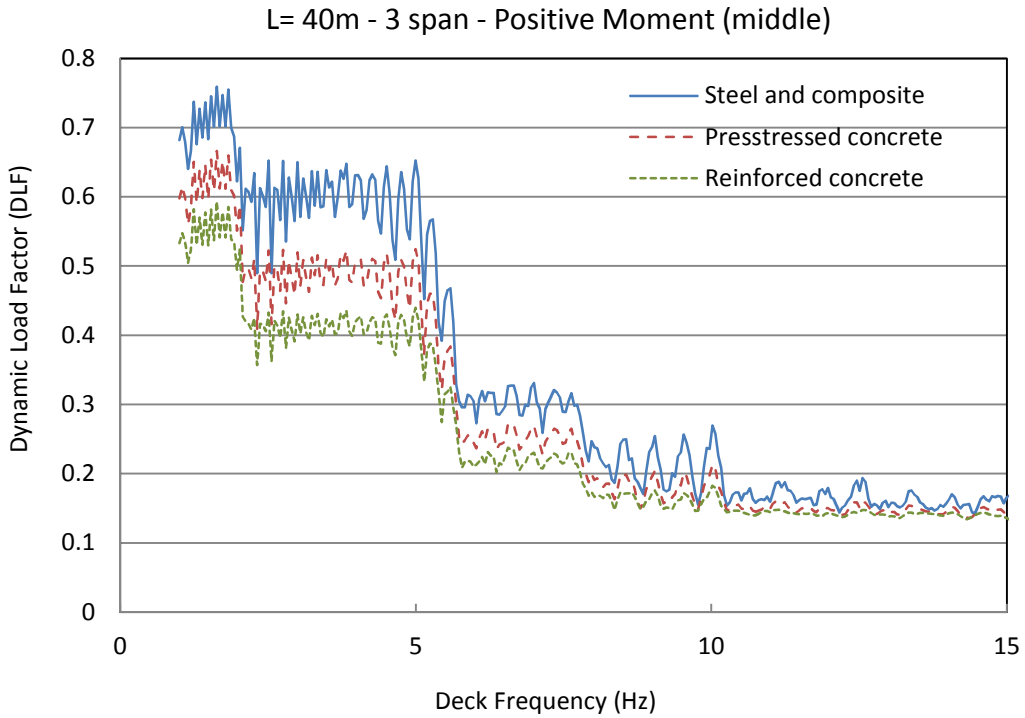

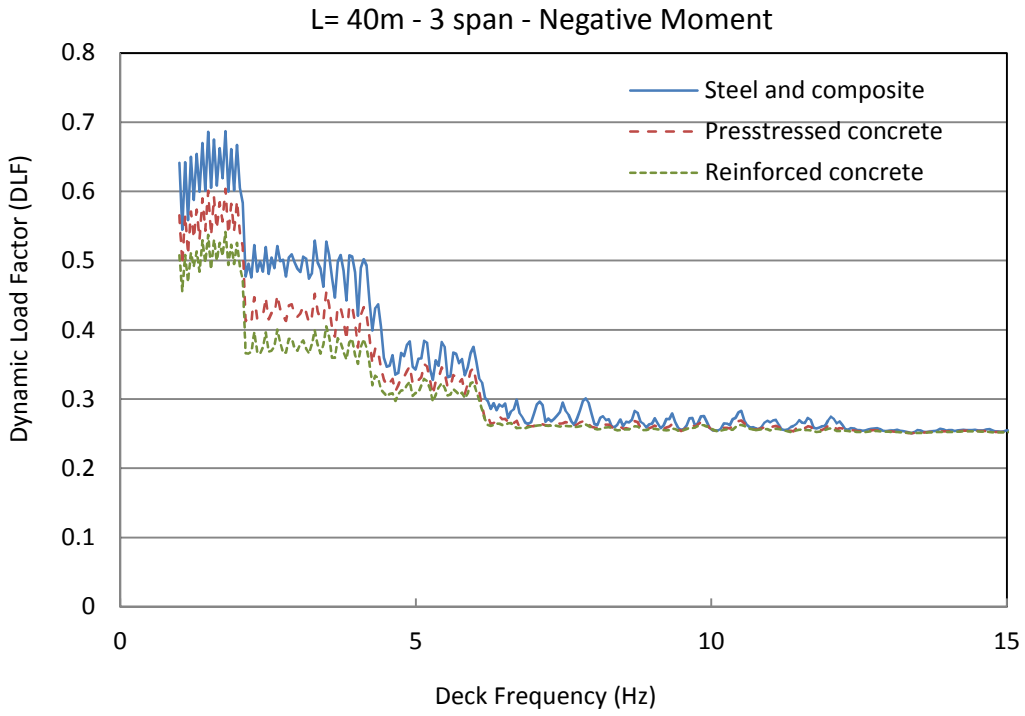

Figure 5-19 (Cont.). Dynamic Load Factors for bending moment in 1-span, 2-span and 3-span bridges, L=40m

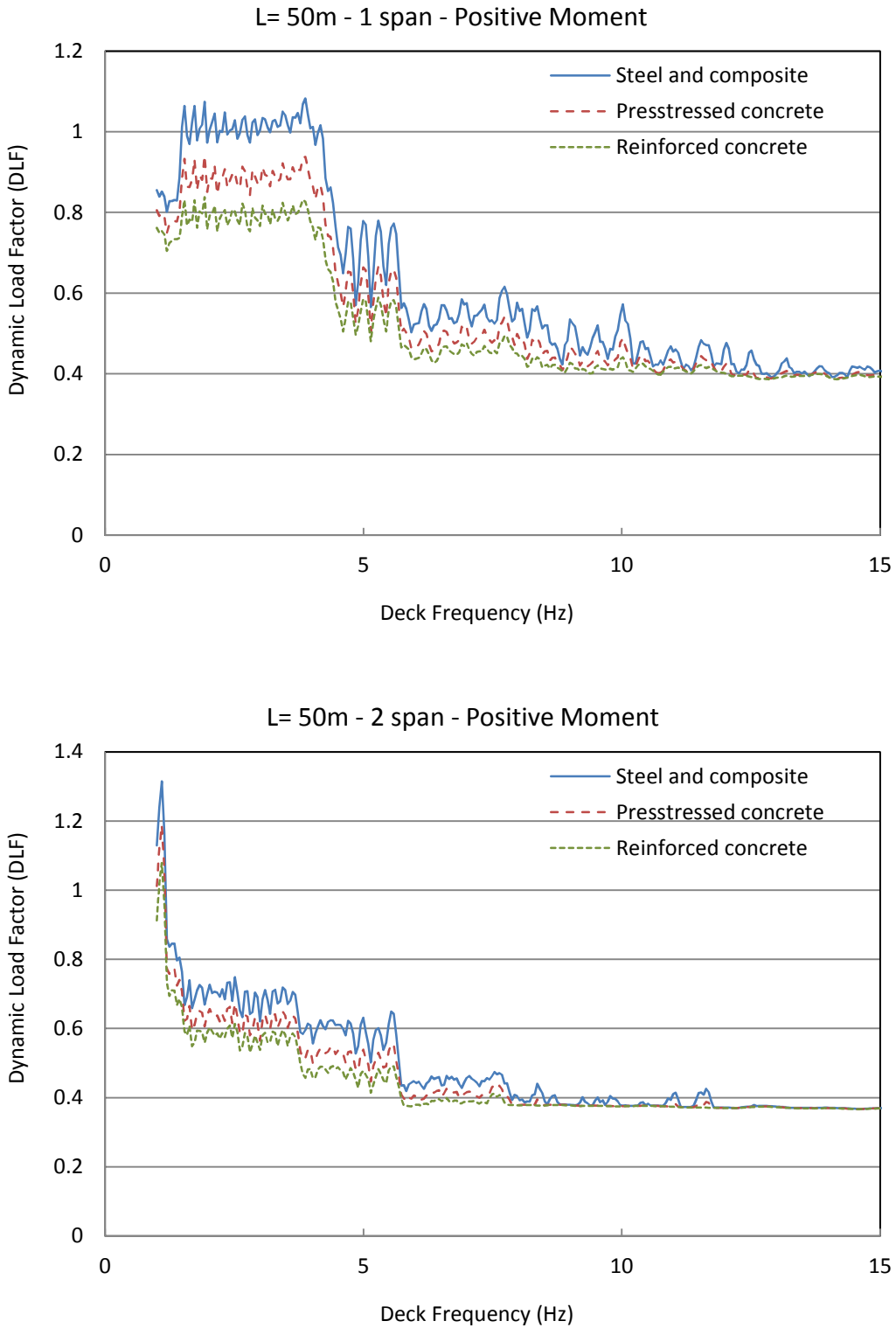

Figure 5-20. Dynamic Load Factors for bending moment in 1-span, 2-span and 3-span bridges, L=50m

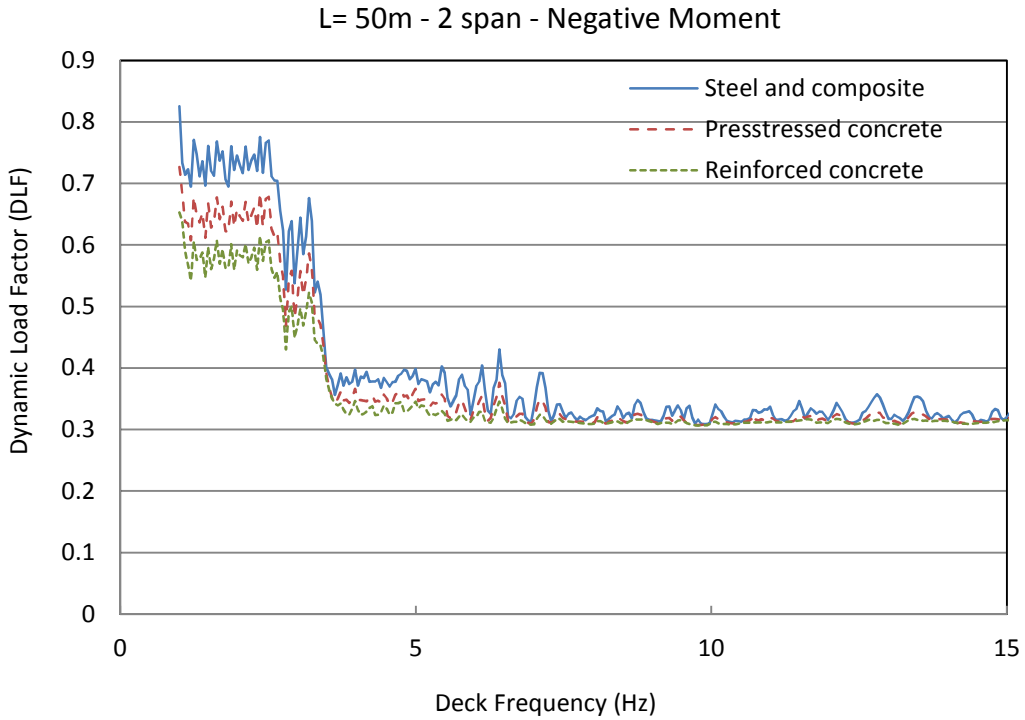

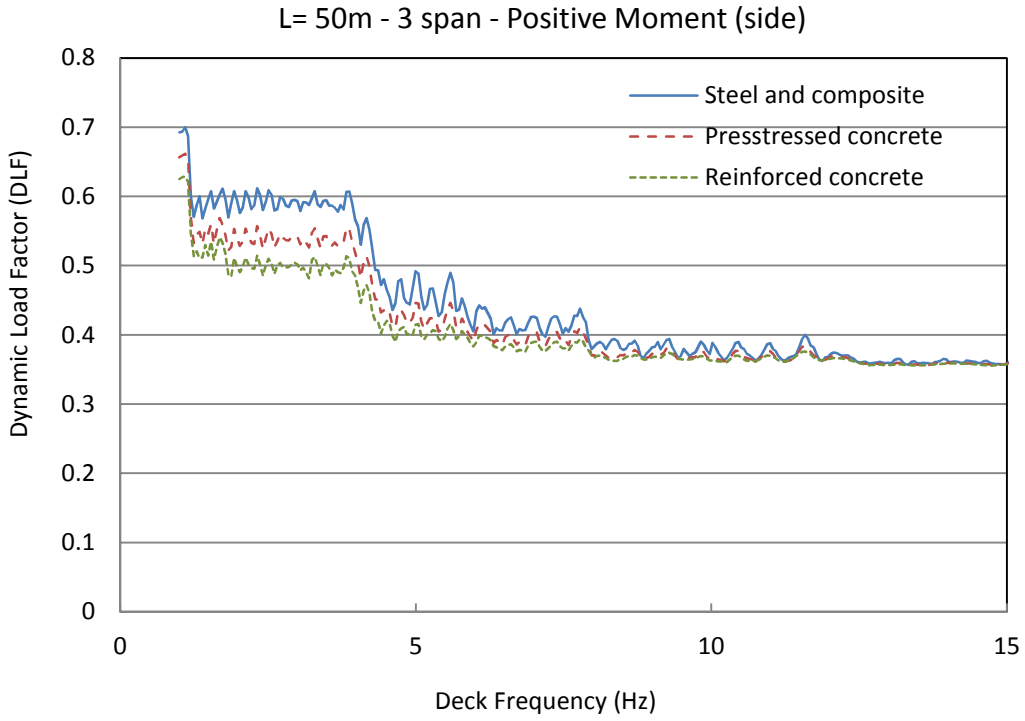

Figure 5-20 (Cont.). Dynamic Load Factors for bending moment in 1-span, 2-span and 3-span bridges, L=50m

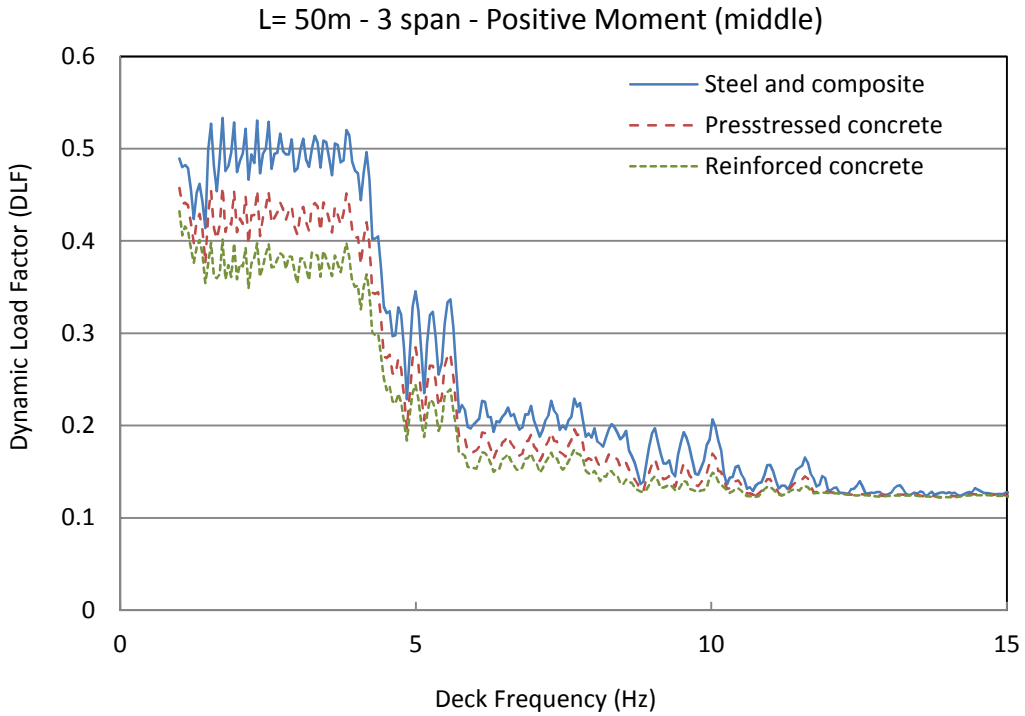

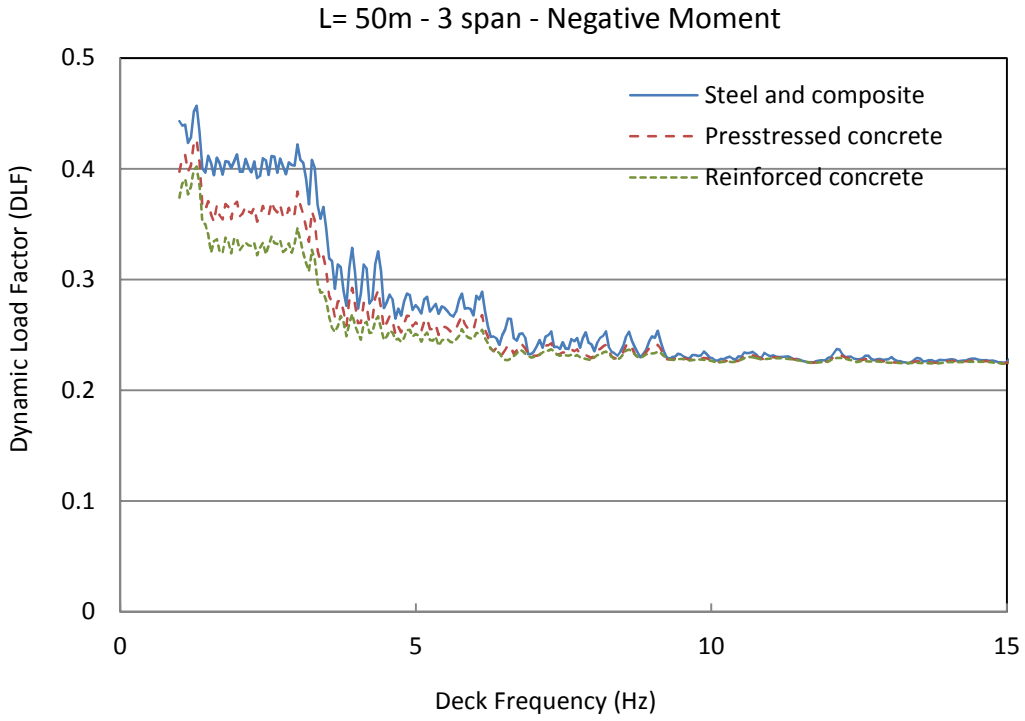

Figure 5-20 (Cont.). Dynamic Load Factors for bending moment in 1-span, 2-span and 3-span bridges, L=50m

For spans longer than 20m, the effect of structural damping in analysis results is more obvious. For instance, 20m simple span bridges (Fig. 5-16) with 0.5, 1.0 and 1.5% of critical damping experience maximum DLF values equal to 5.4, 4.5 and 3.8, respectively. This shows about 17% and 30% reduction in dynamic responses for 0.5% and 1.0% increase in critical damping percentage. Same trend can be observed for positive and negative bending moments in 2-span and 3-span continuous bridges.

Designing a bridge superstructure with a dynamic load factor about 5 does not necessarily result in a bridge superstructure 5 times stronger, due to the fact that the train load is only a part of the load combinations in the design procedure. By using provided DLF diagrams, a designer may decide to avoid the resonance by shifting the superstructure frequency of vibration. This can be done by altering the bridge type, girder spacing, material used, or eventually span length if possible.

5.6. Verification

To verify the applicability of the proposed Dynamic Load Factor (DLF) diagrams, determined strength limit state DLFs by others (Gabaldon et al., 2009; Goicolea, 2009) are compared to the values obtained by using diagrams in previous section. The summarized case studies include 5 to 40-meter simply supported spans bridges. As a set of case studies in Spain, applied load models were conventional loads in Spain rather than the Eurocode HSLM. Expectedly, HSLM recommended by Eurocode should simulate the worst possible case. This is the reason of having most of the proposed DLFs acceptably higher than measured DLFs at resonance in Table (5-4). The only case that calculated DLF based on the Eurocode HSLM is less than case studies is the 20-meter

long span with the "ICE 350E" train load which shows 14% higher DLF in practice. However, the same bridge has experienced less produced bending moment (or displacement) at the midspan (DLF=1.9) for another type of high-speed train, ICE2. This fact shows high dependency of the structural response to the load model and train characteristics which should be taken into account in the final design of the high-speed rail bridges.

Table 5-4. Comparison of proposed DLF values and determined DLFs by others, (a) Gabaldon et al. (2009) and (b) Goicolea (2009)

L (m)	Frequency (Hz)	Damping (%)	Load Model	Experimental/ Other DLF	Proposed DLF
5	16	2.0	ICE 350E	2.8[a]	3.5
7.5	12	2.0	ICE 350E	2.0[a]	2.0
15	5	1.0	TALGO AV2	1.8[b]	4.7
20	4	2.0	ICE 350E	4.0[a]	3.5
20	4	2.0	ICE2	1.9[b]	3.5
30	3	2.0	ICE2	1.2[b]	1.8
40	3	2.0	ICE2	0.45[b]	0.85

5.7. Conclusions

This study investigates the dynamic behavior of high-speed railroad bridges for the strength limit state design. The dynamic response of bridge superstructures, expressed as moment dynamic load factors, is captured in different sections. For this reason, one-span, two-span continuous and three-span continuous bridges are considered with a variety of practical span lengths. Typical girder types with different damping ratios are also considered in analyses. Due to the lack of high speed train models in the United States, the Eurocode models are used in analytical calculations. As opposed to current process of

Eurocode, this study aims to deliver an early-stage, easy to use and diagram-based design methodology, in which the bridge engineer is able to predict and possibly avoid any adverse dynamic effect due to resonance phenomena. Results show that resonance effect can be largely destructive by increasing the bending moments in various sections of the bridge girders. For span lengths of less than 7m, where HSLM-B governs, high DLF values up to 6 are spread over a rather broad range of frequency. As span length increases from 7m to 50m, a trend is visible in diagrams in which they tend to transform into stepped shapes. The effect of higher modes appears to cause this formation for specific frequency zones. While DLF values in low frequency range are extremely high (up to 6), they are often out of the practical frequency range of the superstructures for the considered span lengths. Spans longer than 50m were found not to be a concern in terms of dynamic load factors, thus no diagrams were offered for those cases.

Chapter 6

Conclusions

6.1. Summary and Conclusions

Structural response of bridges to dynamic loads depends on a variety of parameters such as load characteristics, stiffness, mass of the structure and damping. Even though the dynamic analysis of bridges for different load conditions follow the same backbone formulation, the complexity of bridge structures and applied loads makes it impractical to use closed form solutions and analytical techniques in most cases. Numerical techniques such as Finite Element Method and experimental studies can be an alternative for assessing the dynamic response of bridges. These two methods can be particularly helpful in examining complex systems with the possibility of observing nonlinear response.

In this dissertation, different approaches have been utilized to study particular issues regarding dynamic response of highway and railway bridges. Finite element modeling, reliability analysis and analytical approaches have been used to study particular issues regarding the response of bridges to seismic loads, vehicular dynamic loads and high-speed train loads, respectively.

In the first part of the dissertation, seismic vulnerability of an existing curved bridge structure is evaluated using finite element method and fragility analysis. Existing methodology for fragility analysis of regular straight bridges have been used with particular attention to the curved bridge characteristics such as orientation of columns and abutments and the modal response of the bridge structure. Based on the fragility analysis results, the transverse and active deformation of abutments are the most vulnerable issues

for slight damage state, while for higher damage levels, plastic rotation at the lower part of columns is the critical possible damage. Median PGA values which cause slight, moderate, extensive and complete damages (upper bounds) were determined equal to 0.09g, 0.19g, 0.29g and 0.57g, respectively. By applying calculated system fragility curves for each damage level and the possibility of the earthquake intensity in the area, expected damage level and accompanying maintenance costs for each time period can be estimated for the examined bridge structure. Compared to the measured fragility of typical straight multispan continuous steel bridges in the Central and Southern United States by Choi and Jeon (2003), with the median PGA values for 4 damage levels equal to 0.21g, 0.35g, 0.49g and 0.68g, this examined curved bridge is considerably more fragile.

In the second part, the effects of the vehicular impact of the moving loads over highway bridges have been studied using reliability analysis. Relatively high variation in recorded impacts for steel tension and compression members in bridges affects the reliability of designed bridges using the current version of the AASHTO LRFD Bridge Design Specifications (2007). Executed reliability analysis on current yield and fracture design equations for tension members validate a conservative design for yielding and fracture of steel tension members. By increasing current resistance factor for yielding in gross section from $\varphi_y=0.95$ to $\varphi_y=1.00$, the reliability indices are adjusted to the considered target value $\beta_T=3.0$. Also, by suggesting $\varphi_u=0.90$ instead of current resistance factor, $\varphi_u=1.00$, the reliability indices are decreased to the target reliability index $\beta_T=4.5$ for fracture of the net section.

In addition, the analysis results indicate safe behavior of all monitored steel sections designed for axial compression. However, in practical span length ratios ($0.2<r'<0.8$), AASHTO criteria leads to extremely conservative designs in some cases, with β values up to 5.1 for HSS compression members. According to this study, AASHTO LRFD resistance models for compression steel members can be adjusted to achieve a more uniform safety for different slenderness values. For example, for slenderness values equal to 2.0, the average reliability index for all sections is greater than 4.37 (compared to the target reliability index $\beta_T=3.0$).

In the last part, the dynamic behavior of high-speed railroad bridges for the strength limit state design is investigated using analytical methods. For this reason, one-span, two-span continuous and three-span continuous bridges are considered with a variety of practical span lengths. Typical girder types with different damping ratios are also considered in analyses. Eurocode model, as one of the widely accepted high-speed train load models, is used in analytical calculations. As opposed to current process of Eurocode, this study aims to deliver an early-stage, easy-to-use and diagram-based design methodology in which the bridge engineer is able to predict and possibly avoid any adverse dynamic effect due to resonance phenomenon.

Results show that resonance effect can be largely destructive by increasing the bending moments in various sections of the bridge girders. For span lengths of less than 7m, where HSLM-B governs, high dynamic load factor values up to 6 are spread over a broad range of frequency. While DLF values in a low frequency range are extremely high (up to 6), they are often out of the practical frequency range of the superstructures for the

considered span lengths. Spans longer than 50m has been found not to be a concern in terms of dynamic load factors, thus no diagrams are offered for those cases.

Enhanced understanding of bridge structural failures caused by different types of dynamic loads, and estimating their corresponding probability of failure can lead to a more reliable and cost efficient design of bridges. Balancing the cost and safety of structures, as the traditional rule of engineers, should be enriched by considering new concepts of sustainable developments and green construction.

6.2. Contributions

The main purpose of this dissertation is to evaluate the dynamic response of highway and railway bridges to different loads, and for particular issues such as fragility of multispan curved highway bridges, reliability of steel truss bridges, and the resonance of bridge superstructure for high-speed rail bridges. Different techniques including numerical methods and analytical approached have been utilized in determining the dynamic response of bridges to each load category.

6.2.1. Fragility of Multispan Curved Bridges

Fragility analysis methodology is utilized in a step-by-step approach to study seismic vulnerability of a multispan continuous steel curved bridge structure, and comparison has been made to the response of typical straight bridges with the same structural system. The analysis results indicate considerably higher fragility for curved bridges compared to regular straight bridges. Determined median PGA values for slight, moderate, extensive and complete damage states for the examined bridge are 2.33, 1.84, 1.69 and 1.19 times

smaller than the corresponding values calculated for the straight bridges with the same structural system in literature. This fact highlights the priority and need of more attention to curved bridges for retrofitting purposes.

6.2.2. Reliability of Steel Truss Bridges

AASHTO LRFD bridge design criteria for designing steel axial members are re-evaluated using the latest experimental test results. Calculated reliability indices for yielding of steel tension members in highway bridges show that current resistance factor, $\varphi_y=0.95$, may lead to overdesigned sections. Increased resistance factor for the yielding mode, $\varphi_y=1.00$, still showed satisfactory reliability above the target index.

In addition, the conventional resistance factor for the fracture of the net section ($\varphi_u=0.80$) could be increased to $\varphi_u=0.90$ for the observed steel sections.

Furthermore, determined reliability of designed steel compression members using AASHTO LRFD bridge design code for a variety of slenderness values declare safe behavior of designed members with underestimated compression strength in most cases.

6.2.3. Resonance of High-Speed Rail Bridges

Dynamic response of railway bridge superstructure to high-speed trains is studied, and dynamic load factor diagrams for maximum bending moments, applicable in the early stage of the design phase, are proposed. By using proposed diagrams, a designer can determine any possibility of resonance due to the high-speed train loads and choose the most appropriate structural system without doing complex dynamic analysis.

6.3. Future Work

Highlighted possible researches that can be done in the future are summarized in the following paragraphs. Itemized subjects are expected to be relatively fundamental and applicable in a broad range of research in the future:

- A probabilistic data modeling for the presence of live loads and moving vehicles on highway and railroad bridges can be beneficial for any future seismic analysis of bridges. Having the probability density function and related random parameters for the percentage of maximum live load on bridges during earthquakes can improve the accuracy of future fragility analysis and other probabilistic determinations.
- Resistance models for designing compression steel members in the AASHTO LRFD bridge design specifications can be adjusted to achieve a more uniform safety for different slenderness values. Current design equations may lead to relatively high reliability for slenderness values less than 2 (for most steel sections) with a gradual decrease in the reliability of more slender members (Fig. 4-5).
- More investigation of the reliability of steel tension and compression members, applicable in highway bridges, with any updated load and resistance models can be beneficial in clarifying delivered safety of the mentioned members.
- Similar to dynamic load factor diagrams for “strength limit state” design of bridges in high-speed railways, providing initial design diagrams for “service limit state” and estimating produced superstructure accelerations versus different superstructure vibration frequencies can be advantageous in early stage of

designing bridges. Shear dynamic load factors (not presented in this dissertation) will also be determined by the same research team at the University of Nebraska-Lincoln which will be published in near future.

Moving from deterministic to probabilistic approaches in the structural dynamics methodology and developing reliability based design criteria has been a major step to achieve more cost efficient structures. Next step would ideally be a global motivation toward developing "*Sustainability Based*" structural design criteria, by considering not only the economic aspects of the designed structures, but also the environmental and social effects of future structures.

Bibliography

AASHTO, (2011). *AASHTO guide specifications for LRFD Seismic Bridge Design.* 2nd Ed., Washington, DC: American Association of State Highway and Transportation Officials.

AASHTO, (2008a). *Bridging the Gap – Restoring and Rebuilding the Nation's Bridges*. Online publication, American Association of State Highway and Transportation Officials.

AASHTO, (2008b). *Manual for Bridge Evaluation.* 1st Ed., Washington, DC: American Association of State Highway and Transportation Officials.

AASHTO, (2007). *AASHTO LRFD Bridge Design Specifications*. Washington, DC: American Association of State Highway and Transportation Officials.

Agrawal, S. & Jain, A. K. (2009). Seismic analysis of a S-curved viaduct using stick and finite element models. *International Journal of Applied Science, Engineering and Technolology, 5*(3), 184-194.

Ayyub, B. M., & Lai, K. L. (1991). Selective sampling in simulation-based reliability assessment. *International Journal of Pressure Vessels and Piping, 46*, 229-249.

Bennett, R. M., & Najem-Clarke, F. S. (1987). Reliability of bolted steel tension members. *Journal of Structural Engineering, 113*(8), 1865-1872.

Billing, J. R. (1984). Dynamic loading and testing of bridges in Ontario, *Canadian Journal of Civil Engineering, 11,* 833-843.

Buckle, I. G., Friedland, I., Mander, J., Martin, G., Nutt, R., & Power, M. (2006). *Seismic Retrofitting Manual for Highway Structures: Part 1-Bridges*. New York, NY: FHWA/MCEER.

CALTRANS, (2010). *Seismic Design Criteria Version 1.6*. CA: California Department of Transportation.

Chen, S. S., & Harik, I. E. (2012). Dynamic effect of a moving truck on a culvert, *Journal of Bridge Engineering, 17*(2), 382-388.

Chernenko, D. E., & Kennedy, D. J. L. (1991). An analysis of the performance of the welded wild flange columns. *Canadian Journal of Civil Engineering, 18*, 537-555.

Choi, E., DesRoches, R., & Nielson, B. (2004). Seismic fragility of typical bridges in moderate seismic zones. *Engineering Structures, 26*(2), 187-199.

Choi, E., & Jeon, J. C. (2003). Seismic fragility of typical bridges in moderate seismic zones. *KSCE Journal of Civil Engineering, 7*(1), 41-51.

Chopra, A. K. (2007). *Dynamics of structures: Theory and applications to earthquake engineering, 3rd ed*. Upper Saddle River, NJ: Prentice-Hall.

Cornel, A. C., Jalayer, F., Hamberger, R. O., & Foutch, D. A. (2002). Probabilistic basis for 2000 SAC federal emergency management agency steel moment frame guidelines. *Journal of Structural Engineering, 128*(4), 526-533.

Cruz Noguez, C. A. & Saiidi, M. S. (2012). Shake-Table Studies of a Four-Span Bridge Model with Advanced Materials. *Journal of Structural Engineering, 138*(2), 183-192.

CSI, (1998). *SAP2000© Integrated finite element analysis and design of structures*. Berkeley, CA: Computers and Structures Inc.

Dinh, V. N., Kim, K. D., & Warnitchai, P. (2009). Dynamic analysis of three-dimensional bridge-high-speed train interaction using a wheel-rail contact model. *Engineering Structures,* 31(12), 3090-3106.

Ditlevsen, O., & Madsen, H.O. (2005). *Structural reliability methods*. Monograph, Internet edition 2.2.5.

Duan, M., Perdikaris, P. C., & Chen, W. (2000). Impact effect of moving vehicles. In W. Chen & L. Duan (Eds.), *Bridge engineering handbook* (56:1-19). USA: CRC Press.

Ellingwood, B., Galambos, T. V., MacGregor, J. G., & Cornell, C. A. (1980). *Development of a probabilistic based load criterion for American national standard A58*. Washington, DC: US Government.

Eurocode (2002). *Eurocode 1: actions on structures - Part 2: traffic loads on bridges, prEN 1991-2:2002 (E)*. Brussels: European Committee for Standardization.

FEMA, (2003). *HAZUS MH MR4 Technical Manual*. Washington, DC: Federal Emergency Management Agency.

Fryba, L. (1996). *Dynamics of railway bridges.* London: Thomas Telford.

Gabaldon, F., Riqueleme, F., Goicolea, J. M. & Arribas, J. J. (2009). Dynamic analysis of structures under high speed train loads: case studies in Spain. In R. Delgado, R. Calcada, J. M. Goicolea & F. Gabaldon (Eds.), *Dynamics of high-speed railway bridges,* (143-165). London, UK: Taylor & Francis Group.

Goicolea, J. M. (2009). Service limit states for railway bridges in new design codes IAPF and Eurocodes. In R. Delgado, R. Calcada, J. M. Goicolea & F. Gabaldon (Eds.), *Dynamics of high-speed railway bridges,* (1-12). London, UK: Taylor & Francis Group.

Goicolea, J. M., Dominguez, J., Navarro, J. A. & Gabaldon, F. (2002). New dynamic analysis methods for railway bridges in codes IAPF and Eurocode 1. *Proceeding of the Railway Bridges-Design Construction and Maintenance,* Madrid: IABSE.

Hagh-Elsafi, O., Albers, W. F., & Alampalli, S. (2012). Dynamic analysis of the Bentley Creek Bridge with FRP deck. *Journal of Bridge Engineering, 17*(2), 318-333.

Huang, D. (2012). Vehicle-induced vibration of steel deck arch bridges and analytical methodology. *Journal of Bridge Engineering, 17*(2), 241-248.

Huang, D. (2005). Dynamic and impact behavior of half-through arch bridges. *Journal of Bridge Engineering, 10*(2), 133-141.

Hwang, H., Liu, J. B., & Chiu, Y. H. (2001). *Seismic fragility analysis of highway bridges, (Technical report: MAEC RR-4).* Memphis, TN: Mid-American Earthquake Center.

Kennedy, D. L. L., & Gad Aly, M. (1980). Limit state design of steel structures-performance factors. *Canadian Journal of Civil Engineering, 7,* 45-77.

Kwon, O., Kim, E., Orton, S., Salim, H., & Hazlett, T. (2011). *Calibration of the live load factor in LRFD design guidelines.* Hannibal, MO: Missouri Transportation Institute.

Levi, J.M. (2011). *Seismic Response of columns in horizontally curved bridges*, Reno, NV: University of Nevada-Reno.

Li, H., Wakezer, J., & Kwasniewski, L. (2008). Dynamic response of a highway bridge subjected to moving vehicles. *Journal of Bridge Engineering, 13*(5), 439-448.

Martinez-Rodrigo, M. D., Lavado, J., & Museros, P. (2010). Dynamic performance of existing high-speed railway bridges under resonant conditions retrofitted with fluid viscous dampers. *Engineering Structures,* 32(3), 808-828.

McLinn, J. (2010). Major bridge collapses in the US, and around the world. *IEEE Transactions on Reliability, 59*(3), 449-482.

Mohseni, M., Lashgari, M., & Norton, T. R. (2012). Reliability evaluation of steel compression members designed with AASHTO LRFD bridge design code, *Proceedings of the Asian-Pacific Symposium on Structural Reliability and its Applications 2012,* Singapore.

Mohseni, M., & Norton, T. R. (2011). Re-calibration of steel tension members design criteria in AASHTO LRFD bridge design code. *Proceedings of the 11th International Conference on Application of Statistics and Probability in Civil Engineering*, Zurich, Switzerland.

Mohseni, M., & Norton, T. R. (2011). Seismic damage assessment of curved bridges using fragility analysis. *Proceeding of 11th International Conference on Applications of Statistics and Probability in Civil Engineering-ICASP11*, Zurich, Switzerland.

Mohseni, M., & Norton, T. R. (2010). Developing analytical fragility curves for highway bridges. *62nd EERI Annual Meeting*, San Francisco, CA.

Museros, P., & Alarcon, E. (2005). Influence of the second bending mode on the response of high-speed bridges at the resonance. *Journal of Structural Engineering,* 131(3), 405-415.

Mwafy, A., Elnashi, A., & Yen, W. H. (2007). Implications of design assumptions on capacity estimated and demand predictions of multi-span curved bridges. *Journal of Bridge Engineering, 12*(6), 710-726.

Najem-Clarke, F. S. (1985). *Correlation coefficient for yield strength and ultimate strength of structural steel*. Knoxville, TN: Univ. of Tennessee.

NDOR, (2005). *New US-75 SB Bridge to I-480 EB construction drawings*. Lincoln, NE: State of Nebraska.

Nielson, B. G. (2005). *Analytical Fragility Curves for Highway Bridges in Moderate Seismic Zones, PhD Dissertation.* Atlanta, GA: Georgia Institute of Technology.

Nielson, B. G., & DesRoches, R. (2007). Seismic fragility methodology for highway bridges using a component level approach. *Earthquake Engineering and Structural Dynamic, 36,* 823-839.

Nowak, A. S., & Collins, K.R. (2000). *Reliability of structures*. USA: McGraw-Hill.

Nowak, A. S. (1999). *Calibration of LRFD bridge design code (NCHRP Report 368)*. Washington, DC: National Academy Press.

Olsson, A. M. J., & Sandberg, G. E. (2002). Latin Hypercube sampling for stochastic finite element analysis. *Journal of Engineering Mechanics, 128*(1), 121-125.

Padgett, J.E., and DesRoches, R. (2009). "Retrofitted bridge fragility analysis for typical classes of multi-span bridges", *Earthq. Spectra,* Vol. 25, No. 1, pp. 117-141.

Padgett, J. E., Nielson, B. G., & DesRoches, R. (2008). Selection of optimal intensity measures in probabilistic seismic demand models of highway bridge portfolios. *Earthquake Engineering and Structural Dynamic, 37,* 711-725.

Padgett, J. E., & DesRoches, R. (2008). Methodology for the development of analytical fragility curves for retrofitted bridges. *Earthquake Engineering and Structural Dynamic, 37,* 1157-1174.

Padgett, J. E., & DesRoches, R. (2006). Evaluation of bridge retrofit in regions of low-to-moderate seismicity. *Proceeding of the 5th national seismic conference on bridges and highways*, San Francisco, CA: Multidisciplinary Center for Earthquake Engineering Research.

Ren, W., Harik, I. E., Blandford, G. E., Lenett, M., & Baseheart, T. M. (2004). Roebling suspension bridge. II: ambient testing and live-load response, *Journal of Bridge Engineering, 9*(2), 119-126.

Samaan, M., Kennedy, J. B., & Sennah, K. (2007). Impact factors for curved continuous composite multiple-box girder bridges, *Journal of Bridge Engineering, 12*(1), 80-88.

Schmidt, B. J., & Bartlett, F. M. (2002a). Review of resistance factor for steel: data collection. *Canadian Journal of Civil Engineering, 29*, 98-108.

Schmidt, B. J., & Bartlett, F. M. (2002b). Review of resistance factor for steel: resistance distributions and resistance factor calibration. *Canadian Journal of Civil Engineering, 29,*109-118.

Seo, J., & Linzell, D. G. (2012). Horizontally curved steel bridge seismic vulnerability assessment. *Engineering Structures, 34,* 21-32.

Sun, Z., Wang, D., Guo, X., Si, B. & Huo, Y. (2012). Lessons learned from the damaged Huilan Interchange in the 2008 Wenchuan Earthquake. *Journal of Bridge Engineering, 17*(1), 15-24.

Todorovich, P., Schned, D., & Lane, R. (2011) *High-speed rail international lessons for U.S. policy makers*. Cambridge, MA: Lincoln Institute of Land Policy.

Wang, N., O'Malley, C., Ellingwood, B. R., & Zureick, A. H. (2011). Bridge rating using system reliability assessment. I: Assessment and verification by load testing. *Journal of Bridge Engineering, 16*(6), 854-862.

Wang, N., Ellingwood, B. R., & Zureick, A. H. (2011). Bridge rating using system reliability assessment. II: Improvements to bridge rating practices. *Journal of Bridge Engineering, 16*(6), 863-871.

Wardhana, K., & Hadipriono, F. C. (2003) Analysis of Recent Bridge Failures in the United States, *Journal of Performance of Constructed Facilities, 17*(3), 144-150.

Wen, Y. K., & Wu, C. L. (2001). Uniform hazard ground motions for mid-America cities. *Earthquake Spectra, 17*(2), 359-384.

Wright, T., DesRoches, R., & Padgett, J. E. (2011) Bridge Seismic Retrofitting Practices in the Central and Southeastern United States, *Journal of Bridge Engineering, 16*(1), 82-92.

Yashinsky, M. (1998). Performance of bridge seismic retrofits during Northridge Earthquake, *Journal of Bridge Engineering, 3*(1), 1-14.

Yau, J. D. (2001) Resonance of continuous bridges due to high speed trains. *Journal of Marine Science and Technology*, 9(1), 14-20.

Xia, H., & Zhang, N. (2005). Dynamic analysis of railway bridge under high-speed trains, *Computers & Structures,* 83(23-24), 1891-1901.